

**BOLU ABANT İZZET BAYSAL UNIVERSITY
THE GRADUATE SCHOOL OF NATURAL AND APPLIED
SCIENCES**



**EVALUATING TAU-NEUTRINO ENERGY AND DIRECTION
FROM ITS SHOWER OBSERVABLES TO ESTIMATE THE
NUMBER OF EVENTS BY THE PROPOSED ARRAY**

DOCTOR OF PHILOSOPHY

ŞEYMA ATİK YILMAZ

BOLU, MARCH 2019

BOLU ABANT İZZET BAYSAL UNIVERSITY
THE GRADUATE SCHOOL OF NATURAL AND APPLIED
SCIENCES
DEPARTMENT OF PHYSICS



EVALUATING TAU-NEUTRINO ENERGY AND DIRECTION
FROM ITS SHOWER OBSERVABLES TO ESTIMATE THE
NUMBER OF EVENTS BY THE PROPOSED ARRAY

DOCTOR OF PHILOSOPHY

ŞEYMA ATİK YILMAZ

BOLU, MARCH 2019

APPROVAL OF THE THESIS

EVALUATING TAU - NEUTRINO ENERGY AND DIRECTION FROM ITS SHOWER OBSERVABLES TO ESTIMATE THE NUMBER OF EVENTS BY THE PROPOSED ARRAY submitted by **Şeyma ATİK YILMAZ** and defended before the below named jury in partial fulfillment of the requirements for the degree of **Doctor of Philosophy in Department of Physics, The Graduate School of Natural and Applied Sciences of Bolu Abant İzzet Baysal University** in 03/22/2019 by

Examining Committee Members

Signature

Supervisor
Prof.Dr. Haluk DENİZLİ
Bolu Abant İzzet Baysal University



.....

Member
Prof. Dr. Abdülkadir ŞENOL
Bolu Abant İzzet Baysal University



.....

Member
Prof. Dr. Harun KARSLI
Bolu Abant İzzet Baysal University



.....

Member
Prof. Dr. Cüneyt ÇELİKTAŞ
Ege University



.....

Member
Prof. Dr. İlkay TÜRK ÇAKIR
Giresun University



.....

Prof. Dr. Ömer ÖZYURT



.....

Director of Graduate School of Natural and Applied Sciences

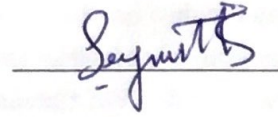


To each of my beloved family members . . .

DECLARATION

I hereby declare that all information in this document has been obtained and presented in accordance with academic rules and ethical conduct. I also declare that, as required by these rules and conduct, I have fully cited and referenced all material and results that are not original to this work.

Şeyma ATİK YILMAZ

A handwritten signature in black ink, reading "Şeyma Atik Yılmaz", is written over a horizontal line. The signature is cursive and includes a small flourish at the end.

ABSTRACT

EVALUATING TAU-NEUTRINO ENERGY AND DIRECTION FROM ITS SHOWER OBSERVABLES TO ESTIMATE THE NUMBER OF EVENTS BY THE PROPOSED ARRAY

PhD THESIS

ŞEYMA ATİK YILMAZ

**BOLU ABANT IZZET BAYSAL UNIVERSITY GRADUATE SCHOOL OF
NATURAL AND APPLIED SCIENCES**

DEPARTMENT OF PHYSICS

SUPERVISOR: PROF. DR. HALUK DENİZLİ

BOLU, 22/03/2019

The detection of Ultra High Energy Cosmic Rays (UHECRs) is an important study in the area of Astroparticle Physics. The air showers having a wide range of energies consist of electromagnetic, muonic and hadronic components which travel in different directions. Since neutrinos having no charge and very small mass interact weakly with matter, they carry the direction information unlike other possible primary cosmic rays (protons, ions, etc.). While the UHE neutrinos travels 1/13 of Earth diameter in Earth crust, they interact with the rock to produce the tau lepton which subsequently create a shower just before it emerges from the crust. The main idea of TAUWER (Tau-Neutrino Multitower Detector Experiment) array is to observe the large angle showers around horizon created by tau decays which produced with charge current interactions of tau neutrinos through the Earth Skimming method and mountain chain screen strategy. The observation of the air showers initiated in Earth crust or mountain chains is a novel idea, is also very effective method to remove interactions with the unwanted sources.

In this study the look-up table is produced for the tau neutrino induced showers including 5 different decay modes in 5 different energies with 4 different development lengths with THIN ON selection about 8000 and without THIN ON selection 900 showers simulated using CORSIKA (COsmic Ray SIMulations for KAscade) program. They are analyzed to correlate the distribution of electromagnetic, muonic and hadronic components with energy and particle density to reconstruct the shower energies. The location of the stations with the arrival time information of the particles are used to determine the direction of the induced showers.

The difference between the calculated and simulated zenith and azimuthal angles are below 0.5 degree for all simulated energies and development lengths. In addition, the expected number of the events for TAUWER array are estimated as 0.17, 0.25, and 0.43 events per year from latest neutrino flux upper limits using both Earth Skimming

method and mountain chain screen strategy. The results of these analysis will be advisory on the optimization of detector array, the placements of detectors, and the determination of the trigger for different characteristic of the showers as energy, the development length and the decay mode.

KEYWORDS: Ultra High Energy Cosmic Ray (UHECR), Tau Neutrino, CORSIKA Simulation, Surface Detector Array, TAUWER



ÖZET

GÖZLEMLENEN DUŞ ÜRÜNLERİNDEN TAU-NÖTRİNOSUNUN ENERJİ VE YÖNÜNÜN BULUNARAK ÖNERİLEN DİZİLİM ARACILIĞIYLA OLAY SAYILARININ BELİRLENMESİ

Doktora Tezi

ŞEYMA ATİK YILMAZ

BOLU ABANT İZZET BAYSAL ÜNİVERSİTESİ

FEN BİLİMLERİ ENSTİTÜSÜ

Fizik Anabilim Dalı

TEZ DANIŞMANI: PROF. DR. HALUK DENİZLİ

BOLU, 22/03/2019

Çok yüksek enerjili kozmik ışınların tespiti Astroparçacık fiziği alanında önemli bir çalışmadır. Çok çeşitli enerjilere sahip duşlar, farklı yönlerde hareket eden müonik, elektromanyetik ve hadronik bileşenlerden oluşur. Yüksüz ve çok küçük bir kütleyle sahip olan nötrinolar madde ile zayıf etkileşime girdiklerinden, diğer olası kozmik ışınların (protonlar, iyonlar, vs.) aksine yön bilgilerini taşırlar. Çok yüksek enerjili nötrinolar, yer kabuğu içerisinde Dünya çapının 1/13 kadarlık bir kısmında seyahat ettikleri sırada yer kabuğu ile etkileşerek meydana getirdikleri tau leptonu kabuktan çıktığı sırada bir duş oluşturur. TAUWER diziliminin ana fikri, Earth Skimming metodu ve sıra dağ stratejisi ile tau nötrinolarının yüklü akım etkileşimleriyle meydana getirdiği tau bozunumları tarafından oluşan yataya yakın geniş açılı duşların gözlemlenmesidir. Özgün bir çalışma olan yer kabuğu içerisinde veya sıra dağlardan geçerek oluşan duşların incelenmesi, aynı zamanda da istenmeyen kaynaklar ile oluşacak etkileşimleri ortadan kaldırmak için oldukça etkili bir yöntemdir.

Bu çalışmada CORSIKA programı kullanılarak, tau leptonunun 5 farklı bozunma kanalında, 5 farklı enerjide, 4 farklı duş gelişim mesafesi için THIN opsiyonu ile 8000 adet, THIN opsiyonsuz 900 adet simüle edilmiş duşu içeren bir benzetim kütüphanesi oluşturulmuştur. Duş enerjilerini yeniden yapılandırmak için bu duşların elektromanyetik, müonik ve hadronik bileşenlerinin dağılımları enerji ve parçacık yoğunluğu ile ilişkilendirilerek analiz edilmiştir. Ayrıca duşların geliş açılarını belirlemek için, istasyonların konum bilgileri ile duş parçacıklarının zaman bilgileri birlikte kullanılır.

Benzetimi yapılan duşlara ait zenit ve azimutal açıları ile hesaplanan değerler arasındaki fark 0.5 derecenin altında kalır. Bunlara ek olarak, TAUWER dizilimi için beklenen olay sayısı, hem Earth Skimming metodu hem de sıra dağ stratejisi

kullanılarak yılda 0.17, 0.25 ve 0.43 olay olarak en güncel üst limit nötrino akıları kullanılarak tahmin edilmektedir. Analiz sonuçları kurulacak dedektör diziliminin optimizasyonu, konumu, dağılımı ile ilgili ve enerji, duş gelişim mesafesi, bozunum modu gibi farklı duş karakterleri için tetiklemenin belirlenmesi gibi konularda ileriye yönelik kararların alınmasında yol gösterici bir nitelik taşımaktadır.

ANAHTAR KELİMELER: Çok Yüksek Enerjili Kozmik Işınlr, Tau Nötrino, Yüzey Dedektör Dağılımı, CORSIKA Simülasyonu, TAUWER



TABLE OF CONTENTS

ABSTRACT	v
ÖZET	vii
TABLE OF CONTENTS	ix
LIST OF FIGURES	xi
LIST OF TABLES	xv
LIST OF ABBREVIATIONS AND SYMBOLS	xvi
ACKNOWLEDGEMENTS	xviii
1. INTRODUCTION	1
2. AIM AND SCOPE OF THE STUDY	12
3. MATERIALS AND METHODS	13
3.1 Simulations of the Air Shower	14
3.1.1 TAUOLA Interface	15
3.1.2 Corsika Simulation Program	15
3.1.2.1 QGSJET Option	15
3.1.2.2 GHEISHA Option	16
3.1.2.3 Horizontal Flat Detector Array	16
3.1.2.4 SLANT Option	17
3.1.2.5 CURVED Atmosphere Option	17
3.1.2.6 INCLINED Observation Plane Option	17
3.1.2.7 UPWARD Option	17
3.1.2.8 STACKIN Option	18
3.1.2.9 ROOTOUT Option	18
3.1.2.10 PLOTSH Shower Plot Production Option	18
3.1.2.11 THIN Option	18
3.2 The Array Geometry	19
4. RESULTS AND DISCUSSIONS	20
4.1 Unthinning of CORSIKA THIN Data	21
4.2 Reconstruction of the Air Showers	31

4.2.1	The Energy Reconstruction	35
4.2.2	The Time Spread	36
4.2.3	The Thickness and the Spherical Shower Front	38
4.2.4	The Limits of the Array	40
4.2.5	Effective Area of the Array	42
4.2.6	Arrival Direction Estimation	42
4.3	Effect of ECUT in the Analysis	49
4.4	Estimation the Number of Expected Shower	53
4.4.1	Probability Calculations	54
4.4.2	Discussions	60
5.	CONCLUSIONS AND RECOMMENDATIONS	64
6.	REFERENCES	66
7.	APPENDICES	71
8.	CURRICULUM VITAE	80

LIST OF FIGURES

	<u>Page</u>
Figure 1.1. The distribution of the cosmic ray flux depending the primary energy (Boezio, 2014; Cronin et al., 1997).	2
Figure 1.2. The demonstration of an air shower (a) produced by a primary gamma ray consists of electron positron pairs and photons, (b) by a nucleus producing various secondary particles like pions, muons, neutrinos, photons, etc. (Bernlöhrr, 1999).	4
Figure 1.3. Schematic view of the development of electromagnetic, muonic and hadronic components of the extensive air shower (Haungs et al., 2015).	5
Figure 1.4. The demonstration of Earth Skimming method where the ν_τ travels through Earth crust and produced a τ shower.	8
Figure 3.1. Flow chart of the procedure followed during the analysis.	13
Figure 3.2. The coordinate system of CORSIKA	16
Figure 3.3. Schematic diagram of the array in (a) the ZX plane, (b)YZ'-plane, the projection of YZ plane on the inclined plane.	19
Figure 4.1. The line equations and their notations of the geometry which belongs to the inclined plane to create the particles in weighted numbers with the unthinning method.	22
Figure 4.2. The position of point P in $z - x$ plane.	25
Figure 4.3. The position of point P^* and P in $z - x$ plane.	26
Figure 4.4. The position of point F and P in $z - x$ plane.	28
Figure 4.5. The distribution of the particles on the circle with PF radius.	28
Figure 4.6. The position of point G in (a) $z - x$ and (b) $z - y$ planes.	29
Figure 4.7. The position of point G^* in (a) $z - x$ and (b) $z - y$ planes.	31
Figure 4.8. The unthinned particles superimposed to the particle thin.	32
Figure 4.9. The arrival directions for point G^* are superimposed to the arrival directions of point P as (a) θ and (b) ϕ distribution	32
Figure 4.10. The variation of particle percentages on the $\pi^- \pi^0$ decay channel with various development lengths.	33
Figure 4.11. The variation of particle percentages on the $\pi^- \pi^+ \pi^-$ decay channel respect to various development lengths.	34

Figure 4.12.	The lifetime of the $\pi^- \pi^0$ and $\pi^- \pi^+ \pi^-$ decay channels respect to various development length in terms of shower energies.	34
Figure 4.13.	The number of e^\pm in the stations versus the radius of the showers grouped in different energies.	35
Figure 4.14.	Particle density in a back or front tile of the station on π^- shower that decay 5 km far from the array plane. The array is composed by 40 horizontal rows and 16 vertical rows with 30 m apart.	36
Figure 4.15.	The time distribution of the stations on π^- shower that decay 5 km far from the array plane. The array is composed by 40 horizontal rows and 16 vertical rows with 30 m apart.	37
Figure 4.16.	The distribution of the number of particles along the radius of the shower and the time difference between the first and last particle on each station as a color code are shown for π^- shower.	37
Figure 4.17.	The mean arrival time for e^\pm in π^- decay channel for 5 km development length as a function of radial distance from core.	38
Figure 4.18.	The spherical shower front for 5 km development length in π^- decay channel.	39
Figure 4.19.	The shower front thickness for π^- channel in 5 km development length.	40
Figure 4.20.	The acceptance of the array for $5 \times 10^8 \text{ GeV}$ in terms of zenith angle.	41
Figure 4.21.	The acceptance of the array for $5 \times 10^8 \text{ GeV}$ in terms of azimuthal angle.	42
Figure 4.22.	The effective area of TAUWER array for all decay channels and development lengths.	43
Figure 4.23.	The zenith angles θ for 27 different showers are evaluated from at least 2 triggered stations.	48
Figure 4.24.	The azimuthal angles ϕ for 27 different showers are evaluated from at least 2 triggered stations.	48
Figure 4.25.	For low energy scale the number of particles for (a) all, (b) μ^\pm and (c) the shower diameters in y-z directions for 0.1 GeV ECUT, (d) total number of particles, (e) μ^\pm number of particles and (f) the shower diameters in y-z directions for 0.05 GeV ECUT.	50

Figure 4.26.	For high energy scale the number of particles for (a) all, (b) μ^\pm and (c) the shower diameters in y-z directions for 0.1 GeV ECUT, (d) total number of particles, (e) μ^\pm number of particles and (f) the shower diameters in y-z directions for 0.05 GeV ECUT.	51
Figure 4.27.	The simulated arrival directions; $\theta_{calculated}$ for hadrons ECUT (a) 0.1 GeV, (c) 0.05 GeV in low energy scale, (e) 0.1 GeV, (g) 0.05 GeV in high energy scale, $\phi_{calculated}$ for hadrons ECUT (b) 0.1 GeV, (d) 0.05 GeV in low energy scale, (f) 0.1 GeV and (h) 0.05 GeV in high energy scale. . .	52
Figure 4.28.	The interaction length of neutrino in rock with respect to neutrino initial energy.	55
Figure 4.29.	The neutrino interaction probability with respect to traveling distance in rock for different neutrino initial energies.	56
Figure 4.30.	The geometrical view of the neutrino skimming from the Earth and using of a nearby mountain as a target while the τ induced shower emerging from the rock to the detector array (not in scale). L-x is the interaction distance for the ν_τ , the interaction point shown as " * " symbol, x is the traveling distance for the τ , and R_\oplus is the Earth radius.	57
Figure 4.31.	The neutrino survival probability with respect to traveling distance in rock for different initial energies.	59
Figure 4.32.	The escape probability of τ with respect to traveling distance for different initial energies.	60
Figure 4.33.	The escape probability of τ with respect to traveling distance for different escape directions from shell.	60
Figure 4.34.	The efficiency of TAUWER array for all decay channels and energies.	61
Figure 7.1.	The zenith angles θ for 27 different showers are evaluated from at least 1 triggered stations.	77
Figure 7.2.	The azimuthal angles ϕ for 27 different showers are evaluated from at least 1 triggered stations.	77
Figure 7.3.	The zenith angles θ for 27 different showers are evaluated from at least 3 triggered stations.	77
Figure 7.4.	The azimuthal angles ϕ for 27 different showers are evaluated from at least 3 triggered stations.	78
Figure 7.5.	The zenith angles θ for 27 different showers are evaluated from at least 4 triggered stations.	78

Figure 7.6.	The azimuthal angles ϕ for 27 different showers are evaluated from at least 4 triggered stations.	78
Figure 7.7.	The zenith angles θ for 27 different showers are evaluated from at least 5 triggered stations.	79
Figure 7.8.	The azimuthal angles ϕ for 27 different showers are evaluated from at least 5 triggered stations.	79



LIST OF TABLES

	<u>Page</u>
Table 4.1. Time it takes to simulate a single shower for different energy and development lengths without THIN option.	20
Table 4.2. The escape probability with respect to θ and ν_τ energy	62
Table 4.3. The number of events for TAUWER array corresponding to the different upper limit flux in $km^{-2}sr^{-1}$ per year.	62
Table 7.1. The number of particles which simulated with THIN off selection for 5 different decay modes in 5 different energies with 4 different development lengths	73
Table 7.2. The number of particles which simulated with THIN on selection for 5 different decay modes in 5 different energies with 4 different development lengths	75

LIST OF ABBREVIATIONS AND SYMBOLS

AGNs	: Active Galactic Nuclei
AGASA	: Akeno Giant Air Shower Array
μ^+	: Antimuon
ϕ	: Azimuthal Angle
CC	: Charged-Current
π^\pm	: Charged Pion
CORSIKA	: Cosmic Ray Simulations for Cascade
EAS	: Extensive Air Shower
EGCRs	: Extra Galactic Cosmic Rays
EM	: Electromagnetic
e^-	: Electron
eV	: Electronvolt
GCRs	: Galactic Cosmic Rays
γ	: Gamma
GRBs	: Gamma Ray Bursts
GeV	: Giga Electronvolt
GZK	: Greisen-Zatsepin-Kuzmin
HiRes	: High Resolution Fly's Eye Experiment
MeV	: Mega Electronvolt
μ^-	: Muon
π^0	: Neutral Pion
PeV	: Peta Electronvolt
PMTs	: Photomultiplier Tubes
e^+	: Positron
SCRs	: Solar Cosmic Rays

<i>sr</i>	: Steradian
SUGAR	: Sydney University Giant Air-shower Recorder
TAUWER	: Tau-Neutrino Multitower Detector Experiment
τ	: Tau Lepton
ν_τ	: Tau Neutrino
TeV	: Tera Electronvolt
UHECRs	: Ultra High Energy Cosmic Rays
θ	: Zenith Angle



ACKNOWLEDGEMENTS

First and foremost, all praise belongs to Almighty Allah for giving me the strength, knowledge, ability and opportunity to complete my PhD studies successfully.

I am heartily thankful to my supervisor, Prof. Dr. Haluk Denizli, who has guided me with his knowledge and giving me countless advice. He always promotes me to develop my PhD studies from the initial to the final level. I am also grateful to him being very patient and kind for me as well as for providing status in a wonderful project.

Besides my supervisor, I also wish to thank to the mentor of TAUWER project, Prof. Dr. Maurizio Iori for giving me precious knowledge about Astroparticle Physics. I am thankful to his leadership when we concluded the studies.

I would like to thank to my thesis advisory committee who Prof. Dr. Abdülkadir Şenol and Prof. Dr. Harun Karşlı for their instructive comments and supportiveness about the studies.

I would like to especially thank my dear husband Dr. Ali Yılmaz for always being by my side when I lost my energy and motivation to work. He always encourages me to study hard and provides valuable help in coding, physics, and academic writing.

Finally but the biggest thanks to each of my beloved family members who supported and encouraged me a lot during my studies, their prayers and good wishes always accompanied me.

I would like to thank to Scientific and Technological Research Council of Turkey (TUBITAK) for financial supporting of this work with a project under the grant number: 114F138.

1. INTRODUCTION

The Earth is exposed by many types of natural radiation which may originate from the natural radioactive materials on the Earth's crust, such as, the radioactive uranium, thorium or potassium in the soil. It may also come from extraterrestrial sources. For example, the protons, heavy nuclei are the charged particles that have most energetic radiations coming from the cosmic background. The electrons, helium, carbon, oxygen, iron, and other nuclei are the primaries compounded from the stars (Patrignani et al., 2017). In earlier, it was expected that the radiation always originates from the natural radioactive materials on the Earth's crust and it was also not known that natural radiation could originate from the cosmic background until the early the 1900s. However, the cosmic rays were discovered with a series of balloon flights in 1912 by Victor Franz Hess (1912) while measuring the variation of ionization in air with rising altitude. Therefore, a decrease was also expected on the radiation level as it traveled towards the top of the atmosphere, although an increase in the radiation level was observed by Hess with these balloon flights. Hess measured once again the radiation during a total solar eclipse to provide the preventing of the Sun's effect, as a possible source. He still measured rising radiation at rising altitudes and concluded that the radiation of very high penetrating power enters from above into the atmosphere. Hess discovered a natural source of the high energy particles and afterwards they are named *cosmic rays* by Millikan.

In Astroparticle Physics, understanding the possible origin of the cosmic rays and regarding them as messenger particles from terrestrial sources are attractive subjects, since there is no clear sign in where they are produced or the source of the production. Especially, when their energies extend to 10^{21} eV, the detection of the cosmic rays becomes more interesting. When the energy per nucleon lower than 10^9 eV, they are dominantly solar cosmic rays. After that energy, the origin of the cosmic rays may suppose as our Galaxy up to the energies of 10^{17-18} eV and the upper energies may be coming from extragalactic sources.

The Figure 1.1 shows the cosmic ray flux as a function of energy (Boezio, 2014; Cronin et al., 1997). The spectrum can be represented by a power law until the knee which is around 10^{15} eV. Around the knee region, the number of particle observed in a year is one or less in 1 m^2 area due to the low flux of the cosmic rays at these energies

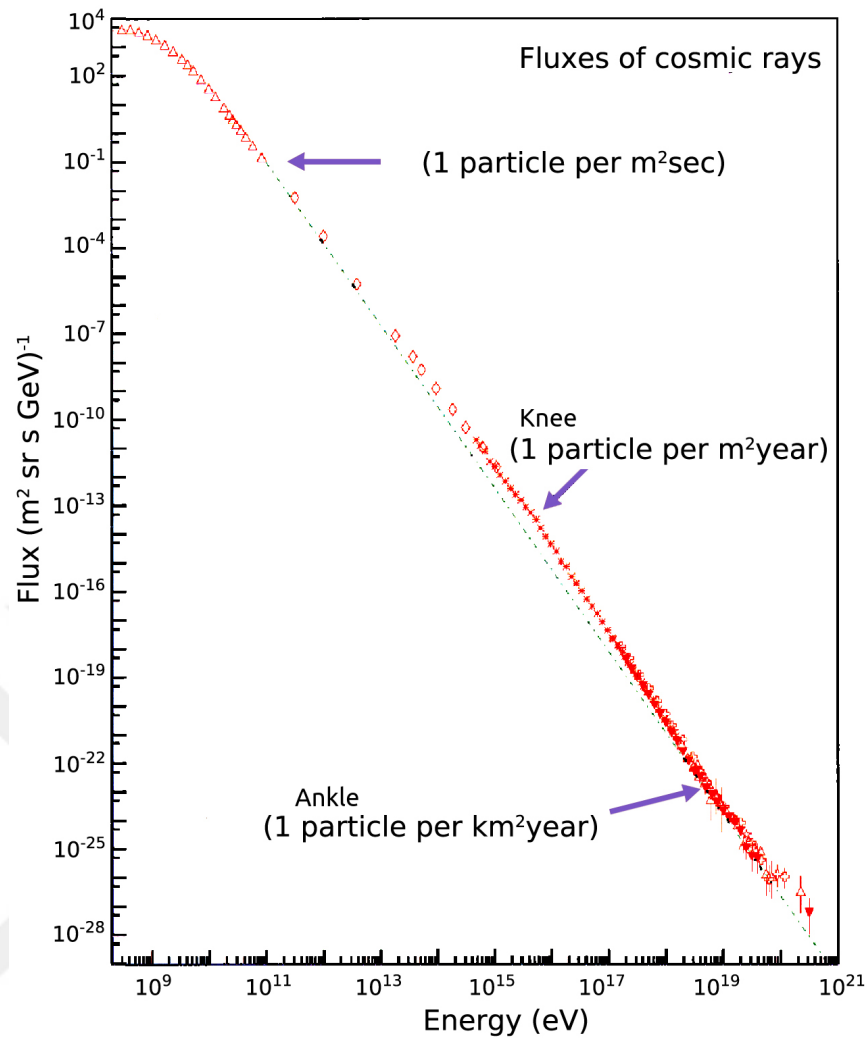


Figure 1.1. The distribution of the cosmic ray flux depending the primary energy (Boezio, 2014; Cronin et al., 1997).

and observations became difficult by the balloons or satellites out of the atmosphere. The ground based arrays have advantages since they can be used in the atmosphere as a detection medium.

The spectrum becomes smooth around 10^{18} eV and it is interpreted as the ankle where the second soft bend begins. The observations about this region is not enough yet, but the Greisen-Zatsepin-Kuzmin (GZK) cutoff forms around $3-5 \cdot 10^{19}$ eV except protons (Greisen, 1966; Zatsepin and Kuzmin, 1966) that defines an upper limit for the energy of cosmic rays from distant origins. This rigid cutoff is originated from the interactions between the protons and the cosmic microwave background on spreading from their origins to Earth. The GZK cutoff was observed by the High Resolution Fly's Eye (HiRes) experiment Sokolsky (2009) and Pierre Auger Observatory (Abraham

et al., 2007).

The cosmic ray sources can be classified in terms of their energies. When the energy is $10^9 eV$ or lower, they can be categorized as solar cosmic rays. On the other hand galactic cosmic rays originated from our galaxy within the energy range of $10^9 - 10^{15} eV$. Above these energies they could be from extragalactic sources. The detailed information is listed as in below for the possible sources.

Solar Cosmic Rays

Solar Cosmic Rays (SCRs) were discovered with the three times increasing in ionization during magnetic storms in 10 years of record period (Forbush, 1946). They are formed by charged particles such as protons, ions and electrons. The energy of the particles, coming from Sun is about MeV range while they are passing through the atmosphere. The solar flares may reach to our atmosphere but their energies can not exactly determined around the GeV scale (Bazilevskaya, 2005).

Galactic Cosmic Rays

The cosmic rays generally refer to the Galactic Cosmic Rays (GCRs) which are formed by shock waves in the supernova explosions inside our Milky Way galaxy (Blasi, 2013). The particles are around GeV range of energy however sometimes they can be reach to PeV energies in the Earth. The GCRs are atomic nuclei like hydrogen and uranium which are interacted with magnetic fields because of being completely ionized. These particles can travel near the speed of light and they have very likely been accelerated around the last few million years.

Extragalactic Cosmic Rays

The Ultra High Energy Cosmic Rays (UHECRs) are called Extragalactic Cosmic Rays (EGCRs) whose energies are up to $10^{21} eV$. There is no certain evidence about their sources due to very low flux but the direction of the cosmic rays indicate that they are originated from out of the Milky Way Galaxy (Aab et al., 2017). The origin of the extragalactic CRs may be caused from the particles, formed in the core of Active Galactic Nuclei (AGN), which means that they may produce neutrinos through the interactions of the accelerated protons and ions with an acceleration disk target

surrounding a central black hole. The UHECRs may also be produced from Gamma Ray Bursts (GRBs) or past galactic GRBs.

The UHECRs from the extragalactic sources pass through the Earth and they create air showers. A high energy cosmic ray loses its energy as a result of the collisions with the air molecules in the atmosphere and disintegrates their energy to produce secondary particles. These secondary particles or cascade are continue to their travel in the atmosphere and create more secondary. When they collide with the air molecules, their energies decreases. The number of secondary particles increases and many low energetic particles are absorbed by the atmosphere. This decreases the total number of secondary particles produced by a primary particle. The action of exchanging the primary energy of a cosmic ray into many lower energy secondary particles is called as Extensive Air Shower (EAS). When the average energy per particle decreases below the 80 MeV , the interactions cause to the absorption of particles and to end of the cascade. That elevation where the cascade begin to die is known as shower maximum (Cheng, 2009). Only the extremely high energy events may reach to the shower maximum at the sea level.

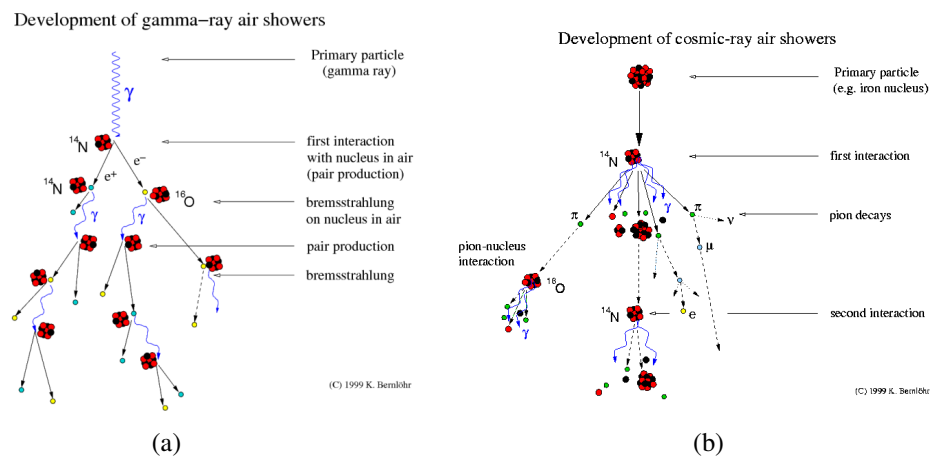


Figure 1.2. The demonstration of an air shower (a) produced by a primary gamma ray consists of electron positron pairs and photons, (b) by a nucleus producing various secondary particles like pions, muons, neutrinos, photons, etc. (Bernlöhr, 1999).

The shower cascade includes different types of particles depending on the primary particle. When a photon is the primary particle, the shower contains electrons, positrons, and gamma rays. The cascade also includes muons, neutrinos, and hadrons while

a nucleus is the primary particle. In Figure 1.2 Bernlöhr (1999), both the gamma and nucleus initiated showers are illustrated as a sample of schematic view of the air shower development.

The EASs are formed from three main components which are electromagnetic, muonic, and hadronic. For example, the components of a proton initiated EAS are nearly 80% γ rays, 15% e^\pm , 2% μ^\pm and 0.2% hadrons.

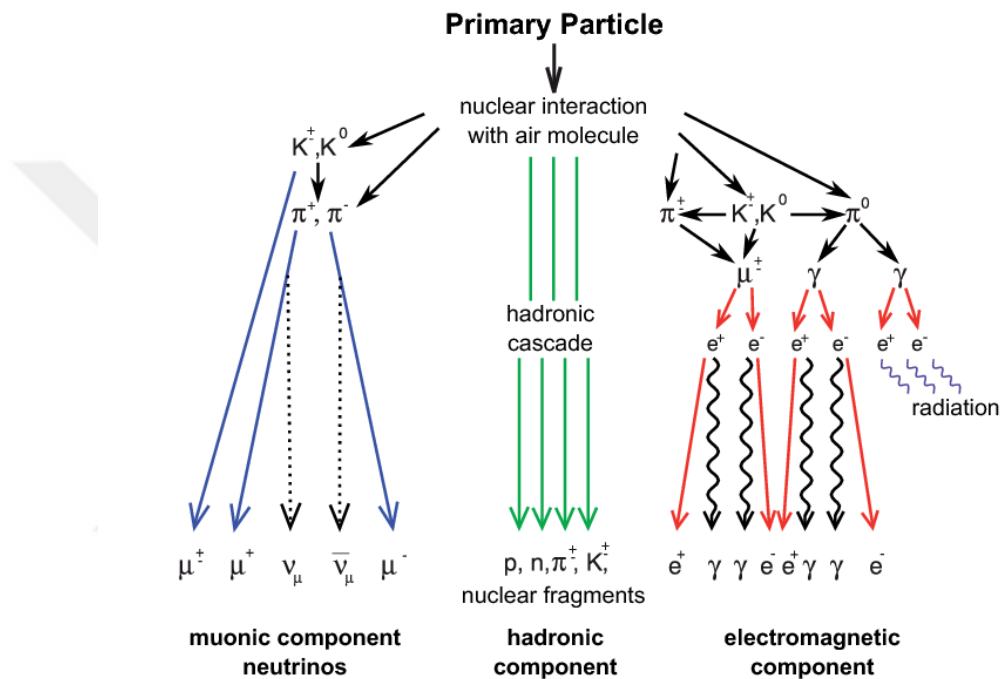


Figure 1.3. Schematic view of the development of electromagnetic, muonic and hadronic components of the extensive air shower (Haungs et al., 2015).

Hadronic Cascade

A hadronic shower is created by the interaction of a proton or nuclei with the atmosphere and the secondary particles are mostly mesons, charged and neutral pions in this hadronic interaction shown in the center of Figure 1.3 (Haungs et al., 2015). When a proton as the primary particle, it gives large amount of its initial energy to the secondary mesons. In the cascade, the number of charged pions is twice than the neutral pions. If these secondary particles are sufficiently energetic, they may be trigger more cascades which they are generally consisted of pions. Below the interaction threshold, hadrons are continue to this process. The neutral pions decay

into two photons and they cover nearly one third of the primary hadron energy.

$$\pi^0 \rightarrow 2\gamma. \quad (1.1)$$

Muonic Cascade

The mesons produced in hadronic cascade, mostly pions, decay via weak interaction into muons and neutrinos according to Equations 1.2 - 1.3 and they occur the muonic cascade shown in the left of Figure 1.3.

$$\pi^+ \rightarrow \mu^+ + \nu_\mu, \quad (1.2)$$

$$\pi^- \rightarrow \mu^- + \bar{\nu}_\mu. \quad (1.3)$$

The charged pions dependently their energies can decay or interact with the air. When charged pions have high energy, they almost interact. Low energy pions decay into muons and muon neutrinos. Muons are also unstable and decay into electrons and positrons.

$$\mu^+ \rightarrow e^+ + \nu_e + \bar{\nu}_\mu, \quad (1.4)$$

$$\mu^- \rightarrow e^- + \bar{\nu}_e + \nu_\mu. \quad (1.5)$$

The interaction of high energetic charged pions create more charged and neutral pions belong to the second generation of shower. The continuum proceeds until the energy of the charged pions are reach to the energy where the decay process is dominant.

Electromagnetic (EM) Cascade

The initial energy of the γ ray is transformed to the secondary particles which they are known as the EM cascade illustrated in the right side of Figure 1.3. This cascade is a combination of pair production and bremsstrahlung which they are shown in Equations 1.6 and 1.7. The EM cascade development is described by the Heitler model that the energy divides in half and the number of particles doubles after each

interaction in the cascade.

$$\gamma (in EM field) \rightarrow e^+ + e^-, \quad (1.6)$$

$$e^\pm (in EM field) \rightarrow e^\pm + \gamma. \quad (1.7)$$

An electron-positron; $e^- - e^+$ pair can be created via the interaction of a gamma ray with the Coulomb field of the atmospheric nuclei and it is called pair production. An electron travels or accesses into a material or a nuclei at high speed, it is interacted by the opposite force of the electrons in the atom, then it will slow down or stop. When it is slowed down, escape from the material with less energy. This energy must be converted to other forms or absorbed by the nuclei. If the e^- is decelerated, an x-ray is radiated by this energy. This phenomenon is called Bremsstrahlung and the x-ray on this process is Bremsstrahlung x-ray.

The charged particles in both EM and hadronic cascade are travel in a dielectric medium (the atmosphere) with a speed greater than the phase velocity of light in that medium and they spread out Cherenkov light behind them in the shape of a cone (Jelley, 1955). This light can be seen as in blue color around a nuclear reactor which is surrounding with the water. This provide to measure the intensity of the reaction in the reactor or the radioactivity of the used nuclear fuel rods. Cherenkov radiation is also used as a particle detector in astrophysical research. The particles, which created by the interaction of the high energy cosmic rays with the atmosphere, can be detected by the Cherenkov effect in the observatories. For example, in the HAWC (High Altitude Water Cherenkov Experiment) experiment, 300 pools each with 200 000 liters of purified water and four Photomultiplier Tubes (PMTs), are used for the measurement of high energy particles from space (Abeysekara et al., 2013).

Earth Skimming

The detection of UHECRs is significant especially ν_s in terms of collecting the information about the source of the cosmic rays or the effect of the neutrino oscillations on the neutrino flavor mixing rate. Since the neutrinos traveled through the large distance without interacting, they have almost equal neutrino flavor mixing rate on the Earth as a result of oscillations. One can test for the existence of neutrino oscillations

by looking for up-going showers from Earth Skimming tau neutrinos (Fargion, 2002).

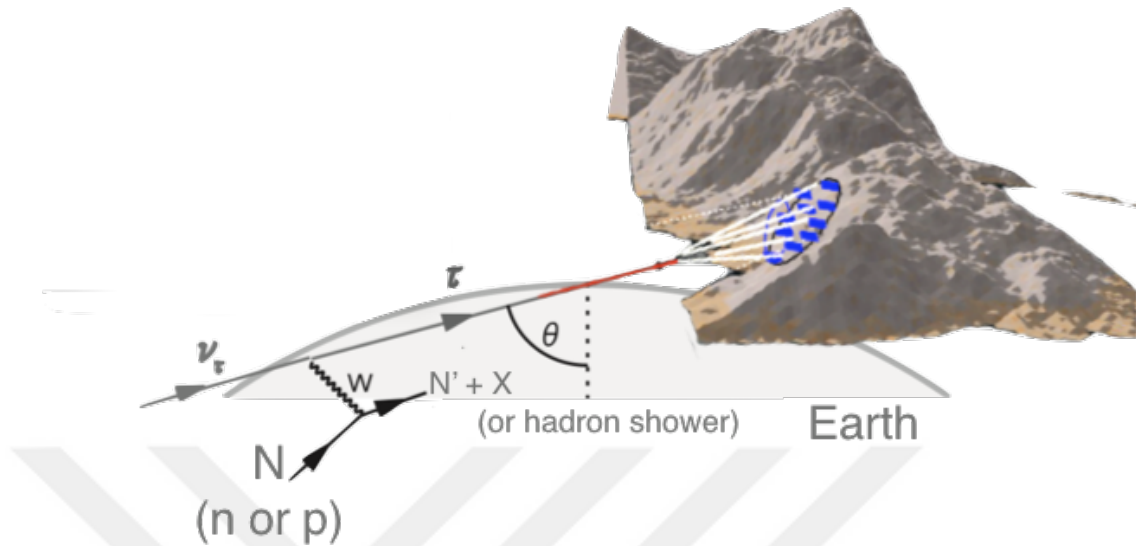


Figure 1.4. The demonstration of Earth Skimming method where the ν_τ travels through Earth crust and produced a τ shower.

The Figure 1.4 shows that, the tau neutrino ν_τ is interacted with the chord of the Earth or a mountain. When it penetrate to the crust, it may collide with the nuclei in the material. This collision causes an interaction between the ν_τ and a nucleus. It creates a tau lepton τ by the charged-current (CC) interaction. When the tau lepton may emerge from the rock before its decay, τ may produce a shower in the atmosphere. This process is named as the Earth Skimming method.

The importance of the Earth or a material in this process is to provide an intensive environment as a target which will increase the interaction rate. The rocks are quite convenient for providing this dense environment.

The detection techniques

Designing the many different detectors for the detection of Ultra High Energy Cosmic Rays is due to the effort to detect the cosmic rays in the best way. The area of the detector array is very important to detect precisely the very high energetic particles. The experiments on UHECRs are made to learn many of the uncertain information, and researches are still ongoing about them.

The first array is constructed by John Linsley, Livio Scarsi and Bruno Rossi in New Mexico in the early of 1960s as Volcano Ranch detector array with 8 km^2 area.

The detectors on this array are consisted of scintillators and the experiment published the detection of the cosmic rays with the energy of $10^{20} eV$ and higher values (Linsley et al., 1961).

SUGAR (Sydney University Giant Air-shower Recorder) (1968-1979) is the first detector set up in the southern hemisphere and consists of 47 stations established on an area of $70 km^2$. At these stations, scintillators with an effect area of $6 m^2$ are below the ground as $1.5 m$ inside liquid filled tanks. With this array, a cosmic ray with an energy of $10^{18} eV$ was detected in a direction close to the center of the galaxy (Bellido et al., 2001). The data obtained from this experiment is also a unique result for later studies and it has been tested by AGASA and Pierre Auger experiments.

AGASA (The Akeno Giant Air Shower Array) is the world's largest surface detector distribution consisting of 111 scintillator detectors with a surface area of $2.2 m^2$, totally covering an area of $100 km^2$. With this experiment the world's second biggest cosmic ray recorded with an energy $2 \times 10^{20} eV$ (Hayashida et al., 1994).

The Haverah Park experiment was constructed in United Kingdom with water Cherenkov tanks in totally $12 km^2$ area. Each water tank have a PMT on the top surface. The experiment was collected data for 20 years, and was switched off in 1987. The estimation of the primary energy with the density of particles in the shower core is developed as a new technique (Lawrence et al., 1991).

The Fly's Eye experiment is consist of 2 fluorescence telescopes separated by $3.4 km$ from each other. These telescopes made by mirrors with a $1.6 m$ diameter and in center of the mirrors there are 12 or 14 PMTs. The total of 880 PMTs scan the all sky with their $\sim 5^\circ$ field of view. The Fly's Eye experiment published the result of their claim about an event with energy of $3 \times 10^{20} eV$ which originate in the contemporary era of the Universe (Bird et al., 1993). The Fly's Eye experiment was operated the High Resolution Fly's Eye cosmic ray observatory (HiRes) as an extension of the original experiment. It is an upgraded version of the experiment with larger mirrors, smaller PMTs, and more sophisticated electronics (Bird et al., 1994).

The IceCube experiment located in South Pole is a neutrino observatory with a cubic-kilometer particle detector made of the Antarctic ice. The experiment consist of a surface array named IceTop and a more dense part is inside the ice named DeepCore detectors. The DeepCore detectors are under the surface inside 86 boreholes with

mounted vertical strings. 5160 digital optical modules (DOMs), have PMTs and other electronics, are arranged from 1450 m to 2450 m depth on the strings and each strings are hold 60 DOMs (Achterberg et al., 2006). Also the surface detector array, IceTop have 81 stations which are located on top of the strings (Abbasi et al., 2013). A high energy neutrino with an energy of $\sim 290 \text{ TeV}$ was observed in 2017 by IceCube Neutrino Observatory (IceCube Collaboration et al., 2018).

The Pierre Auger observatory have two types of array as the surface detector stations and the collection of air fluorescence telescopes. In this hybrid detector system, two methods are applied independently. The first method is the water-Cherenkov detectors for the surface detector array which detect the interaction of the high energy particles with water. The second method is the observation of the ultraviolet light emitted high in the Earth's atmosphere with the fluorescence telescopes (Abraham et al., 2004). The Pierre Auger observatory published an observation of the inclined events with energies exceeding $4 \times 10^{18} \text{ eV}$ between January 2004 and December 2013 (The Pierre Auger Collaboration, 2015).

Another surface detector array is KASCADE (KARlsruhe Shower Core and Array DETector) experiment which launched in 1996 in Karlsruhe, Germany. The stations are located on an area of $200 \times 200 \text{ m}^2$ with 252 stations separated by 13 m. KASCADE aims to observe particles which comes from the air showers with the energy of 1 PeV and above (Antoni et al., 2003). The CORSIKA program was created to simulate the development of these particle showers for the KASCADE experiment.

The surface detector arrays have been generally designed and installed to detect the downward showers. However, cosmic rays also travel to the upward through the Earth.

TAUWER (The TAU-neutrino multitoWER Detector Experiment) is planned as an experiment which collaboration of Carnegie Mellon University from USA, 'La Sapienza' University of Rome from Italy and Bolu Abant Izzet Baysal University from Turkey. In TAUWER experiment, it is planned to observe the horizontal and upward air showers through the interaction of tau neutrinos with the Earth's crust on the detector array constructed at a mountain surface. The stations consisting of scintillator detectors positioned facing down from the mountain surface planned to detect UHE ($\sim 0.1 - 100 \text{ EeV}$) ν_τ induced showers formed while passing through 1/13 part of the

Earth's crust and exit to the atmosphere based on the Earth Skimming strategy (Fargion et al., 1999; Zas, 2005).



2. AIM AND SCOPE OF THE STUDY

The main purpose of this thesis is to propose and optimize an array to detect UHE neutrinos. To reach this goal the tau neutrino induced showers are simulated using CORSIKA simulation program to build a look-up table with the 5 different decay modes of ν_τ and each modes have 5 different energy scales in 4 development lengths.

The detection of large angle ν_τ induced showers around horizon is obtained by applying the Earth Skimming method and mountain chain screen strategy with an inclined detector array which has 0.5 km^2 area on the mountain surface. The particle distribution on different decay modes, the shower core, the estimation of the energy from the particle distributions and the arrival directions for each simulated shower are evaluated and used to estimate the number of events in a year with the array proposed in this thesis.

3. MATERIALS AND METHODS

Tau neutrino (ν_τ) induced showers are simulated to study their properties extensively on the mountain slope. To obtain ν_τ induced showers from ν_τ decay to tau lepton (τ) in the energy range 10^{16} eV - 10^{19} eV, the generations are accomplished with selected tools. First one of these tools is the TAUOLA interface Was and Jadach (1992) which used to decay τ to its different decay channels. The secondary particle of ν_τ induced showers are simulated with CORSIKA simulation program using the output of TAUOLA. The Figure 3.1 shows the production of the simulated showers in a flow diagram.

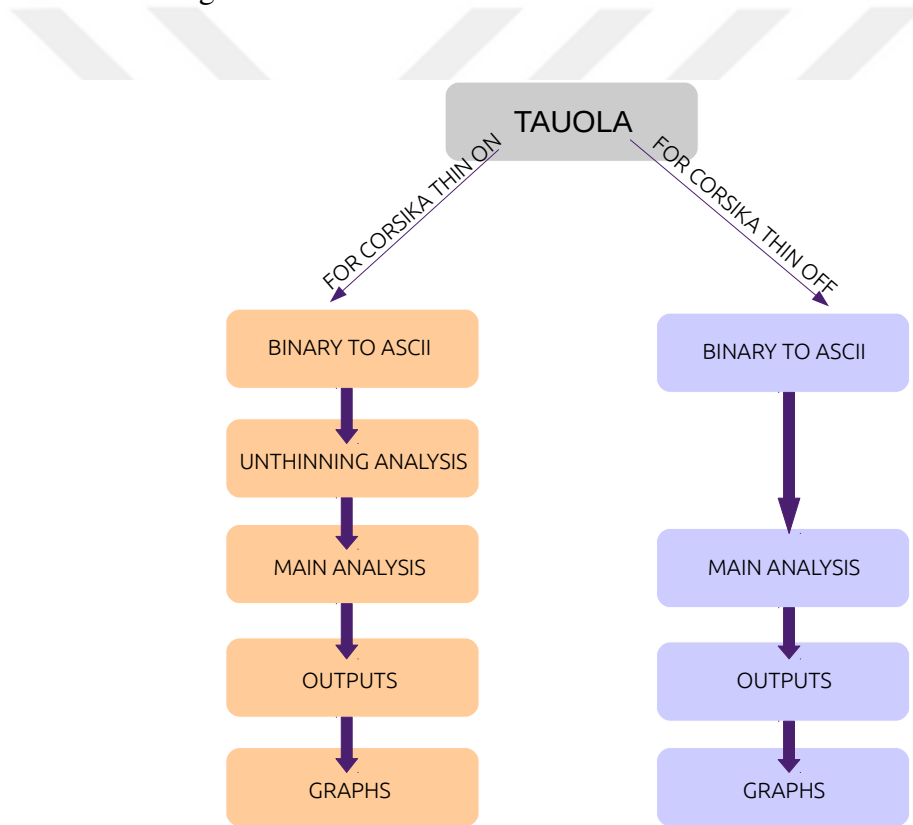


Figure 3.1. Flow chart of the procedure followed during the analysis.

The simulations are generated the following decay modes of τ (π^- , $\pi^- \pi^0$, $\pi^- \pi^+ \pi^-$, $\pi^- \pi^0 \pi^0$, $\pi^- \pi^+ \pi^- \pi^0$) that involves 64 % of the tau branching ratio. The expected ν_τ induced showers are studied to optimize and identify the performance of the TAUWER array.

CORSIKA (COsmic Ray SIMulations for KAScade), is a simulation program based on the Monte Carlo technique, developed for the KASCADE experiment. This program has been developed to study the properties and production of atmospheric showers, taking into account the decays and interactions of the nuclei in the atmosphere, hadrons, muons, electrons and photons. It can create the secondary particles with different types, energies, locations, directions and arrival times in an air shower and they can pass from a selected observation level. The required options for the array's geometry on the CORSIKA are compiled for the production of τ induced showers. In this study, the Quark Gluon String model with JETs (*QGSJET*) model is used for hadronic interactions in high energies and the Gamma Hadron Electron Interaction Shower code (*GHEISHA*) is selected for low energy interactions. Other selected options are; *Horizontal flat detector array*, *SLANT*, *CURVED*, *INCLINED*, *UPWARD*, *STACKIN*, *ROOTOUT*, *PLOTSH Shower Plot Production* and *THIN* (when THIN option is used).

The required input cards to run the CORSIKA Heck et al. (1998) (modified version of 6.99) program are compiled with the selected options which created separately to each decay channel, energy and shower development length, and the planned inclined plane of the observation. Thus, it is possible to produce showers in the desired energy, shower development length and decay channel. To simulate the τ induced showers, a Dell R815 Server (2U) 4 AMD Opteron 6380, 2.5 GHz, 32 Kernel, 128 GB memory, 1600 MHz featured calculation system are used and 60 of the 64 virtualized kernels are continuously used throughout the entire run. The duration of the simulations depends on THIN (ON / OFF), energy, shower development length and decay channel. For example, when the THIN option is not activated, the $\pi^- \pi^0$ decay channel shower changes from 10 hours ($10^{16}eV$) to about 600 hours ($10^{18}eV$) while in the $\pi^- \pi^- \pi^+$ decay channel showers can be generated between 20 and 1800 hours.

3.1 Simulations of the Air Shower

The all programs, codes, interfaces or options used in the simulation of the data for this thesis are briefly explained in this section.

3.1.1 TAUOLA Interface

TAUOLA Interface is a library based on the Monte Carlo algorithms. The interface can perform τ lepton decays and the output like τ generation can be attached to any Monte Carlo program. To generate τ decays, the TAUOLA interface is used FORTRAN language with the defining its spin state and the frame which the decay became. The detection of tau neutrino is made by observation the τ induced shower which is produced in the charge current (CC) tau-neutrino interaction. In this study, the ν_τ to τ decay has been simulated using the TAUOLA program (Was and Jadach, 1992).

3.1.2 Corsika Simulation Program

CORSIKA (COsmic Ray Simulation KAScade) is a simulation program based on the Monte Carlo technique developed for the KASCADE experiment in Karlsruhe, Germany. This program has been developed to study the properties and production of atmospheric showers, taking into account the decays and interactions of the nuclei in the atmosphere, hadrons, muons, electrons and photons. The options are compiled which required for the production of the τ induced showers with CORSIKA. In this study, the QGSJET 6 model was used for hadronic interactions in high energies and the GHEISHA routine for low energy interactions.

The CORSIKA program writes the 'binary' information of the type, momentum, position, weight and time of all particles on the observation plane specified on the entry card, after simulating the shower development length. This data is analyzed in more detail using the developed codes.

3.1.2.1 QGSJET Option

Quark Gluon String model with JETs (QGSJET) is purposed to study the high energy hadronic interactions of the elastic scattering by hadron - nucleon collisions. The newest version is *QGSJET-II-04* and is improved compared to original QGSJET. It can be given reliably results for hadronic cross section measurements (Ostapchenko, 2006). The related model of the QGSJET can be selected when the simulation is constructed.

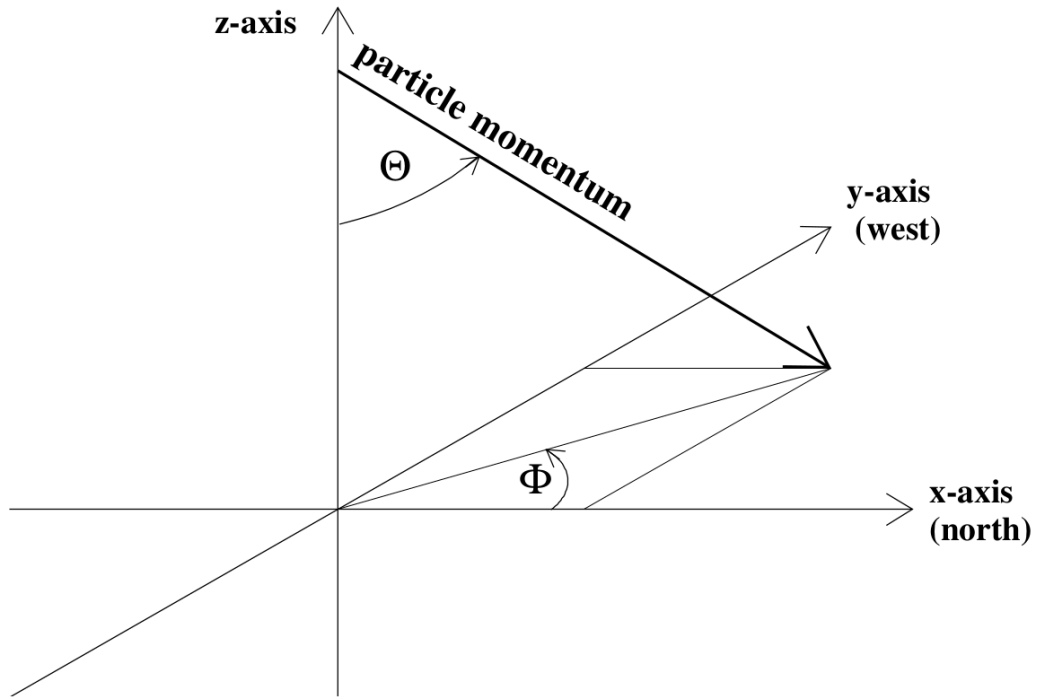


Figure 3.2. The coordinate system of CORSIKA

3.1.2.2 GHEISHA Option

Gamma Hadron Electron Interaction Shower code (GHEISHA) is used for the low energetic hadronic interactions as hadronic collisions up to 100 GeV . This package is generally used in the GEANT simulation program. GHEISHA can be handled the reaction kinematics properly. GHEISHA and FLUKA also operate the different momentum distributions for mesons in terms of secondary particle distribution, energy deposition and atmospheric ionization (Mishev and Velinov, 2013).

3.1.2.3 Horizontal Flat Detector Array

The horizontal flat detector array is selected as detector geometry while installing the CORSIKA simulation program. The detector array is constructed in a mountain surface and this surface is a flat place. Also the type of the detectors is not a non-flat; volume detector or vertical string detector. The flat detectors are used in well known experiments such as KASCADE or Pierre Auger Observatory.

3.1.2.4 SLANT Option

The SLANT option is used for the very inclined showers to acquire the ionization energy loss, the deflection within the Earth's magnetic field and the generation of Cherenkov photons. They can be obtain while the charged hadronic primaries on their path between entering the atmosphere and the first interaction point (Heck and Pierog, 2013).

3.1.2.5 CURVED Atmosphere Option

The CURVED option is an atmospheric feature which suitable for the showers with large zenith angles above $\approx 70^\circ$. Within small zenith angles the Earth's atmosphere is supposed as completely flat in spite of that the atmosphere is getting curved with the zenith angle increase. The CURVED option provides the ionization energy loss, deflection with the Earth's magnetic field and the generation of Cherenkov photons for charged hadronic primaries on their path between entering the atmosphere and the first interaction point (Heck and Pierog, 2013).

3.1.2.6 INCLINED Observation Plane Option

INCLINED option is define the inclined observation plane besides the horizontal observation plane which is predefined automatically in CORSIKA. In the input card the keyword INCLIN specify the geometry of the inclined sampling plane. In this thesis the observation plane is a mountain slope and it can be define with a inclined plane.

3.1.2.7 UPWARD Option

The UPWARD option is selected to process the upward traveling particles in the simulated data. The zenith angle is determined the direction of the shower between $0^\circ < \theta < 70^\circ$ and $110^\circ < \theta < 180^\circ$ for primary particles. In the simulated data for this thesis, the UPWARD option is used to obtain the horizontal and upward showers obey to the Earth Skimming technique.

3.1.2.8 STACKIN Option

The STACKIN option is used to combine all the parameters which define the secondary particles simulated in CORSIKA. For example, the altitude of the first interaction, shower axis or first interaction start may be used to write out the parameters of the secondary particles to a file.

3.1.2.9 ROOTOUT Option

The ROOTOUT option is useful to write the output in 'DATA.root' file in root format. This provides the particle output data without storing the huge particle output data file MPATAP. It may be fast and easy way to store the output files.

3.1.2.10 PLOTSH Shower Plot Production Option

The shower plot production can be set with the PLOTSH option to write the start and end points of each particle track for the electromagnetic, muonic and hadronic component. These start and end points written to files are particle identification, energy (in GeV), x_{start} , y_{start} , z_{start} (all in cm), t_{start} (in sec), x_{end} , y_{end} , z_{end} (all in cm), and t_{end} (in sec). When the THIN option is on, the particle weight is also written.

3.1.2.11 THIN Option

THIN option of the CORSIKA simulation program can be applied to particles of a shower in the same branch; writes them as a single particle then it gives a weight equal to the total number of particles on that branch. If the energy of the primary particle is $E_0 > 10^{16}$ eV, the duration of the simulation is very long. The THIN mode produces outputs spending much less time compared with the normal (UNTHIN) mode. The THIN option can be used to saving time while the simulation of data. The ratio of the energy of the primary particle to the energy of all the secondary particles produced ($\epsilon_{th} = E/E_0$) determines the THIN level. When the THIN option is selected, the THIN level is used as $\epsilon_{th} = 10^{-6}$ in this thesis. In the output data, particles have identity, position (x, y, z), momentum (p_x , p_y , p_z and p_{tot}), direction angles (θ , ϕ) and weight number for THIN option.

3.2 The Array Geometry

The TAUWER array can detect the upward tau induced showers produced by the tau-neutrino interaction. This array is a large surface array with stations pointing at the horizon to detect particles of the air showers produced by large zenith angle. The primary particle ν_τ uses the matter in front of the array as interaction target. To collect the secondary particles of this shower, the array is constructed on an inclined surface. The array consists of 640 stations (40×16) which are placed 30 m apart and located on 30° inclined plane of the mountain slope. Each station, *named tower*, in Figure 3.3(a) constructed by two scintillator tiles ($40 \times 20 \text{ cm}^2$) separated by 160 cm and pointed below the horizon (approximately 2.5°) to measure upward moving showers coming from ν_τ interactions with the Earth's crust. This setup covers approximately 0.5 km^2 on the mountain surface, as in Figure 3.3(b).

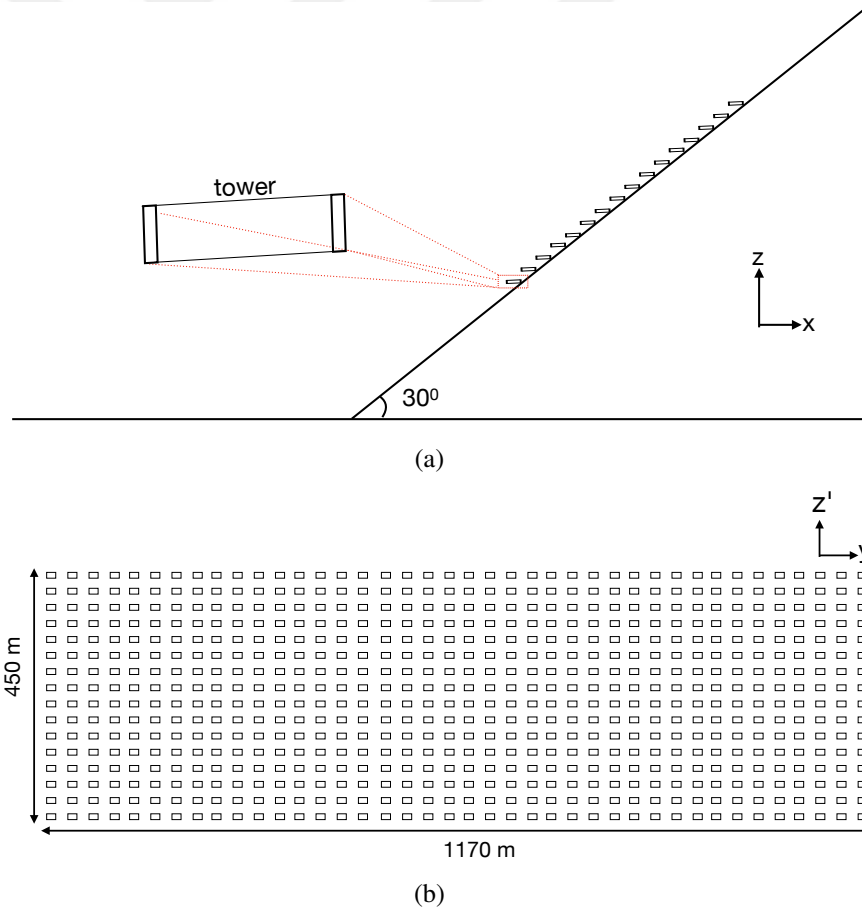


Figure 3.3. Schematic diagram of the array in (a) the ZX plane, (b)YZ'-plane, the projection of YZ plane on the inclined plane.

4. RESULTS AND DISCUSSIONS

The main goal is to estimate the performance of the array proposed in this thesis for Earth Skimming method and mountain chain screen strategy. Therefore CORSIKA is used to produce showers with different energies, decay modes and development lengths. Since the particles in the same branch are discarded with THIN option in CORSIKA as described in Section 3.1.2.11, showers are also simulated with THIN option to reduce the production time. This massive production provides better statistics to understand the performance of the array. In order to accurately use the data with THIN option, an unthinning method will describe in Section 4.1 is developed for restoring the information lost during thinning procedure in CORSIKA.

Table 4.1. Time it takes to simulate a single shower for different energy and development lengths without THIN option.

Development Length (km)	Energy (GeV)	Time (hours)
3	10^7	3 - 6
	$5x10^7$	12 - 50
	10^8	20 - 140
	$5x10^8$	125 - 245
	10^9	210 - 600
5	10^7	5 - 13
	$5x10^7$	10 - 62
	10^8	25 - 130
	$5x10^8$	120 - 245
	10^9	250 - 600
7	10^7	5 - 20
	$5x10^7$	11 - 78
	10^8	20 - 135
	$5x10^8$	100 - 245
	10^9	200 - 600
10	10^7	6 - 16
	$5x10^7$	10 - 75
	10^8	22 - 132
	$5x10^8$	125 - 245
	10^9	210 - 600

The production time of one shower for both options has energy dependence. So the higher energy of the primary particle is the longer it takes to simulate the shower. For the analysis, data is produced with 5 different decay modes of tau neutrino (π^- ,

$\pi^- \pi^0, \pi^- \pi^+ \pi^-, \pi^- \pi^0 \pi^0, \pi^- \pi^+ \pi^- \pi^0$) with 5 different energy region ($10^7 GeV, 5 \times 10^7 GeV, 10^8 GeV, 5 \times 10^8 GeV, 10^9 GeV$) and 4 development lengths ($3 km, 5 km, 7 km, 10 km$). Each set has 80 and 9 showers with and without THIN option, respectively. This corresponds to production of total 900 showers without THIN option and 8000 showers with THIN option. The detailed number of particles for mountain surface, array and the center of the array which simulated without THIN option for 5 different decay modes in 5 different energies with 4 different development lengths are given in Appendix-A.

Table 4.1 summarize the simulation time range of one shower without THIN option. For example, the simulation time for $10^8 GeV$ energy in 4 different development length changes between 20 – 140 hours for one shower. With THIN option this decreases to the range between 1 – 7 hours. It took 3 years to complete the production of the data used in this thesis with a 64 core Dell R815 (2U) server.

4.1 Unthinning of CORSIKA THIN Data

The THIN option in the CORSIKA simulation program follows the secondary particles in same branch of the showers which have an energy above $10^7 GeV$. It drops the particles to one particle and gives a weight according to THIN level. Only a fraction of the secondary particles is followed in the shower development. This reduces the computing time. There are methods in the literature Estupiñán et al. (2015); Stokes et al. (2012) to unthin data produced with THIN option in CORSIKA. Therefore a method called '*unthinning*' is developed to recover the lost particle information of simulated showers by using CORSIKA THIN output. The unthinning method provides to obtain very similar distributions of the particles by comparison with the original data.

The unthinning method is developed in terms of the geometrical structure of the shower along the inclined plane to obtain the real number of particles on that plane. For this purpose, the numbered lines on the Figure 4.1 are used to obtain the equations of the shower planes. In order to comprehend the marked points, some details can be given. The position and direction information of the particles (P_x, P_y, P_z) in point P at the inclined plane are used to obtain the P^* point on the shower axis. Then the point F , which is the closest point from point P to the plane of the shower, is found. Using

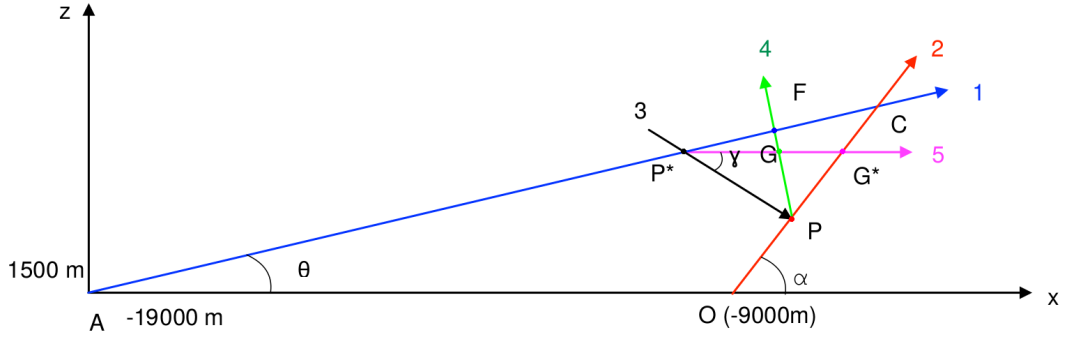


Figure 4.1. The line equations and their notations of the geometry which belongs to the inclined plane to create the particles in weighted numbers with the unthinning method.

the Monte Carlo method, some points are produced in a circle perpendicular to the axis of the shower in a radius of PF . The number of these points are obtained equal to the weight information of the particles on the THIN option. To obtain the real number of particles on the mountain surface, the equations of the lines are written as in below;

$$(z - z_A) = B(x - x_A)^i, \quad (4.1)$$

$$(z - z_O) = A(x - x_O)^{ii}, \quad (4.2)$$

$$(z - z_P) = D(x - x_P)^{iii} (\overrightarrow{P^*P}), \quad (4.3)$$

$$(z - z_P) = B^*(x - x_P)^{iv} (\overrightarrow{PF}), \quad (4.4)$$

$$(z - z_G) = aa(x - x_G)^v (\overrightarrow{P^*G}), \quad (4.5)$$

$$(x - x_G) = bb(y - y_G)^{vi}. \quad (4.6)$$

where; $A = \tan(\alpha)$, $B = \tan(\theta)$ and $B^* = \tan(90 - \theta)$ and the details of aa , bb and D will be given in the text. Equation 4.1 shows the shower axis of the THIN data, Equation 4.2 is the the slope of the inclined plane in terms of $(z - x)$ and Equation 4.3 is the direction of the particles at point P using the momentum information. The point P^* where the intersection of the particles passing through the point P is found by

ⁱshower axis

ⁱⁱinclined plane on mountain slope

ⁱⁱⁱusing momentum info to get direction and find P^*

^{iv}line PF , to find perpendicular crossing point on shower axis

^vline passing through P^* and G to find G^* on the mountain plane

^{vi}particle distribution in 3D

solving the Equations 4.1 and 4.3.

The point F on the shower axis is the vertical distance from the point P to this plane and Equation 4.4 defines the line through the points P and F . The perpendicular line starts from the point P to the shower axis and G is a point on this line. The particles on the point P are randomly produced, in terms of their weights written on THIN data, with Monte Carlo generator within a radius as PF . A line, which started from point P^* , passes through the point G . The solution of the Equations 4.2 and 4.5 together gives the point G^* which are the new coordinates of the particles on the inclined plane as the weighted numbers. The result of these solutions is named as unthinning and in this result the direction of the particles is not degenerated.

To create unthinning data set from CORSIKA thinning output files; the THIN mode is selected as 10^{-6} . The first shower of the simulated THIN data is used to perform the analyzation. The above equations, which belongs to different lines or plane, are shown in Figure 4.1 to calculate unthinning shower where;

$$A = \tan(\alpha), \alpha = 30^\circ, \quad (4.7)$$

$$B = \tan(\theta), \theta = (\theta_{rad} \cdot \frac{180^\circ}{\pi})^\circ - 90^\circ, (\theta = 2.27^\circ, \theta_{rad} = 1.61 \text{ rad}) \quad (4.8)$$

$$B^* = \tan(90^\circ - \theta), (\tan(1.57 - \theta \cdot \frac{\pi}{180^\circ})) \quad (4.9)$$

for calculation of D in Equation 4.3 we have to look p_z momentum is positive or negative, then we have two options for D as in below;

$$\text{if } (p_z < 0); ddd = \tan^{-1}(|\frac{p_z}{p_x}|) - (\theta_{rad} - 1.57), \quad (4.10)$$

$$\text{if } (p_z > 0); ddd = \tan^{-1}(|\frac{p_z}{p_x}|) + (\theta_{rad} - 1.57) \quad (4.11)$$

where p_z and p_x are the momentum of z and x coordinates. $D = \tan(ddd)$ where ddd is equal to γ in Figure 4.1.

$$\text{if } (p_z < 0); D = -\tan(ddd) \quad (4.12)$$

To evaluate slopes of G^* points, if the value of P^* greater than G point, then we

change the sign of slopes;

$$aa = (x_G - x_{P^*}) \rightarrow \text{if } (x_{P^*} > x_G) \text{ then; } aa = -aa, \quad (4.13)$$

$$bb = (z_G - z_{P^*}) \rightarrow \text{if } (z_{P^*} > z_G) \text{ then; } bb = -bb. \quad (4.14)$$

As a brief explain of this study, the upward and inclined (curved) geometry is used in the simulation as an input data. These events have been generated with a large zenith angle $\theta = 92.27^\circ$ and supposed as the detector array being on an inclined plane with an angle $\alpha = 30^\circ$.

The output of this simulation includes the particle properties such as particle type, its momentum (total momentum and belongs to each of x,y and z coordinates) and position (in 3D) as well as weight to it. The study was done to obtain real position and amount of particles on inclined plane which is on the mountain surface (array plane). To make this work, the calculations are started from equation of planes on the schematic definition of the TAUWER detector array used for CORSIKA simulation as in Figure 4.1. The numbered lines and equations solved to obtain position of particles in each direction. For example in step 1, a particle transferred from inclined plane to shower axis named as P and P^* points, respectively. To obtain the radius of shower, vertical components of point P to point F are calculated in step 2 as x_F and z_F . The radius of shower; PF is calculated using circle formula;

$$(x - h)^2 + (y - k)^2 = r^2 \quad (4.15)$$

as the center being at the point (h, k) and the radius being r . Thereafter the finding of PF , new particles are generated with Monte Carlo random generator with ratio each particle's weight to obtain the real numbered particles from unweighted one's by the unthinning method. In here there is a correction for position of particles. When they created by Monte Carlo, their positions start from the origin of coordinate system. But this coordinate system has not same starting point with the studied system. Then to eliminate this difference, the F coordinate to z component of the point G . In step 4, the coordinates of these random particles calculated with achieved formulas from the line equations. With this last step, the unthinning particles on the inclined

plane are obtained.

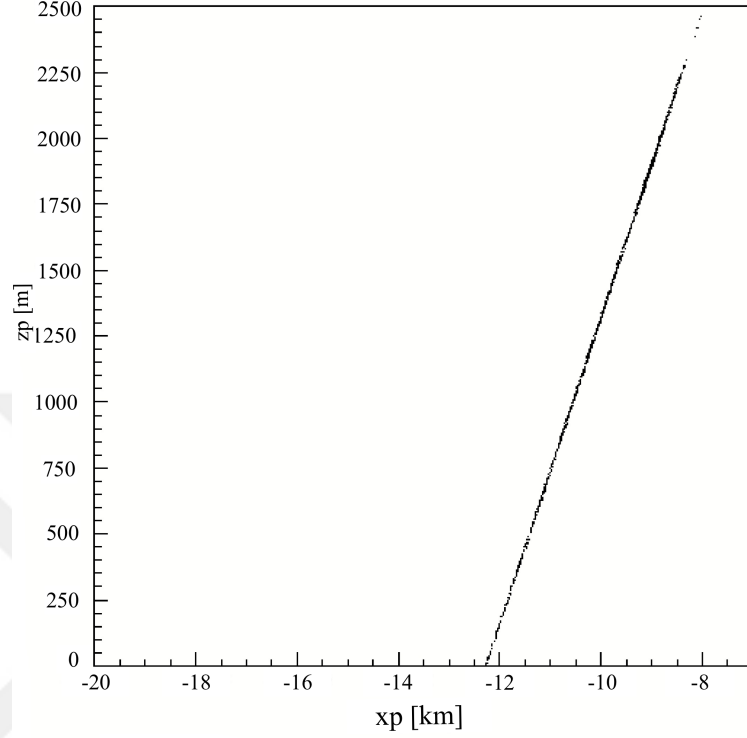


Figure 4.2. The position of point P in $z - x$ plane.

The distribution of the particles from THIN data is depicted in Figure 4.2. The Equations 4.1 and 4.3 are used to obtain position on P^* for particles. For instance, the Equation 4.3 is multiplied by -1 and summed up with each other to find x_{P^*} . The results are given in following equations;

$$(z_P - z_A) = B(x - x_A) - D(x - x_p), \quad (4.16)$$

$$x(B - D) = z_P - z_A + B.x_A - D.x_p \quad (4.17)$$

The solution of Equations 4.16 and 4.17 gives the x_{P^*} coordinates of the point P^* .

$$x_{P^*} = \frac{z_P - z_A + B.x_A - D.x_p}{B - D} \quad (4.18)$$

To find z_{P^*} coordinate, two sides of Equations 4.1 and 4.3 are multiplied by D and B respectively, then obtained following equations;

$$D(z - z_A) - B(z - z_P) = BD.(x_P - x_A), \quad (4.19)$$

$$z(D - B) - D.z_A + B.z_P = BD.(x_P - x_A) \quad (4.20)$$

z_{P^*} can be found from the equation as follows

$$z_{P^*} = \frac{BD.(x_P - x_A) + D.z_A - B.z_P}{D - B} \quad (4.21)$$

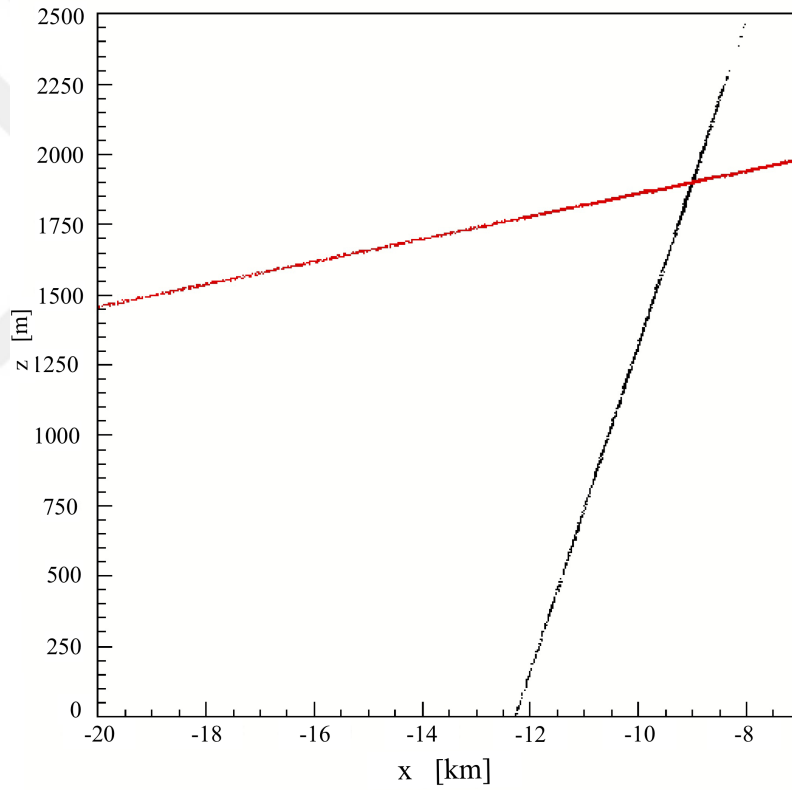


Figure 4.3. The position of point P^* and P in $z - x$ plane.

The calculated x_{P^*} and z_{P^*} coordinates plotted in Figure 4.3 as superimposed to x and z coordinates. Black points are represented by the point P for each particle in the output file and along the inclined plane. Red points are produced by point P^* and they are on the shower axis as expected. As can be seen from the Figure, the number of the particles have not changed but they are moved to point P^* .

Using Equations 4.1 and 4.4 x and z coordinates of the point F can be obtained.

To find x_F subtract Equation 4.4 from Equation 4.1;

$$z_P - z_A = x(B - B^*) + B^* \cdot x_P - B \cdot x_A \quad (4.22)$$

then x_F is;

$$x_F = \frac{z_P - z_A - B^* \cdot x_P - B \cdot x_A}{B - B^*}. \quad (4.23)$$

To find z_F each equation divided its coefficient then the Equation 4.4 is subtracted from 4.1;

$$\frac{1}{B} \cdot (z - z_A) - \frac{1}{B^*} \cdot (z - z_P) = x_P - x_A \quad (4.24)$$

and z_F is obtained as;

$$z_F = \frac{B \cdot B^* \cdot (x_P - x_A) + B^* \cdot z_A - B \cdot z_P}{B^* - B} \quad (4.25)$$

Figure 4.4 shows the distribution of the closest point to the shower axis which called as point F . Depending on the position P of the particle below or above of the shower axis, point F may be before or after from the inclined plane.

After this step to obtain the radius of the circular plane where is generated as random points between the points P and F ;

$$PF = \sqrt{(x_P - x_F)^2 + (z_P - z_F)^2} \quad (4.26)$$

Figure 4.5 is the distribution of the distance PF . This indicates that most of the particles are around 100 m radius.

Using Monte Carlo to generate random numbers in a perpendicular plane to the shower axis, y_G and z_G are obtained. For the calculation of x_G ;

$$x_G = \frac{z_G - z_P + B^* \cdot x_P}{B^*} \quad (4.27)$$

The x , y and z coordinates of point G are depicted in Figure 4.6 as in left side z versus x and in right side z versus y . In Figure 4.6(a), total 177820 points are generated on the G point. Figure 4.6(b) is the Monte Carlo points on a plane with a random PF

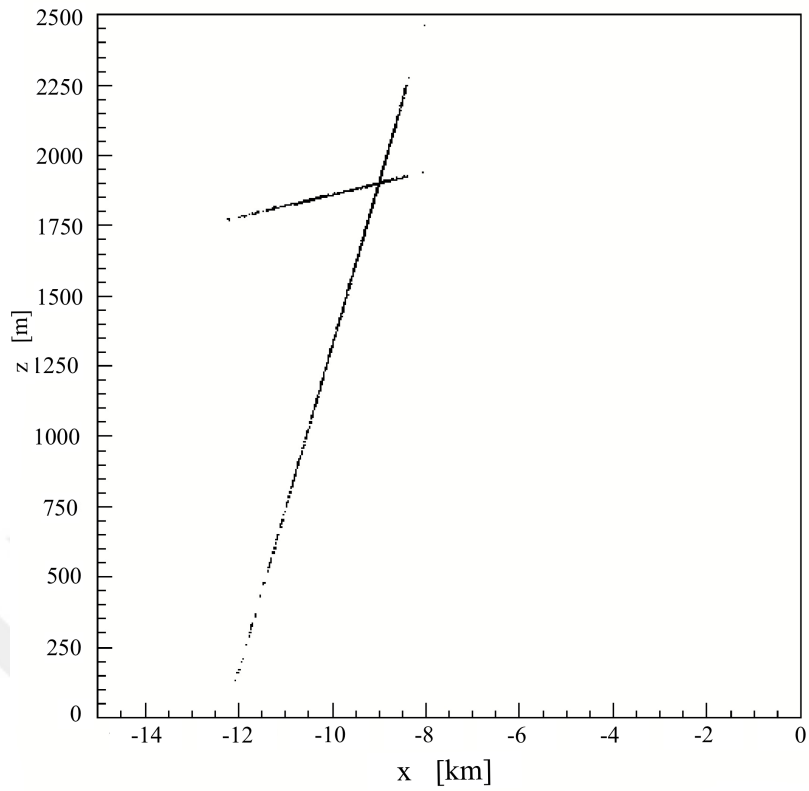


Figure 4.4. The position of point F and P in $z - x$ plane.

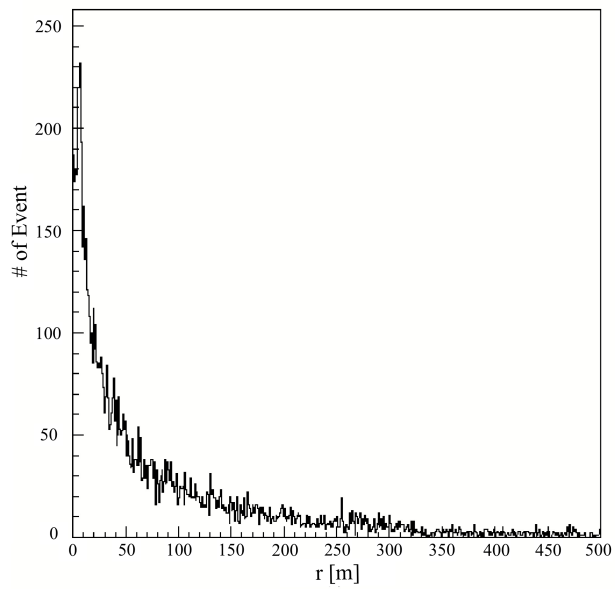


Figure 4.5. The distribution of the particles on the circle with PF radius.

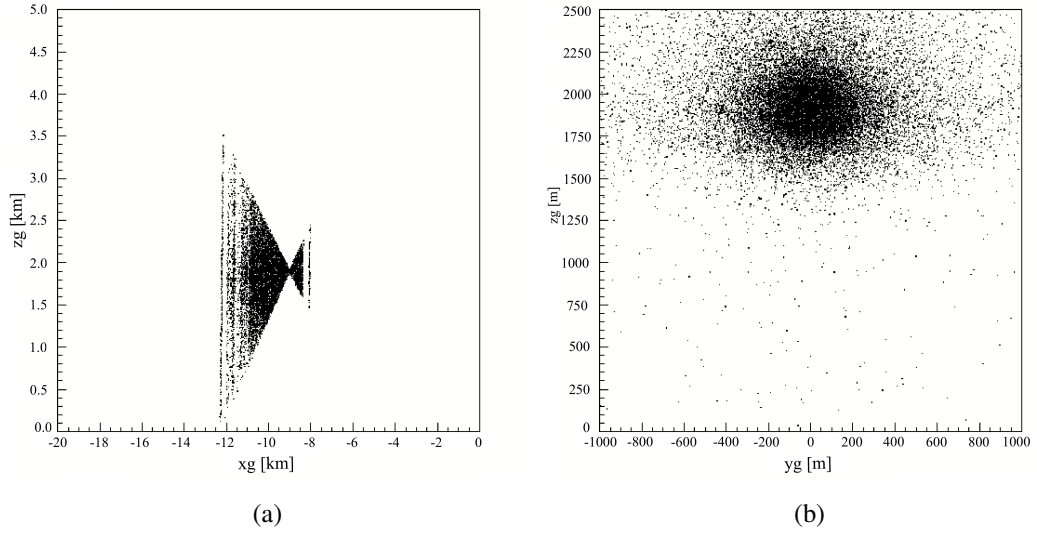


Figure 4.6. The position of point G in (a) $z - x$ and (b) $z - y$ planes.

for each particle. The created points in terms of the particle weights are symmetric. And it is indicating that there is no bias on the analysis so far.

In this step, x , y and z are calculated for G^* . For the calculation of x_{G^*} and z_{G^*} points Equations 4.2 and 4.5 are used.

$$A \cdot x - A \cdot x_P = z - z_P \quad (4.28)$$

$$x = \frac{z - z_P + A \cdot x_P}{A} \quad (4.29)$$

$$z = z_P + A \cdot x - A \cdot x_P \quad (4.30)$$

and in result of the combination of these two equations, the relation can be obtained;

$$\frac{z - z_{P^*}}{z_G - z_{P^*}} = \frac{x - x_{P^*}}{x_G - x_{P^*}} \quad (4.31)$$

where x_{P^*} and z_{P^*} are defined from the Equations 4.13 and 4.14 as,

$$aa \cdot (z - z_{P^*}) = (x - x_{P^*}) \cdot bb \quad (4.32)$$

Hereafter, x is used in relation between Equation 4.2 and 4.5 then added in to

Equation 4.32;

$$aa \cdot z - aa \cdot z_{P^*} = \frac{(bb \cdot z - bb \cdot z_P + bb \cdot A \cdot x_P)}{a} - bb \cdot x_{P^*} \quad (4.33)$$

where z represents z_{G^*} ;

$$z_{G^*} = \frac{A \cdot aa \cdot z_{P^*} - bb \cdot z_P + bb \cdot A \cdot x_P - bb \cdot x_{P^*} \cdot A}{A \cdot aa - bb} \quad (4.34)$$

then calculation for x_{G^*} the Equations 4.30 and 4.32 are solved together;

$$aa \cdot (z_P + A \cdot x - A \cdot x_P) - aa \cdot z_{P^*} = (x - x_{P^*}) \cdot bb \quad (4.35)$$

$$aa \cdot A \cdot x - x \cdot bb = aa \cdot A \cdot x_P + aa \cdot z_{P^*} - aa \cdot z_P - x_{P^*} \cdot bb \quad (4.36)$$

then x_{G^*} is;

$$x_{G^*} = \frac{aa \cdot A \cdot x_P + aa \cdot z_{P^*} - aa \cdot z_P - bb \cdot x_{P^*}}{A \cdot aa - bb} \quad (4.37)$$

and lastly y_{G^*} is obtained following equations which have same slopes;

$$x - x_{P^*} = m \cdot (y - y_{P^*}) \quad (4.38)$$

$$x - x_G = m \cdot (y - y_G) \quad (4.39)$$

from these 2 equations;

$$\frac{x - x_{P^*}}{y - y_{P^*}} = \frac{x - x_G}{y - y_G} \quad (4.40)$$

$$x \cdot y - x \cdot y_G - x_{P^*} \cdot y + x_{P^*} \cdot y_G = x \cdot y - x \cdot y_{P^*} - x_G \cdot y + x_G \cdot y_{P^*} \quad (4.41)$$

therefore y_{G^*} is as follows;

$$y_{G^*} = \frac{y_G \cdot x - y_G \cdot x_{P^*}}{aa} \quad (4.42)$$

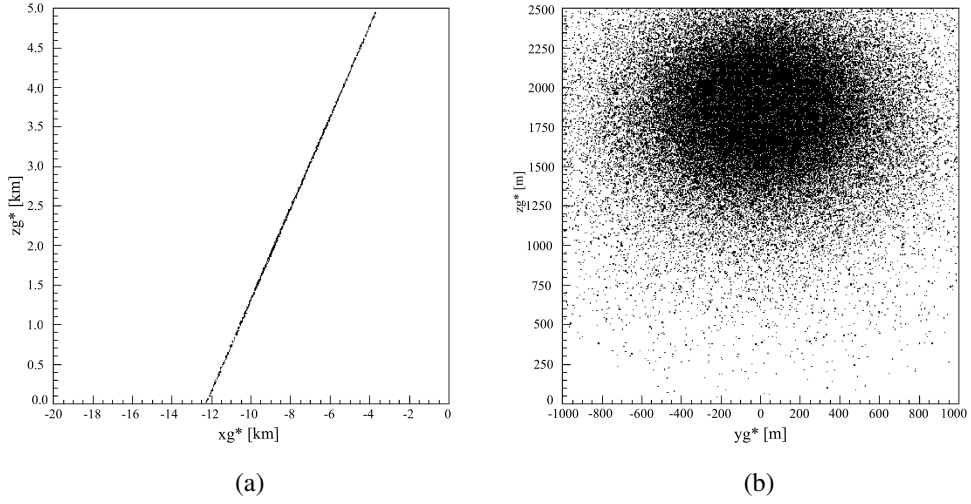


Figure 4.7. The position of point G^* in (a) $z - x$ and (b) $z - y$ planes.

Figure 4.7(a) shows the z_{G^*} versus x_{G^*} plot for the entire shower. This graph represents the shower axis on the mountain surface with all particles real weights. Total 2901091 particles plotted to see the shower axis in the $x - z$ plane. Figure 4.7(b) shows the z_{G^*} versus y_{G^*} for all particles of the shower and their weights taken equal to real values of particles.

As the final configuration of the dedicated TAUWER array geometry, the Figure 4.8 shows the unthinned inclined plane is superimposed to the thin inclined plane on the mountain slope. The red z_P vs x_P plot which define the thin inclined plane is superimposed to the black unthinned inclined plane which that z_{G^*} vs x_{G^*} . Started from coordinates of $P(x, y, z)$ and momentum, and generate P_{G^*} coordinates (x, y, z) . There is a symmetry distribution on the inclined plane and no bias introduced.

It can be seen also from the Figure 4.9, the arrival directions of the examined shower have similar distributions for zenith (θ) and azimuthal (ϕ) angles in both point P and G^* . The arrival directions of the shower are around 2.5° (it is $\theta - 90$) and 0.001° for θ and ϕ , respectively.

4.2 Reconstruction of the Air Showers

In this section, the basic shower reconstruction procedure is studied in terms of the methods that are commonly applied to detector arrays. Section includes the

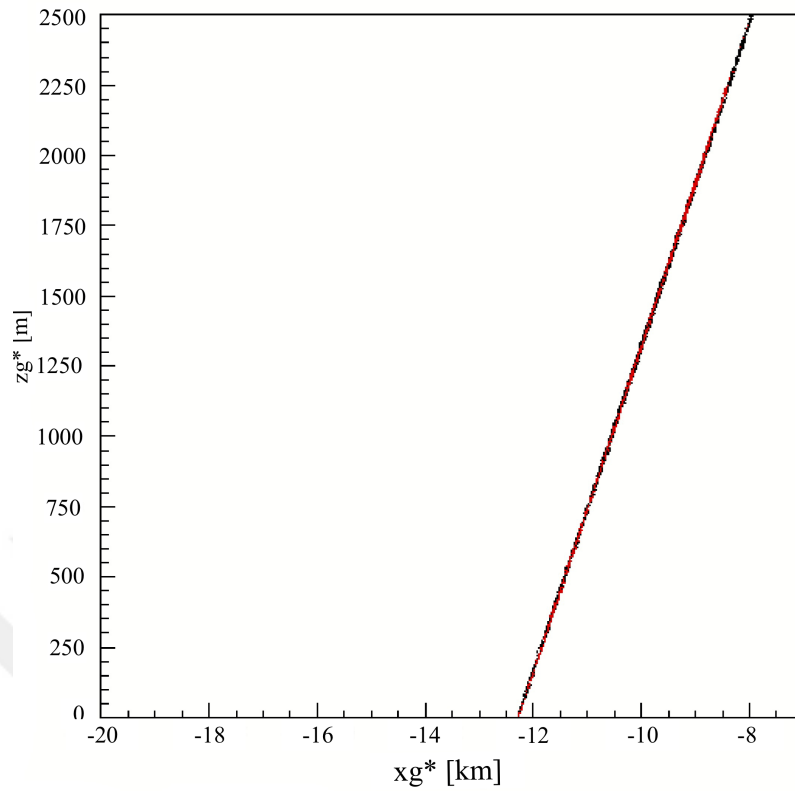


Figure 4.8. The unthinned particles superimposed to the particle thin.

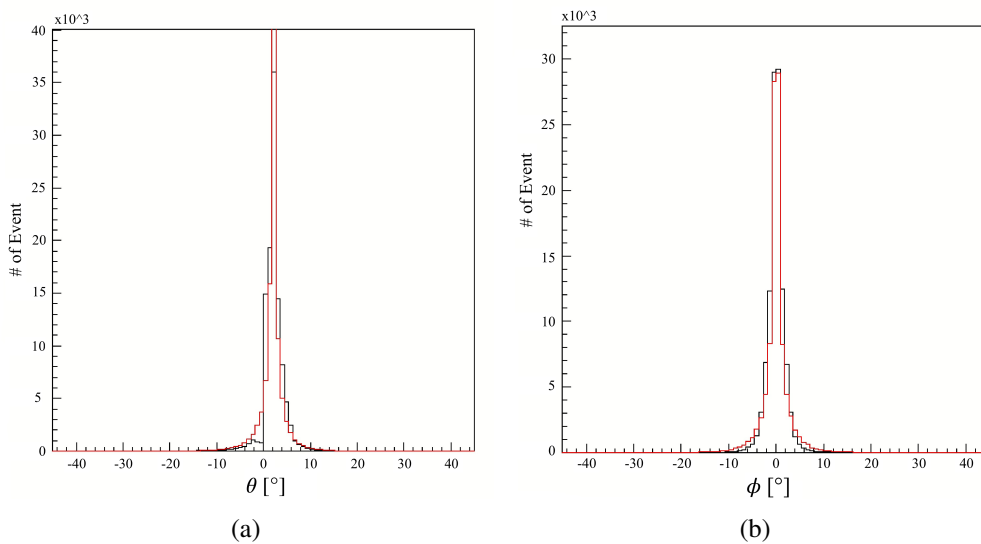


Figure 4.9. The arrival directions for point G^* are superimposed to the arrival directions of point P as (a) θ and (b) ϕ distribution

examination of the simulated showers with respect to the particle percentages, the

lifetime of the decay channels, the energy classification with the density of particles in triggered stations mean arrival times, spherical shower front, and the thickness of the shower front. Also the effective area and the acceptance of the array are studied.

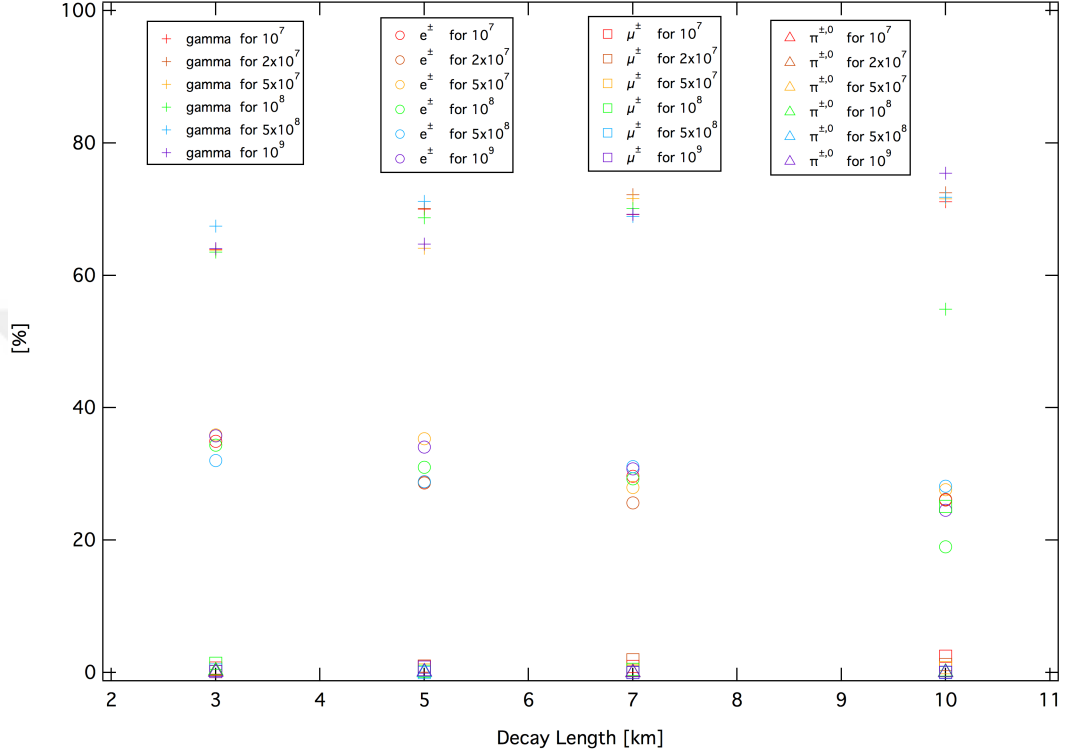


Figure 4.10. The variation of particle percentages on the $\pi^- \pi^0$ decay channel with various development lengths.

The simulated showers include different types of particles such as electrons, muons, pions, etc. The variation of the particles are examined for each development length and energy and the Figure 4.10 shows these results. The most existing particles in the showers are γ s as nearly 60% and above for each energy and development length in the $\pi^- \pi^0$ channel. The e^\pm s follow secondly almost 20 – 40% of the total particles. The μ^\pm s and $\pi^{\pm,0}$ s have similar percentages in the total number of particles.

In Figure 4.11, the most existing particles in the $\pi^- \pi^+ \pi^-$ channel are γ s around 60% as in the $\pi^- \pi^0$ channel. The percentage of γ s increase slightly with the rise of the development length. The e^\pm s have almost same distribution with the $\pi^- \pi^0$ channel. The percentage of μ^\pm s are increase due to the π^\pm in the decay channel. The $\pi^{\pm,0}$ s have similar percentages with the $\pi^- \pi^0$ channel.

The lifetime of the $\pi^- \pi^0$ and $\pi^- \pi^+ \pi^-$ showers are examined in terms of their energies and development lengths and Figure 4.12 shows the results. In 3 km and 7 km

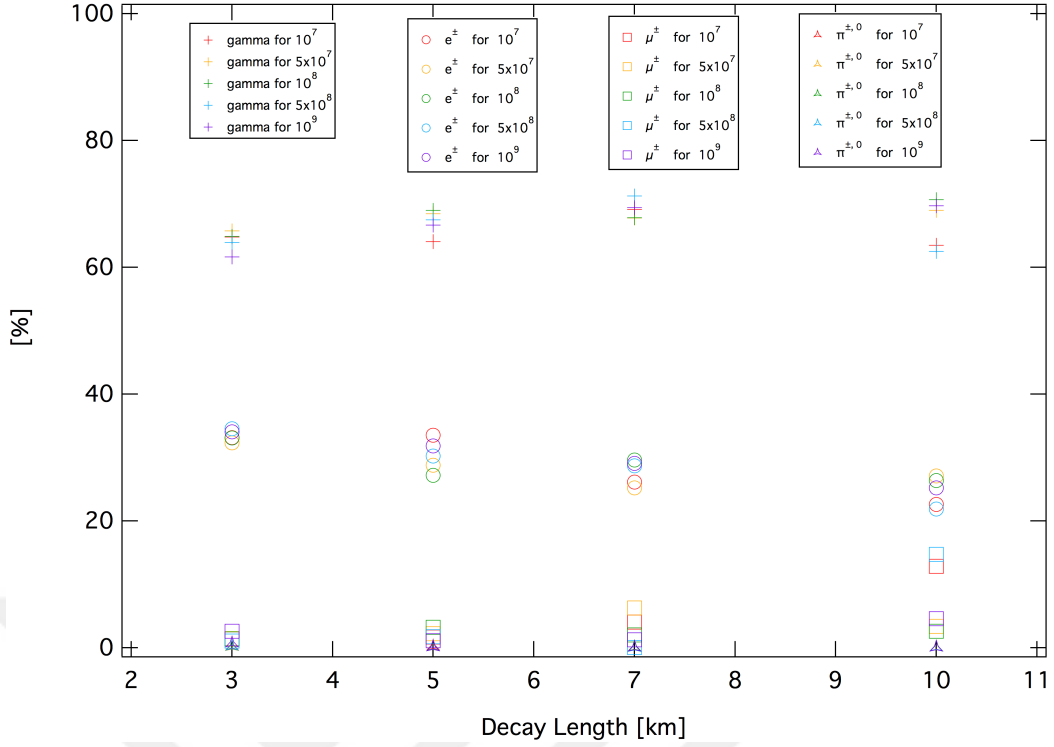


Figure 4.11. The variation of particle percentages on the $\pi^- \pi^+ \pi^-$ decay channel respect to various development lengths.

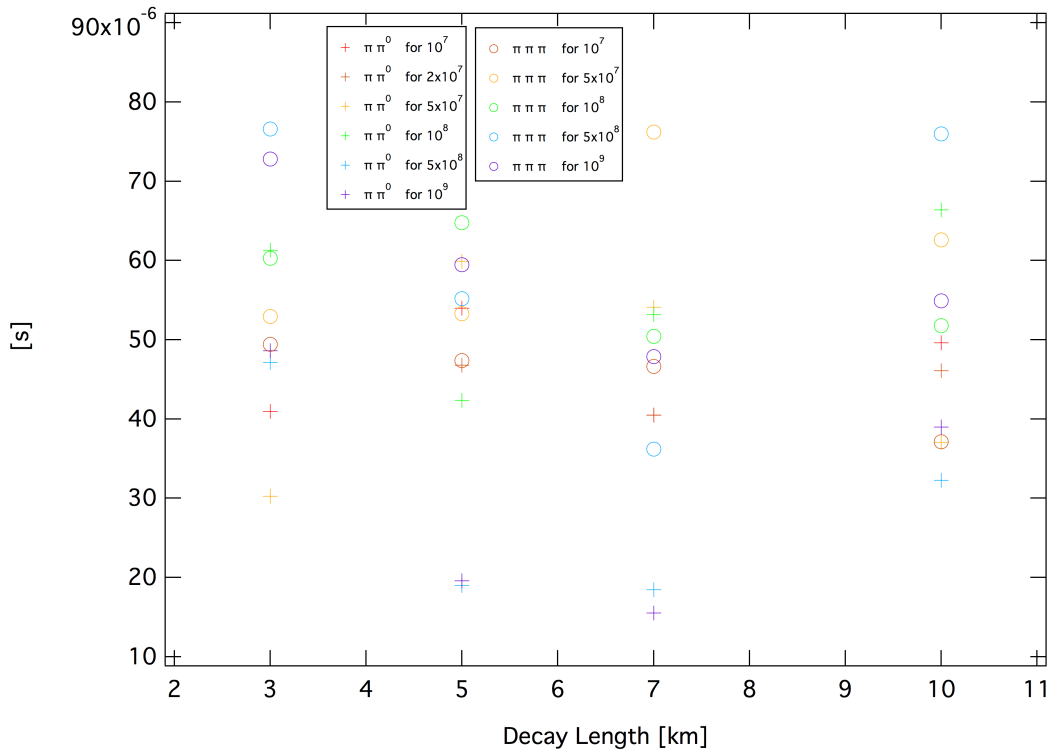


Figure 4.12. The lifetime of the $\pi^- \pi^0$ and $\pi^- \pi^+ \pi^-$ decay channels respect to various development length in terms of shower energies.

development lengths, $\pi^-\pi^+\pi^-$ showers with the 10^7 GeV, 5×10^7 GeV, 5×10^8 GeV and 10^9 GeV energies have bigger lifetime than $\pi^-\pi^0$ showers except 10^8 GeV. The lifetime of the showers in $\pi^-\pi^+\pi^-$ decay channel are higher than $\pi^-\pi^0$ showers in 10^7 GeV, 10^8 GeV, 5×10^8 GeV and 10^9 GeV energies for 5 km. In biggest development length, $\pi^-\pi^+\pi^-$ showers are bigger than $\pi^-\pi^0$ showers in terms of lifetime for 5×10^7 GeV, 5×10^8 GeV and 10^9 GeV energies on the contrary $\pi^-\pi^0$ channel has long lifetime in the energies 10^7 GeV and 10^8 GeV.

4.2.1 The Energy Reconstruction

The goal of the analysis is to determine the groups for different energies ranging from 10^8 GeV to 10^9 GeV. The procedure of the energy reconstruction is started from precisely determining of the shower core on the array. The e^\pm number in each station and their distance to the core are determined. The number of e^\pm per station, where at least one e^\pm for each station, plotted as a function of the radial distance from core. This plot provides to group the different energy scales using number of e^\pm per station.

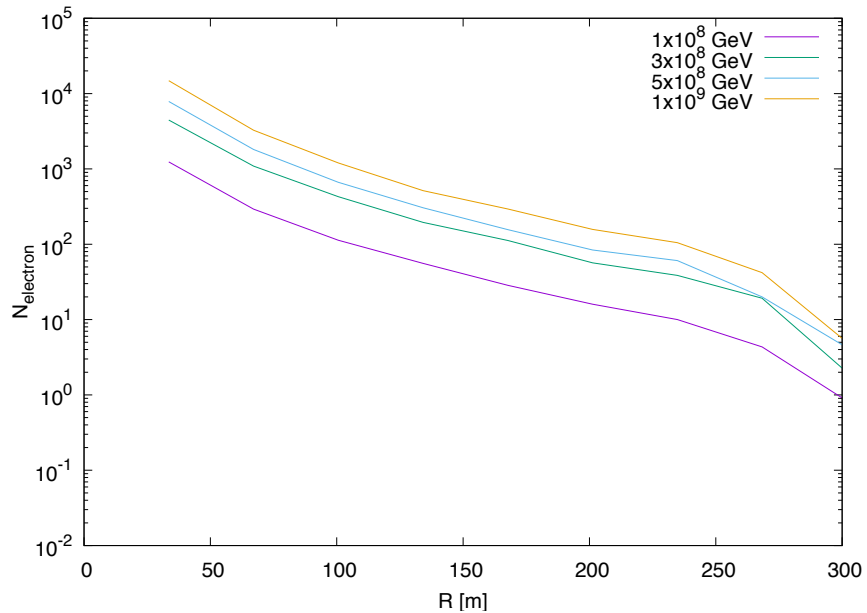


Figure 4.13. The number of e^\pm in the stations versus the radius of the showers grouped in different energies.

The showers are grouped into 4 different energy scales as in Figure 4.13 in terms of their energies ranging from 10^8 GeV to 10^9 GeV. It can be seen that there is an

exponential relationship between the grouped energies and the radial distance from core. Also the energy of the shower can be separated looking by the number of e^\pm as a function of the radial distance.

4.2.2 The Time Spread

In this section, the simulated upward EASs via π^- decay channel are selected to observe the performance of the array placed on the inclined plane. The energy of selected showers, developed in a 5 km development length are ranging from 10^7 GeV to 10^9 GeV. The simulated tau showers on π^- decay channel are discussed in terms of the time spread of the particles on the array for the possible trigger decision in this energy range.

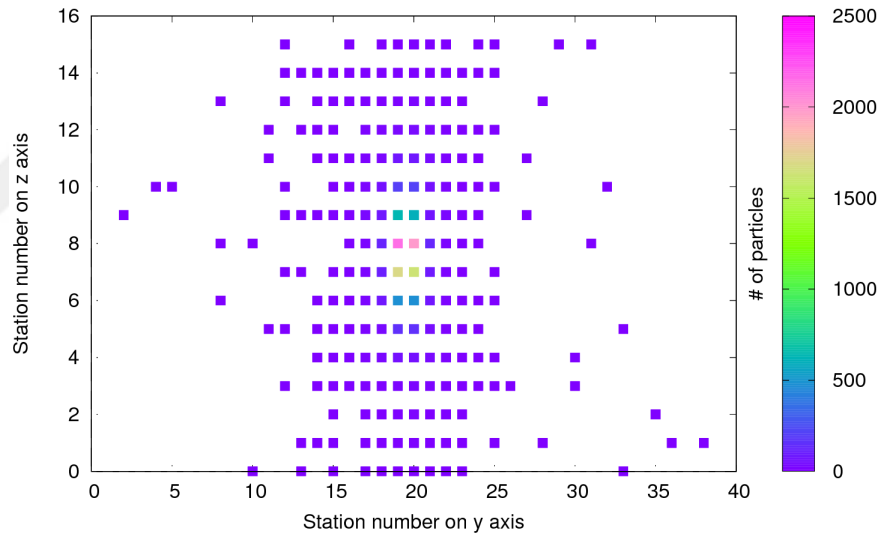


Figure 4.14. Particle density in a back or front tile of the station on π^- shower that decay 5 km far from the array plane. The array is composed by 40 horizontal rows and 16 vertical rows with 30 m apart.

Figure 4.14 shows the particle distribution on the array and referred to the center of the shower. The color code shows the number of particles on the tiles and the most hit tiles are pink tiles on the center of the array. From these simulation studies, it results the signature of tau shower, is a very high-density electron cluster centered on the tau flight path. The maximum number of hits in a single station for tau shower at 1000 PeV ranges from 1500-2500 hits on the center.

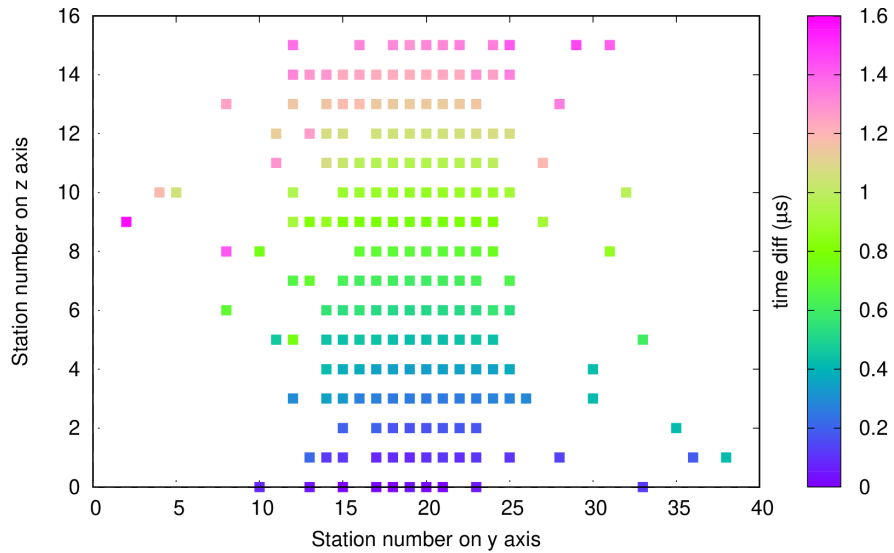


Figure 4.15. The time distribution of the stations on π^- shower that decay 5 km far from the array plane. The array is composed by 40 horizontal rows and 16 vertical rows with 30 m apart.

The timing spread is computed by looking at the arrival times of all hits in a shower, identifying the earliest, and subtracting that from the rest, so each of the showers has the same relative timing reference. The color map corresponds to time difference from earliest to latest. According to Figure 4.15, one shower has $1.6 \mu s$ time window.

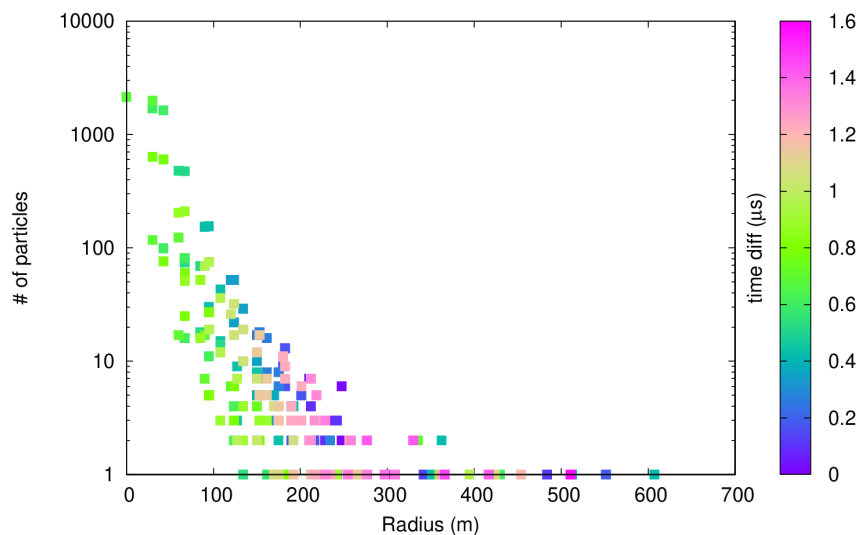


Figure 4.16. The distribution of the number of particles along the radius of the shower and the time difference between the first and last particle on each station as a color code are shown for π^- shower.

The average timing spectrum for π^- decay channel between 10^7 GeV and 10^9 GeV for τ induced showers that hit any scintillator in the 640 stations has been studied. The timing spread of the stations is computed by looking at the arrival times of all hits in a shower, identifying the earliest which is selected as relative timing reference and we find a time delay in a (4x4) sub-array around the center of the shower covers approximately $0.3 \mu s$.

The radius of the shower is evaluated from 1 or more hitted stations and the first fired station is selected as the reference point for x, y and z coordinates. The Figure 4.16 shows that both number of the particles and the time window of the selected shower versus the radius of that shower. The most of the particles are around the first 100 m of the shower and they have nearly 300 ns time window. After first 100 m on the shower, the time difference on the stations are getting bigger than that.

4.2.3 The Thickness and the Spherical Shower Front

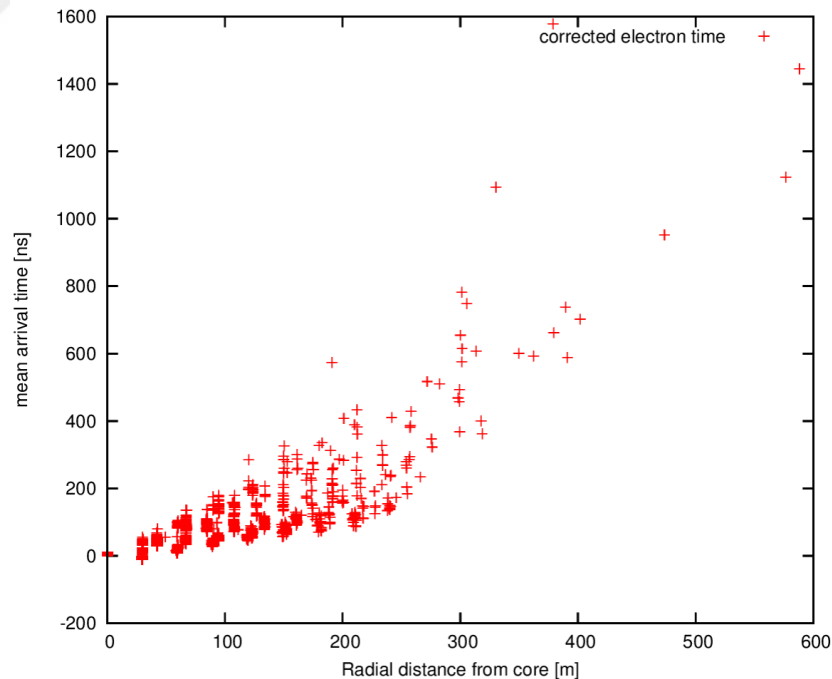


Figure 4.17. The mean arrival time for e^\pm in π^- decay channel for 5 km development length as a function of radial distance from core.

The time reported in the output file of CORSIKA for each particle is the time

when particle arrives to the mountain surface. However, there is a small amount of time difference between the detectors and the mountain surface. For this reason, corrected time may be calculated for the particles passing through the detectors. The results for e^\pm are given in Figure 4.17. The time correction is made for the particles hit to the detectors which their positions and time informations are known from the data simulated in CORSIKA. The known time informations of the particles are the arrival times to the 30° inclined mountain surface. The time difference is calculated from the distance between particle position on mountain surface and the position of the detector. The mean arrival time also determined as a function of radial distance from core as in Figure 4.17. The result also shows that the spherical shower front with the increasing mean arrival time in far from the core.

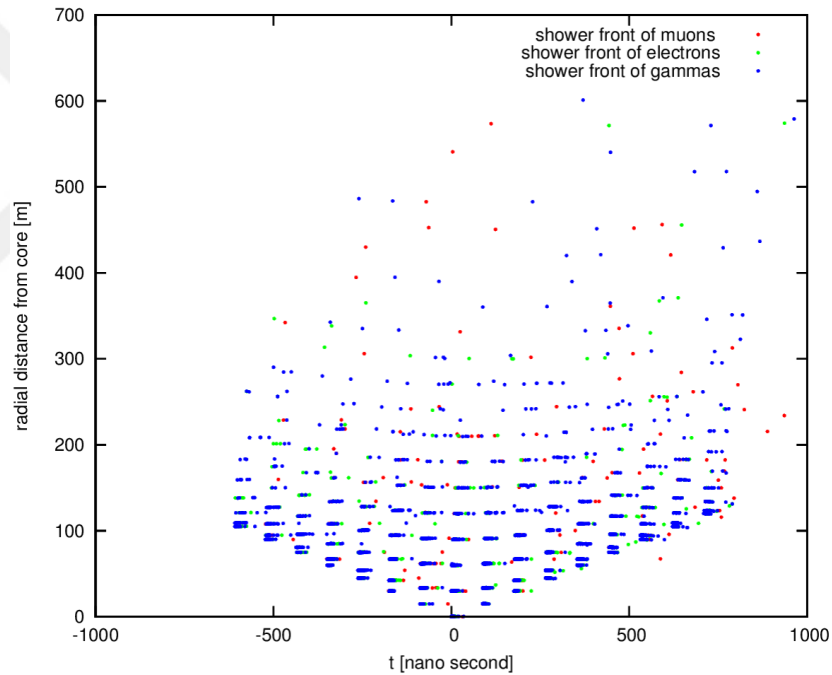


Figure 4.18. The spherical shower front for 5 km development length in π^- decay channel.

The Figure 4.18 shows the γ , e^\pm and μ^\pm radial distance from core as function of arrival time. The blue points refer to γ , green points to e^\pm and red points to μ^\pm . The figure expresses that the distribution of these particles in a shape of spherical shower front with the change of arrival times. Some of these particles are positioned on the right side of the graph depend to excess number of station on right side.

In order to determine the time structure of the spherical shower front, the procedure presented by Agnetta et al. (1997) is performed. The standard deviation is determined

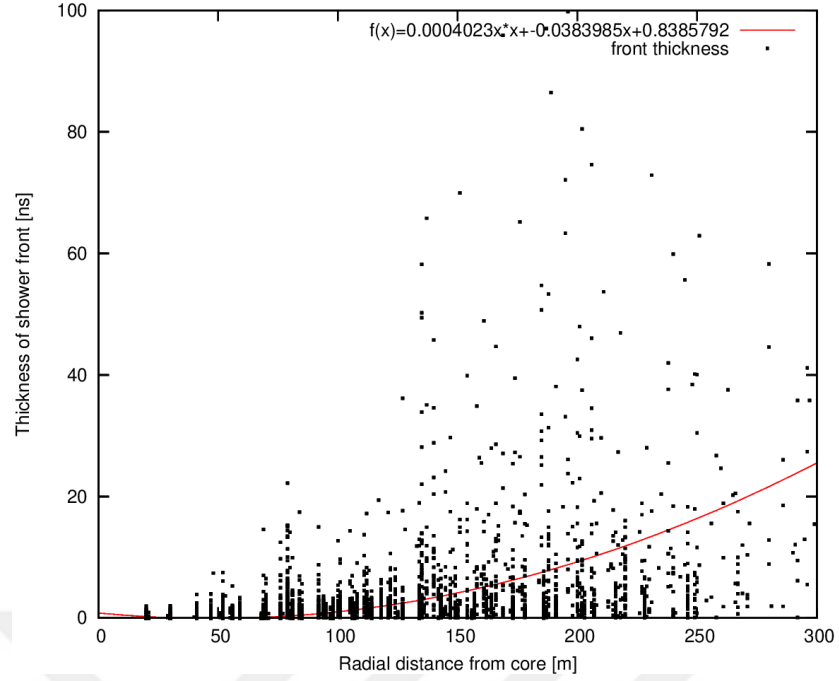


Figure 4.19. The shower front thickness for π^- channel in 5 km development length.

as;

$$\sigma = \sqrt{\sum_{i=1}^{w_i} \frac{(t_i - t_{mean})^2}{w_i - 1}} \quad (4.43)$$

where t_{mean} is mean delay time, w_i is number of particle on each station;

$$t_{mean} = \sum_{i=1}^{w_i} \frac{t_i}{w_i} \quad (4.44)$$

The Figure 4.19 shows the thickness of the shower as a function of radial distance from core and the fit depicts the shower front thickness exponentially increase with the radial distance. The thickness is increase especially far from the shower core depending to the characteristic of the spherical shower front. Linsley and Scarsi (1962) also determined the shower front curvature using μ^\pm and e^\pm . They reported that, the radius of curvature of the e^\pm front increases at bigger core distances as can be seen in Figure 4.19.

4.2.4 The Limits of the Array

The design for a detector array is important for an accurate detection. One of these optimize parameters is to specify the limits of the detector array. To obtain the zenith and azimuthal angle for array, the upper and lower limits are basically determined from the location of the stations. A parabolic fit is applied to these limits. For instance to get the acceptance of the array center, the zenith and azimuthal angles are weighted with the number of particles on each detector.

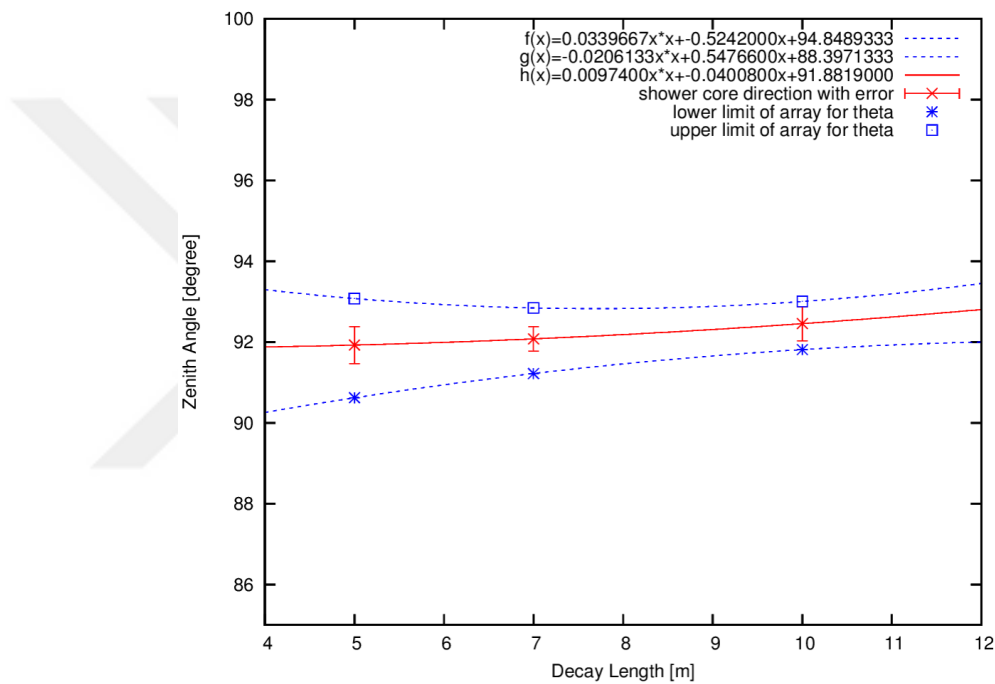


Figure 4.20. The acceptance of the array for 5×10^8 GeV in terms of zenith angle.

The Figure 4.20 shows the zenith θ angle limits of the detector array as a result of parabolic fit. In the graph, the particles of the showers having different development lengths are examined in terms of upper and lower limits and also for a main acceptance for these particles on the stations. The fits results show that, the upper limit for θ is 94.8° and lower limit is 88.4° for 5×10^8 GeV energy. The acceptance of the array for showers in the same features is about 92° . This shows that the simulated showers can be totally detectable with this array in terms of zenith angle.

The Figure 4.21 shows the azimuthal ϕ angle limits of the detector array as a result of parabolic fit. The fits results show that, the upper limit for ϕ is about 18°

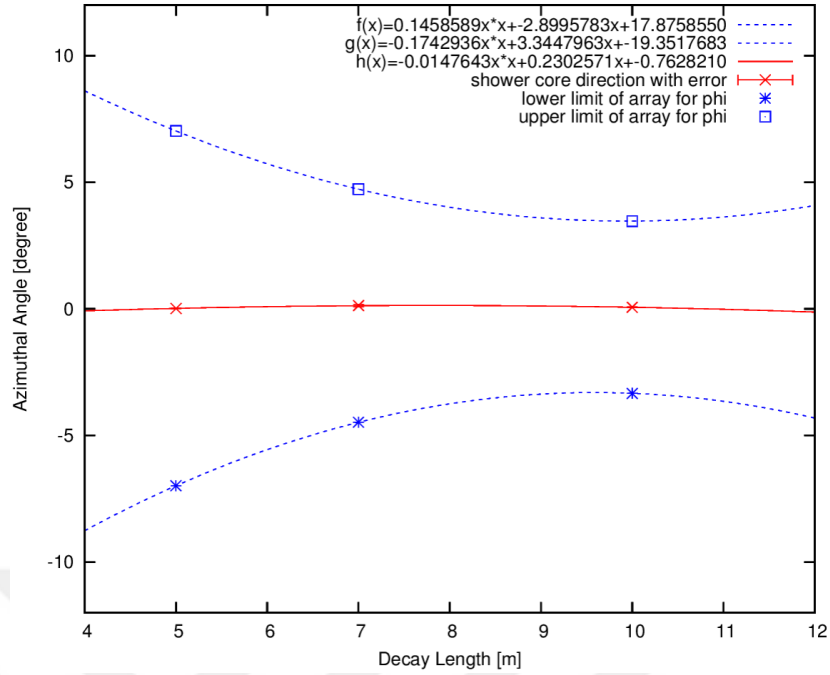


Figure 4.21. The acceptance of the array for $5 \times 10^8 \text{ GeV}$ in terms of azimuthal angle.

and lower limit is -19° for the showers with an energy of $5 \times 10^8 \text{ GeV}$ and different development lengths. The acceptance of the array for the showers in the same features is about 0.8° . This shows that the simulated showers can be totally detectable with this array in terms of azimuthal angle.

4.2.5 Effective Area of the Array

The effective area of the TAUWER array is determined for all reconstructed energies and all decay modes of tau. For this determination, the number of hits per station is selected as at least 1 and upper. These particles can be obtained in an area between 0.058 km^2 and 0.103 km^2 , 0.127 km^2 and 0.153 km^2 , 0.150 km^2 and 0.172 km^2 , 0.175 km^2 and 0.198 km^2 for 10^8 GeV , $3 \times 10^8 \text{ GeV}$, $5 \times 10^8 \text{ GeV}$ and 10^9 GeV energy scales, respectively. That means, the maximum used area of the array is 20%, 30%, 34% and 40% for energies 10^8 GeV , $3 \times 10^8 \text{ GeV}$, $5 \times 10^8 \text{ GeV}$ and 10^9 GeV , respectively.

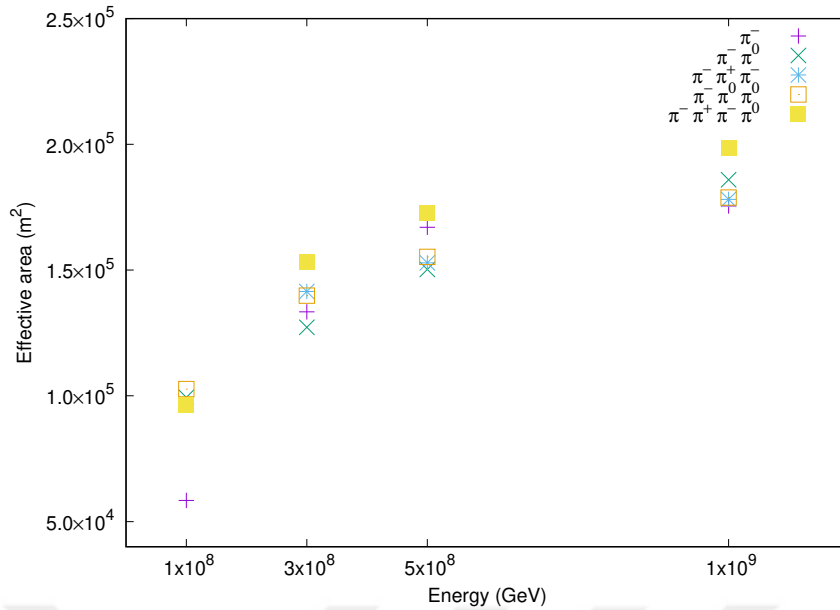


Figure 4.22. The effective area of TAUWER array for all decay channels and development lengths.

4.2.6 Arrival Direction Estimation

The estimation of the arrival direction has an important role on the reconstruction of the extensive air showers. Many different techniques have been performed (Acharya et al., 1993; Aglietta et al., 1993; Ashton et al., 1979; Kh, 2016; Krawczynski et al., 1996; Mayer, 1993). The arrival direction may be estimated with the arrival times of the particles on the shower front using coordinates (x_i, y_i, z_i) of the detector stations. These particles are the first arrived shower front particles for flat detector arrays in contrast to inclined surface detector arrays like in a mountain surface. The first arrived particles to the arrays on the inclined plane are generally in the bottom edge of the shower front. But these particles do not give the information about the shower core. Therefore to accurately determine the shower core is important. Accordingly the arrival time of the core has to be precisely found. Then the time of the core is used in the determination of the arrival direction by *Chi-Square function*.

A good way to obtain the arrival direction of the primary particle is to get exact location of the shower core. In order to find the shower core, the location of the detectors on the mountain surface, how many particles are passed from this position and the shower information of these particles are recorded by counting the particles passing through the detectors. This information is used to find the shower core of the

particles on the detector distribution. In Equation 4.45, x_{core} , y_{core} , z_{core} , which are the core coordinates, are found to be weighted by the total number of coordinates of the particles. *Weight* means the number of the particles on the each detector.

$$x_{core} = \frac{\sum_i(x_i \cdot w_i)}{\sum_i(w_i)}, \quad y_{core} = \frac{\sum_i(y_i \cdot w_i)}{\sum_i(w_i)}, \quad z_{core} = \frac{\sum_i(z_i \cdot w_i)}{\sum_i(w_i)} \quad (4.45)$$

Afterwards, the coordinates of the shower core are found according to the weights of the particles, the core time is determined using the distance between the core location and the most triggered detector coordinates (x_{max} , y_{max} , z_{max}). The core distance is defined by following equation;

$$d_{core} = \sqrt{(x_{max} - x_{core})^2 + (y_{max} - y_{core})^2 + (z_{max} - z_{core})^2} \quad (4.46)$$

When the core location is upper than the location of the most triggered detector in terms of z coordinates, the core time t_{core} is found by subtracting the *correction value* from the first coming particle time of the most triggered detector otherwise it has to be adding. The *correction value* means the time frame that can be taken with the speed of light c to the distance d_{core} .

$$if \quad z_{max} > z_{core} \quad t_{core} = t_{max} - \frac{d_{core}}{c}, \quad (4.47)$$

$$if \quad z_{max} < z_{core} \quad t_{core} = t_{max} + \frac{d_{core}}{c}. \quad (4.48)$$

The estimation of the arrival direction is a basic procedure for reconstruction of an EAS. There are many kind of reconstruction procedure using different shower variables like the density and the coordinates of the particles and arrival time informations. Also the structure of the detector array is effective on the calculation of the arrival direction.

The more comprehensive investigations for the showers are started with the presence of the core location and time. In order to determine the arrival directions of the showers, a minimization is applied to the coordinates and time using the Minuit program (James and Roos, 1975). The most common method used in the literature for

finding of the arrival direction of the EAS is to fitting the recorded arrival time to the expected arrival time to detectors and minimize them as given below (Kh, 2016).

$$\chi^2 = \sum_{i=1}^N w_i (t_i^{exp} - t_i^{rec})^2 \quad (4.49)$$

where N is the number of stations and w_i is the total number of the particles in each station and it called as *weight*. The simplest form of t^{exp} is given by the Plane Front Approximation and the plane is

$$\hat{\mathbf{n}} \cdot (\mathbf{r}_i - \mathbf{r}_{core}) = c \cdot (t_i - t_{core}) \quad (4.50)$$

where $\hat{\mathbf{n}} = (n_x, n_y, n_z)$ is the unit vectors on the EAS shower axis. If this equation is rewritten;

$$n_x(x_i - x_{core}) + n_y(y_i - y_{core}) + n_z(z_i - z_{core}) = c(t_i - t_{core}) \quad (4.51)$$

The minimization of χ^2 solution in the limit of $n_x^2 + n_y^2 + n_z^2 = 1$ is;

$$\chi^2 = \sum_i^N w_i (n_x(x - x_{core}) + n_y(y - y_{core}) + n_z(z - z_{core}) - c(t_i - t_{core}))^2 \quad (4.52)$$

After this step, by obtaining the normal vectors of the shower plane as n_x, n_y, n_z , the arrival direction of the shower is determined.

$$\begin{aligned} n_x^2 x_i^2 + n_y^2 y_i^2 + n_z^2 z_i^2 + 2n_x n_y x_i y_i + 2n_x n_z x_i z_i + 2n_y n_z y_i z_i - 2c n_x x_i (t_i - t_{core}) - \\ 2c n_y y_i (t_i - t_{core}) - 2c n_z z_i (t_i - t_{core}) + c^2 (t_i - t_{core})^2 \end{aligned} \quad (4.53)$$

When the function in minimization is written as a more clear statement, the new expression is in Equation 4.53.

$$\frac{\partial \chi^2}{\partial n_x} = 0, \quad \frac{\partial \chi^2}{\partial n_y} = 0, \quad \frac{\partial \chi^2}{\partial n_z} = 0, \quad \frac{\partial \chi^2}{\partial t_{core}} = 0 \quad (4.54)$$

The new expression is now suitable to apply the solutions on Equation 4.54. For each normal of the plane, the partial derivatives are applied and they give 4 equations in below;

$$2n_x \langle x_i^2 \rangle + 2n_y \langle x_i \cdot y_i \rangle + 2n_z \langle x_i \cdot z_i \rangle + 2ct_{core} \langle x_i \rangle = 2c \langle x_i \cdot t_i \rangle \quad (4.55)$$

$$2n_x \langle x_i \cdot y_i \rangle + 2n_y \langle y_i^2 \rangle + 2n_z \langle y_i \cdot z_i \rangle + 2ct_{core} \langle y_i \rangle = 2c \langle y_i \cdot t_i \rangle \quad (4.56)$$

$$2n_x \langle x_i \cdot z_i \rangle + 2n_y \langle y_i \cdot z_i \rangle + 2n_z \langle z_i^2 \rangle + 2ct_{core} \langle z_i \rangle = 2c \langle z_i \cdot t_i \rangle \quad (4.57)$$

$$2cn_x \langle x_i \rangle + 2cn_y \langle y_i \rangle + 2cn_z \langle z_i \rangle + 2c^2 t_{core} = 2c^2 \langle t_i \rangle \quad (4.58)$$

where;

$$\langle x_i \rangle = \frac{1}{w_i} \sum_{i=1}^N x_i, \quad \langle x_i^2 \rangle = \frac{1}{w_i} \sum_{i=1}^N x_i^2, \quad \langle x_i t_i \rangle = \frac{1}{w_i} \sum_{i=1}^N x_i t_i, \dots \quad (4.59)$$

and so on. The Equations 4.56- 4.58 are simultaneous equations and they can be solved using matrices. When these four simultaneous equations are put to matrix form,

$$\begin{pmatrix} 2\langle x_i^2 \rangle & 2\langle x_i \cdot y_i \rangle & 2\langle x_i \cdot z_i \rangle & 2c\langle x_i \rangle \\ 2\langle x_i \cdot y_i \rangle & 2\langle y_i^2 \rangle & 2\langle y_i \cdot z_i \rangle & 2c\langle y_i \rangle \\ 2\langle x_i \cdot z_i \rangle & 2\langle y_i \cdot z_i \rangle & 2\langle z_i^2 \rangle & 2c\langle z_i \rangle \\ 2c\langle x_i \rangle & 2c\langle y_i \rangle & 2c\langle z_i \rangle & 2c^2 \end{pmatrix} \cdot \begin{pmatrix} n_x \\ n_y \\ n_z \\ t_{core} \end{pmatrix} = \begin{pmatrix} 2c\langle x_i \cdot t_i \rangle \\ 2c\langle y_i \cdot t_i \rangle \\ 2c\langle z_i \cdot t_i \rangle \\ 2c^2 \langle t_i \rangle \end{pmatrix} \quad (4.60)$$

the solutions of the matrix form are;

$$n_x = \frac{\begin{pmatrix} 2c\langle x_i \cdot t_i \rangle & 2\langle x_i \cdot y_i \rangle & 2\langle x_i \cdot z_i \rangle & 2c\langle x_i \rangle \\ 2c\langle y_i \cdot t_i \rangle & 2\langle y_i^2 \rangle & 2\langle y_i \cdot z_i \rangle & 2c\langle y_i \rangle \\ 2c\langle z_i \cdot t_i \rangle & 2\langle y_i \cdot z_i \rangle & 2\langle z_i^2 \rangle & 2c\langle z_i \rangle \\ 2c^2 \langle t_i \rangle & 2c\langle y_i \rangle & 2c\langle z_i \rangle & 2c^2 \end{pmatrix}}{\begin{pmatrix} 2\langle x_i^2 \rangle & 2\langle x_i \cdot y_i \rangle & 2\langle x_i \cdot z_i \rangle & 2c\langle x_i \rangle \\ 2\langle x_i \cdot y_i \rangle & 2\langle y_i^2 \rangle & 2\langle y_i \cdot z_i \rangle & 2c\langle y_i \rangle \\ 2\langle x_i \cdot z_i \rangle & 2\langle y_i \cdot z_i \rangle & 2\langle z_i^2 \rangle & 2c\langle z_i \rangle \\ 2c\langle x_i \rangle & 2c\langle y_i \rangle & 2c\langle z_i \rangle & 2c^2 \end{pmatrix}} \quad (4.61)$$

$$n_y = \frac{\begin{pmatrix} 2\langle x_i^2 \rangle & 2c\langle x_i \cdot t_i \rangle & 2\langle x_i \cdot z_i \rangle & 2c\langle x_i \rangle \\ 2\langle x_i \cdot y_i \rangle & 2c\langle y_i \cdot t_i \rangle & 2\langle y_i \cdot z_i \rangle & 2c\langle y_i \rangle \\ 2\langle x_i \cdot z_i \rangle & 2c\langle z_i \cdot t_i \rangle & 2\langle z_i^2 \rangle & 2c\langle z_i \rangle \\ 2c\langle x_i \rangle & 2c^2\langle t_i \rangle & 2c\langle z_i \rangle & 2c^2 \end{pmatrix}}{\begin{pmatrix} 2\langle x_i^2 \rangle & 2\langle x_i \cdot y_i \rangle & 2\langle x_i \cdot z_i \rangle & 2c\langle x_i \rangle \\ 2\langle x_i \cdot y_i \rangle & 2\langle y_i^2 \rangle & 2\langle y_i \cdot z_i \rangle & 2c\langle y_i \rangle \\ 2\langle x_i \cdot z_i \rangle & 2\langle y_i \cdot z_i \rangle & 2\langle z_i^2 \rangle & 2c\langle z_i \rangle \\ 2c\langle x_i \rangle & 2c\langle y_i \rangle & 2c\langle z_i \rangle & 2c^2 \end{pmatrix}} \quad (4.62)$$

$$n_z = \frac{\begin{pmatrix} 2\langle x_i^2 \rangle & 2\langle x_i \cdot y_i \rangle & 2c\langle x_i \cdot t_i \rangle & 2c\langle x_i \rangle \\ 2\langle x_i \cdot y_i \rangle & 2\langle y_i^2 \rangle & 2c\langle y_i \cdot t_i \rangle & 2c\langle y_i \rangle \\ 2\langle x_i \cdot z_i \rangle & 2\langle y_i \cdot z_i \rangle & 2c\langle z_i \cdot t_i \rangle & 2c\langle z_i \rangle \\ 2c\langle x_i \rangle & 2c\langle y_i \rangle & 2c^2\langle t_i \rangle & 2c^2 \end{pmatrix}}{\begin{pmatrix} 2\langle x_i^2 \rangle & 2\langle x_i \cdot y_i \rangle & 2\langle x_i \cdot z_i \rangle & 2c\langle x_i \rangle \\ 2\langle x_i \cdot y_i \rangle & 2\langle y_i^2 \rangle & 2\langle y_i \cdot z_i \rangle & 2c\langle y_i \rangle \\ 2\langle x_i \cdot z_i \rangle & 2\langle y_i \cdot z_i \rangle & 2\langle z_i^2 \rangle & 2c\langle z_i \rangle \\ 2c\langle x_i \rangle & 2c\langle y_i \rangle & 2c\langle z_i \rangle & 2c^2 \end{pmatrix}} \quad (4.63)$$

Too much calculations have been implemented to obtain the normal vectors n_x , n_y , n_z of the shower plane. The results provide the condition of $n_z^2 = 1 - n_x^2 + n_y^2 < 0$.

The equations are solved and they give the results in below;

$$\begin{aligned} \theta &= \cos^{-1}(n_z) \\ \phi &= \sin^{-1}\left(\frac{n_y}{\sin(\theta)}\right) \end{aligned} \quad (4.64)$$

On the other hand, the reconstructions of the arrival direction of the EAS are also performed by the minimization of the χ^2 fit with same variables of the EAS. All the minimization procedure is applied by the Minuit of the CERN library. This application provides to save the time.

The arrival direction of the τ induced shower is calculated with the core locations and the core time based on the minimization of the normal vectors of each plane by both hand solving and the Minuit library. The coordinates of the stations which

triggered by the e^\pm and their arrival times are put into the calculation of the normal vectors (n_x, n_y, n_z) of the EAS.

The core location $(x_{core}, y_{core}, z_{core})$ is determined using number of particles and the locations of the detectors. For the arrival direction of the shower the number of the e^\pm are selected at least 2 in a station then these stations are taken into account. Also the energy of the primary particle range between $100 PeV$ and $1000 PeV$ with $7 km$ development length.

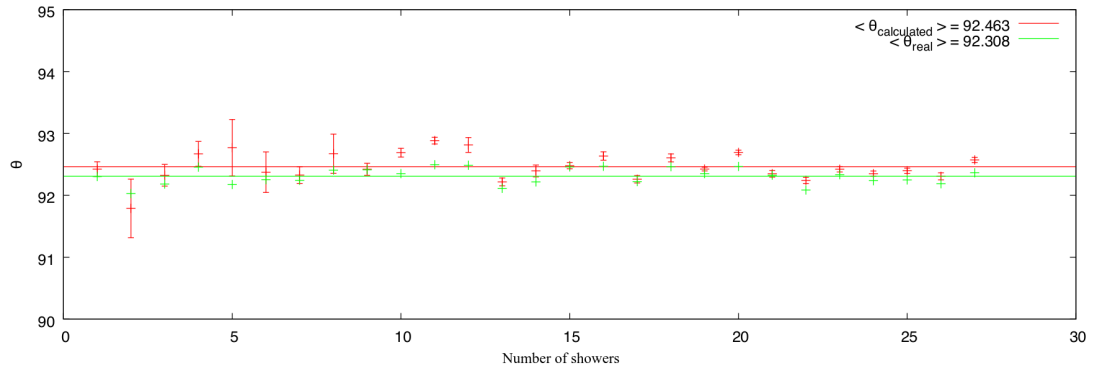


Figure 4.23. The zenith angles θ for 27 different showers are evaluated from at least 2 triggered stations.

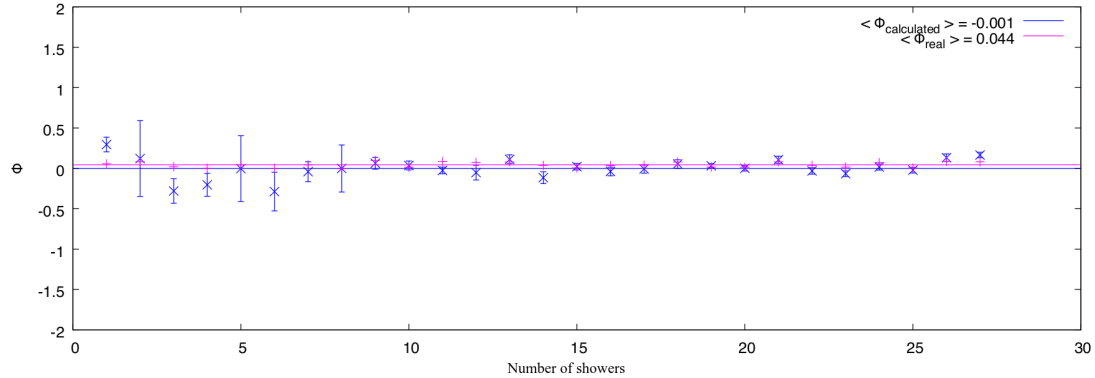


Figure 4.24. The azimuthal angles ϕ for 27 different showers are evaluated from at least 2 triggered stations.

The Figures 4.23 and 4.24 shows the arrival directions which θ and ϕ for 27 different shower in the same energy range. The arrival directions θ and ϕ are estimated with an error of 0.16° and 0.045° , respectively. The detailed results for arrival direction are given in Appendix-B.

4.3 Effect of ECUT in the Analysis

CORSIKA has many properties in the creation of the EASs with several options. The user can configure the input card of CORSIKA to achieve the desired result. ECUT, is an option which defined as the low energy cut-off of the particle kinetic energy for hadrons, muons, electrons and photons.

The effect of the different ECUT values is investigated in terms of the detected particles in two different primary particle energy range for $\pi^- \pi^0$ decay channel. Shower development length is selected as 5 km and the shower energy changes between $10^7 \text{ GeV} - 5 \times 10^8 \text{ GeV}$. The energy ranges grouped as low and high for $\sim 10^7 \text{ GeV}$ and $\sim 10^8 \text{ GeV}$ and each group has 9 showers. The chosen ECUTs are 0.05 GeV and 0.1 GeV for both hadrons and muons in this study. The results of doubling the energy cut is compared for particle distribution on the same detector array distributed on the mountain slope for upward τ induced shower detection and these results are published (Atik Yılmaz et al., 2018).

The array with a large zenith angle is constructed as an inclined plane on a mountain surface to catch the Earth Skimming ν_τ . The analyzation is made to determine the number of particles (total, γ , e^\pm , μ^\pm) on the mountain surface, array, the center of the shower and the width of the shower in 2 direction (y, z) as well as the reconstruction of shower directions (zenith and azimuthal angles) with different arrival directions. The width of the shower is defined from the number of hits on the detectors. The different ECUT values and shower energies are related with the analysis.

The total number of particles (all types) are shown in Figure 4.25(a) as on the inclined plane, on the array and around the center of the array with blue, red and green colors, respectively. The energy scale is lower and ECUT value is 0.1 GeV for hadrons and muons. Figure 4.25(b) is also for low energy scale with ECUT in 0.1 GeV case for hadrons and muons. It shows that μ^\pm numbers on the inclined plane, array and around the center of the array with blue, red and green colors, respectively. In Figure 4.25(c) for each showers, the diameter of the showers (in y, z directions) are plotted from the detected particles in the stations. The diameter of the showers are approximately 140 m and 136 m for y and z directions, respectively. Figure 4.25(d), 4.25(e) and 4.25(f) are for ECUT value of 0.05 GeV for hadrons and muons. When the results are compared with the ECUT value applied as 0.05 GeV , the total number of

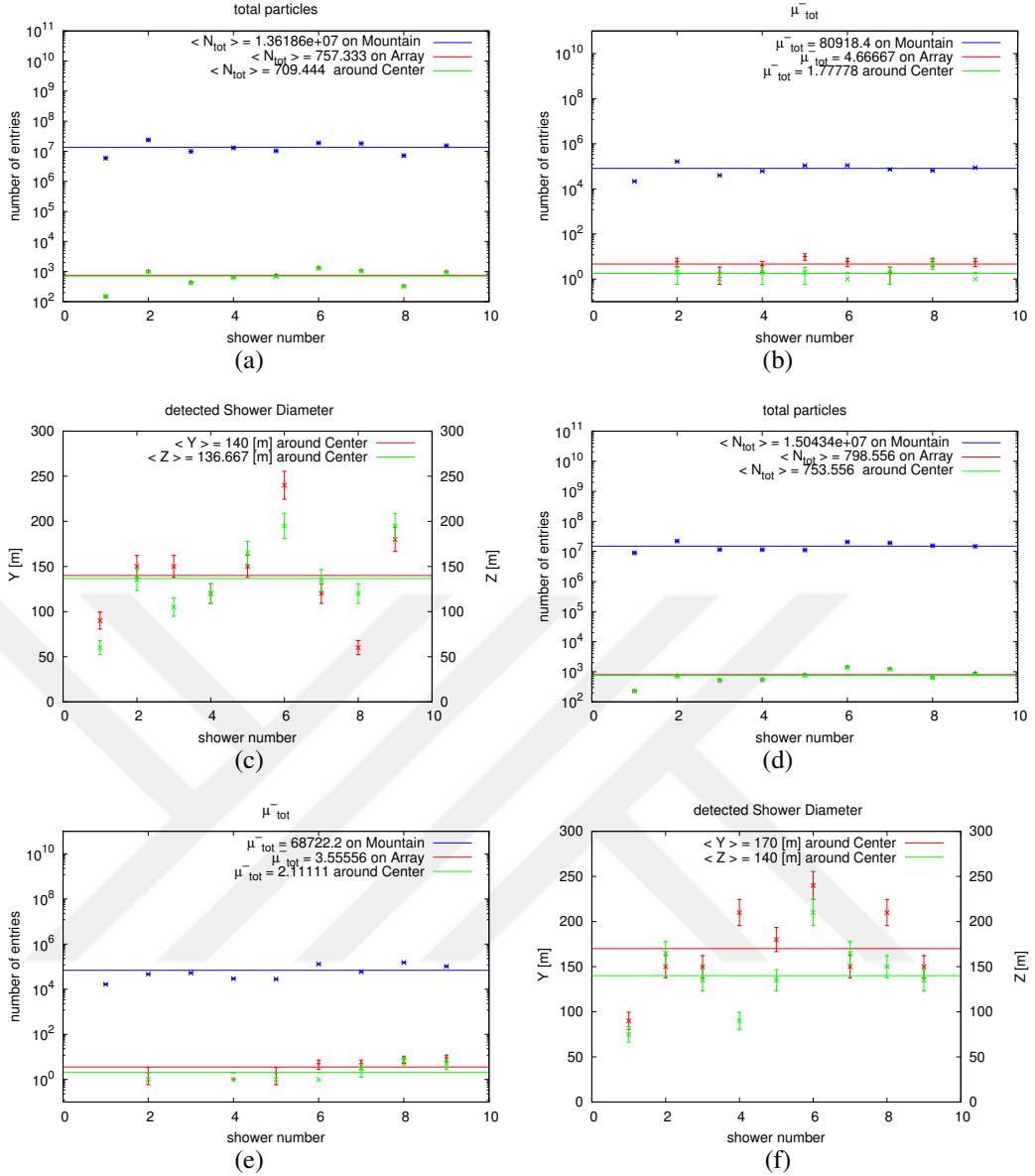


Figure 4.25. For low energy scale the number of particles for (a) all, (b) μ^\pm and (c) the shower diameters in y-z directions for 0.1 GeV ECUT, (d) total number of particles, (e) μ^\pm number of particles and (f) the shower diameters in y-z directions for 0.05 GeV ECUT.

particles on the mountain plane, on the array and around the center of the array increase as 10%, 5% and 6%, respectively. The ECUT for hadrons and muons is reduced by half, the number of μ^\pm decreases on mountain plane and stay within the statistics error on the array and around the center of the array. The average diameter of 9 different showers increases 30 m in y direction and decreases 4 m in z direction when the ECUT value is 0.05 GeV. Furthermore the area of the showers increases as 19% approximately with

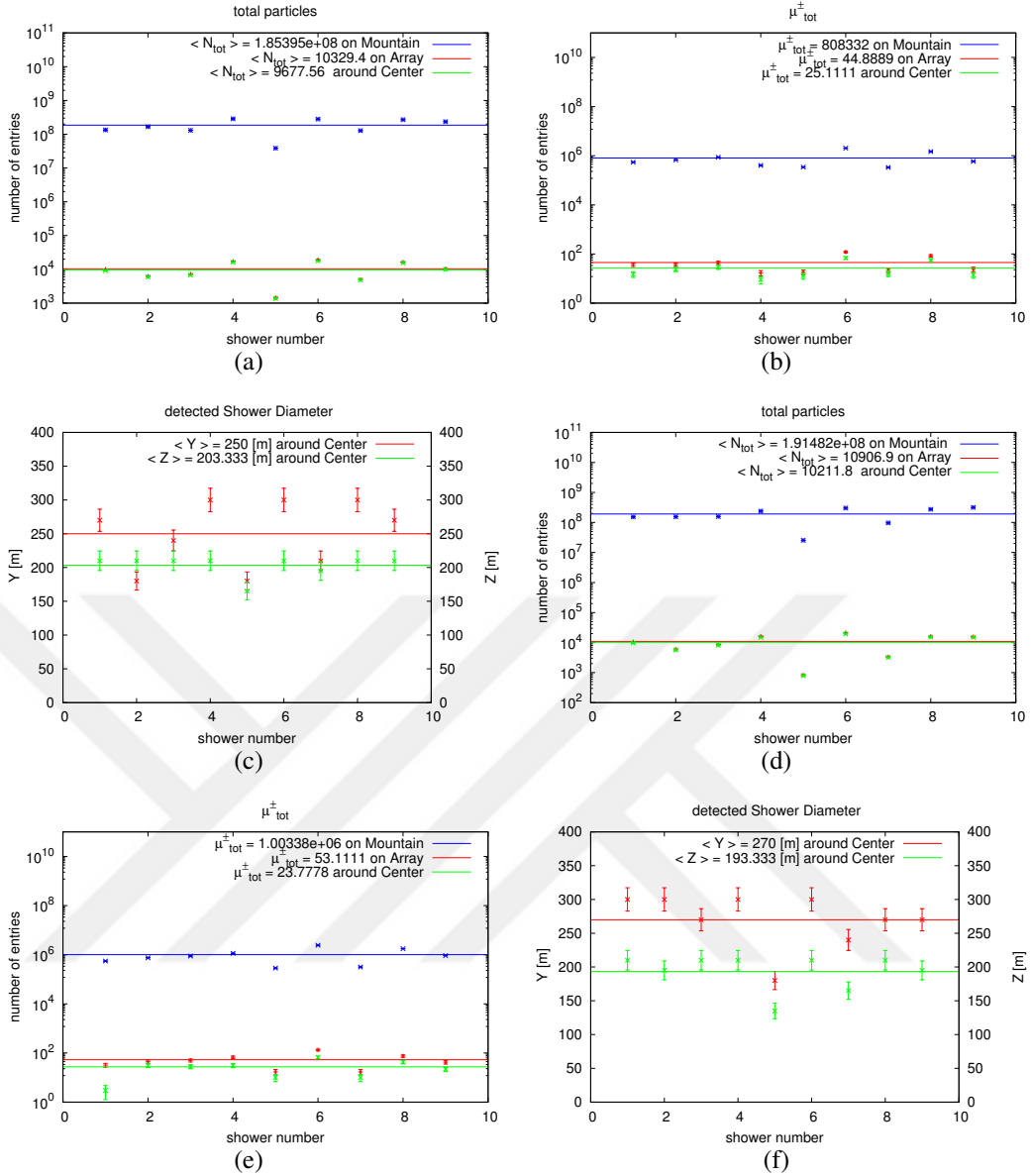


Figure 4.26. For high energy scale the number of particles for (a) all, (b) μ^\pm and (c) the shower diameters in y-z directions for 0.1 GeV ECUT, (d) total number of particles, (e) μ^\pm number of particles and (f) the shower diameters in y-z directions for 0.05 GeV ECUT.

the decreasing of ECUT on hadrons and muons.

Figure 4.26(a), (b) and (c) show the total number of particles and the number of μ^\pm on the detection plane and the diameters of showers in high energy scale for ECUT value equals to 0.1 GeV and when ECUT value equals to 0.05 GeV they are shown in Figure 4.26(d), (e) and (f). When the ECUT value is changed from 0.1 GeV to 0.05

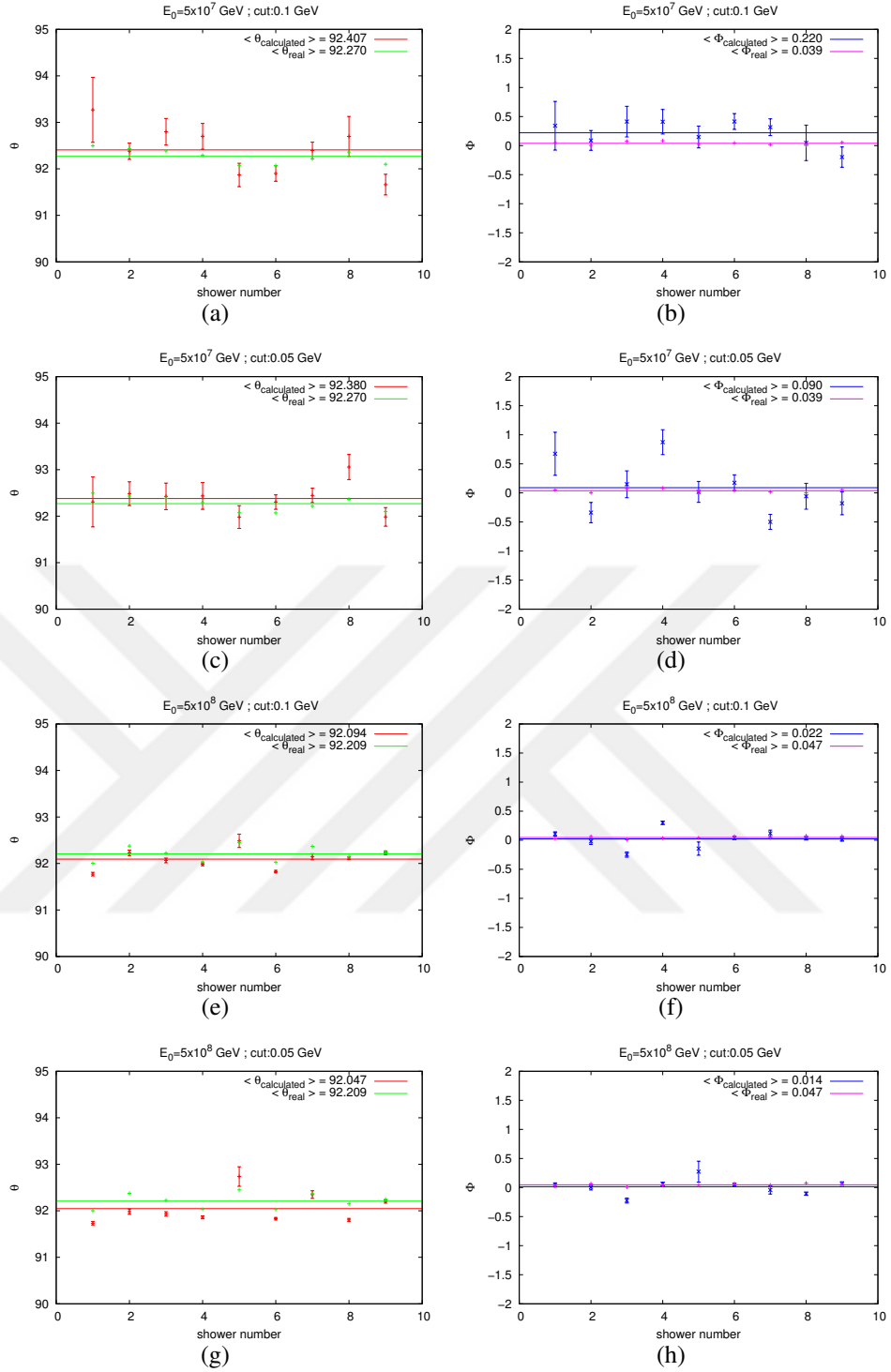


Figure 4.27. The simulated arrival directions; $\theta_{calculated}$ for hadrons ECUT (a) 0.1 GeV, (c) 0.05 GeV in low energy scale, (e) 0.1 GeV, (g) 0.05 GeV in high energy scale, $\phi_{calculated}$ for hadrons ECUT (b) 0.1 GeV, (d) 0.05 GeV in low energy scale, (f) 0.1 GeV and (h) 0.05 GeV in high energy scale.

GeV the number of total particles increases about 3% on the mountain surface, 6% on

the detector plane and around the center of the detector array. Also the number of μ^\pm on the mountain surface and the detector array increases while around the center of the array is not changing. The size of the shower on the inclined plane which specified from trigger at least 5 hits in the stations, is not changing by the reducing of the ECUT value. The diameter of the showers are 250 m in y direction and it increases 20 m and 203 m in z direction and it decreases as 10 m. Therefore the area of the showers increases as 4% approximately with the decreasing of ECUT on hadrons and muons. The area at the low energy scale increases more than at the high energy scale due to the smaller increase on the diameter in y direction and the decrease in the z direction.

The arrival directions (θ and ϕ) are calculated by the procedure which given in Section 4.2.6. The calculated arrival directions of the simulated showers are shown in Figure 4.27. The arrival directions are not affected significantly by changing the ECUT on hadrons and muons. In the low energy scale $\theta_{calculated}$ is 0.14° off for 0.1 GeV hadron ECUT and 0.11° off for 0.05 GeV hadron ECUT while $\phi_{calculated}$ is 0.18° off for 0.1 GeV hadron ECUT and 0.05° off for 0.05 GeV hadron ECUT. In the high energy scale $\theta_{calculated}$ has 0.12° off for 0.1 GeV, 0.16° off for 0.05 GeV and $\phi_{calculated}$ has nearly 0.03° off for both hadron ECUT values.

4.4 Estimation the Number of Expected Shower

The knowledge about the UHECRs are still in an insufficient level depending the low amount of data especially for the energies above 1000 PeV. Many collaboration have been developed different types of array Aartsen et al. (2017); Abbasi et al. (2013); Abeysekara et al. (2013); Abreu et al. (2012a); Bellido et al. (2001); Sokolsky (2011); The Pierre Auger Collaboration et al. (2015) to detect or collect the information about the cosmic rays. Also the ultrahigh energy neutrinos can be detected with the ground based detector arrays both coming from the atmosphere (downward going) or from the Earth crust (upward going or Earth skimming) especially for the tau neutrinos (Aartsen et al., 2016; Abreu et al., 2012b; Aramo et al., 2005; Asaoka and Sasaki, 2013; Iori et al., 2014). The ν_τ detection is important due to have knowledge about the astrophysical ν_τ flux and the origins of them. Up to now there has been no distinct detection of the high energetic ν_τ . In this section, the number of the showers on the TAUWER array is estimated using different ν flux upper limits reported by IceCube

from 3 and 9 years of data, respectively (Aartsen et al., 2016, 2014), (Aartsen et al., 2018).

In this section, the probabilities for neutrino's charged-current interaction with the Earth shell and decay of generated τ lepton will be estimated. By combining them together the probabilities of showers generated from τ neutrinos with different energies and incident angles is derived. The simulation results of the expected shower for TAUWER array will also be displayed at the end of this section and comparisons will be made between these results for latest upper limit fluxes.

4.4.1 Probability Calculations

The ν_τ flux is depended to the neutrino cross section because of they formed in the neutrino conversion to tau lepton. The number of expected shower on the array depends to the neutrino flux, the cross section of the interaction and the target. So the cross section has to be known to determine how many shower can be observed in this array.

There are two types of neutrino interactions; charged - current interaction and neutral current interaction. In charged - current interaction, the neutrino is converted to the charged lepton and in neutral current interaction, the neutrino transfers its energy and momentum to the interacted particle. The charged - current interactions happen with the changing of a W^\pm boson, while in neutral current interactions Z^0 is changed.

The interaction of the ν_τ with the nucleus in the Earth shell through charged - current interaction is interested since a τ lepton to generate a shower for detection on the TAUWER array. The charged-current interaction can be represented as,

$$\nu_\tau N \rightarrow \tau X \quad (4.65)$$

where N is a nucleus.

The cross section for charged-current interaction of neutrino between the energy 10 PeV and 10^6 PeV according to *CTEQ4-DIS* within 10% based on the study by (Gandhi et al., 1998) as;

$$\sigma_{CC} = 5.53 \times 10^{-36} \text{cm}^2 \left(\frac{E_\nu}{1\text{GeV}} \right)^{0.363} \quad (4.66)$$

where E_ν is the energy of neutrino.

The neutrino interaction length L_{int} in rock can be derived as

$$L_{int} = \frac{1}{\sigma_{CC} N_A \rho_{rock} / A} \quad (4.67)$$

where $N_A = 6.022 \times 10^{23} mol^{-1}$ is the Avogadro's number, $\rho_{rock} = 2.65 g/cm^3$ is the density of rock and $A = 1 g/mol$ is the molar mass of neutron. The tau neutrino ν_τ has short interaction length in rock at high energies than lower energies as in Figure 4.28. The charged - current interaction length of τ neutrino is about 1818 km for 50 PeV and 613 km for 1000 PeV.

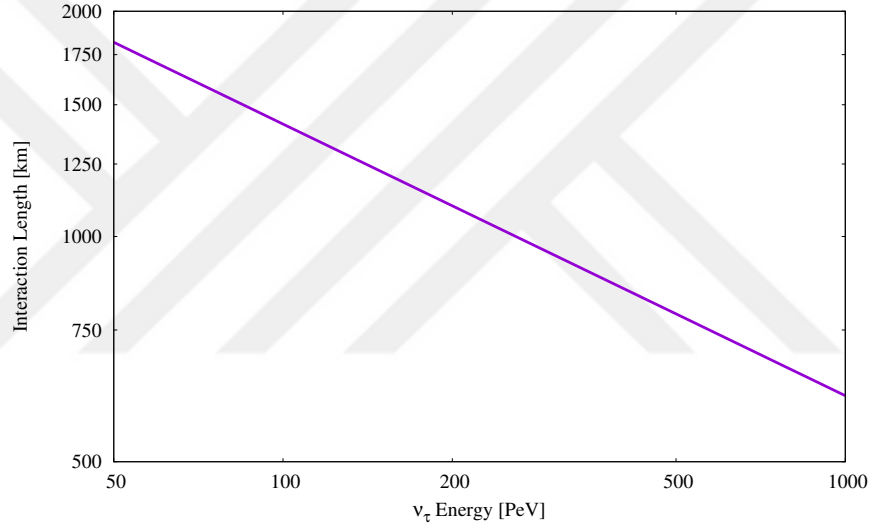


Figure 4.28. The interaction length of neutrino in rock with respect to neutrino initial energy.

The probability of ν_τ traveling from inserting point to the point of the charged - current interaction happens in rock is obtained by the formula;

$$P_{int} = \int_0^L e^{-\frac{(L-x)}{L_{int}}} \frac{dx}{L_{int}} \quad (4.68)$$

where L is the path through the Earth's crust and $(L - x)$ is the traveling distance before the interaction. The distance L integrated as 50 km and dx represents the short distance for the charged-current interaction with rock to generation of a τ lepton. Figure 4.29 shows the interaction probabilities of ν_τ for various initial neutrino energies in terms of traveling distance in rock. When neutrino travels along a mountain

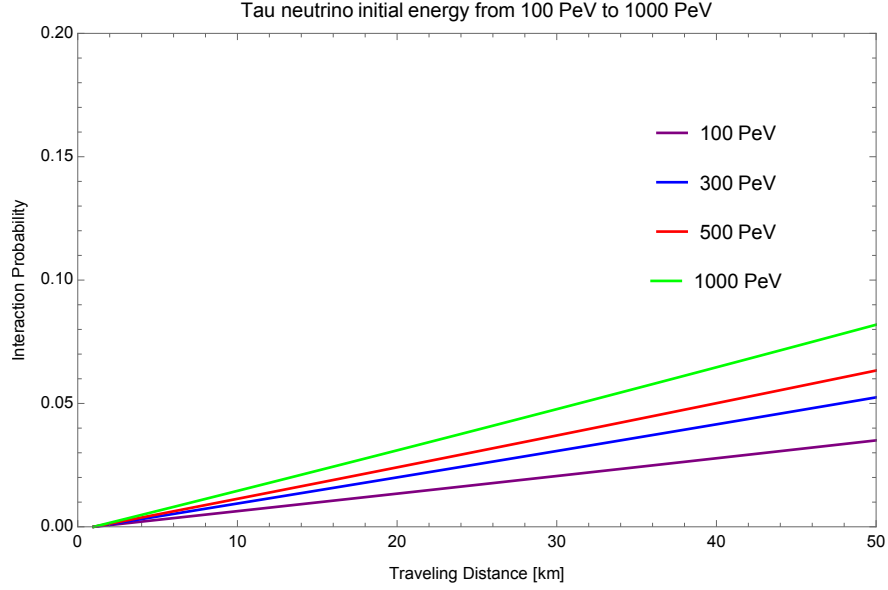


Figure 4.29. The neutrino interaction probability with respect to traveling distance in rock for different neutrino initial energies.

in front of the array as in upper left side of the Figure 4.30, we can use the relation $L = 2\pi R \cos(\pi - \theta)$ with $\theta \leq 90$ for the 'screening effect' and the radius of the Earth is $R = 6371$ km. The screen is selected as 100 km to obtain τ induced air shower.

As in Figure 4.30 the ν_τ travels a distance $(L - x)$ along the Earth's crust and interacts with the rock at the "*" point. It produces a τ lepton by the charged-current interaction, it travels through a distance (x) before emerging from the rock, hence it interacts with the atmosphere, and starts to develop a shower which can be detected by the array on the mountain slope.

In the simulations it also considered as; a mountain chain in front of the array shown in Figure 4.30 as a "screen" to improve the tau emerging shower produced when the neutrino interaction with the mountain chain. The thickness of the mountain chain is considered as 100 km. The initial energy of the τ is to be minimum 10 PeV to escape from the rock before its decay in order for both the Earth Skimming ν_τ method ($> 90^\circ$) and the mountain chain screen strategy ($\leq 90^\circ$). The threshold distance of travel between the interaction point and the surface of τ has to be enough to generate a shower in the air else the shower detection probability will be zero. So, the maximum traveling distance of τ may determined as 50 km in the Earth shell depending on its initial energy.

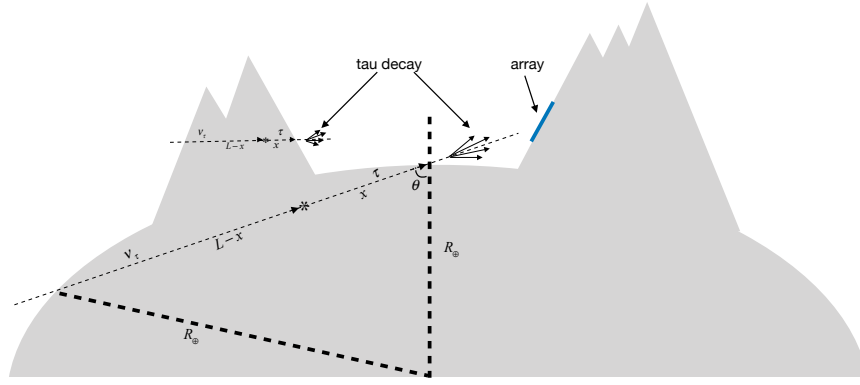


Figure 4.30. The geometrical view of the neutrino skimming from the Earth and using of a nearby mountain as a target while the τ induced shower emerging from the rock to the detector array (not in scale). $L-x$ is the interaction distance for the ν_τ , the interaction point shown as "*" symbol, x is the traveling distance for the τ , and R_\oplus is the Earth radius.

The lepton inelasticity for the interaction is defined as y ,

$$y \equiv \frac{E_\nu - E_\tau^i}{E_\nu} \quad (4.69)$$

where E_ν is the initial energy of ν_τ and E_τ^i is the energy of the τ lepton when it is generated. $\langle y \rangle$ is nearly 0.2 for the analytic approximations by Reference (Dutta et al., 2005). Dependently the average inelasticity, the tau energy E_τ^i is $0.8 E_\nu$. So, the τ lepton starts the traveling with the energy E_τ^i and it loss some of the energy which can be described as,

$$\left\langle \frac{dE_\tau}{dx} \right\rangle = -(\alpha + \beta E_\tau) \rho_{rock} \quad (4.70)$$

where dx is the traveling distance of tau in Earth's crust, α represents the ionization energy loss and is nearly $2 \times 10^{-3} \text{ GeVcm}^2/g$ and β represents the energy loss from Bremsstrahlung, pair production and photonuclear interaction.

The different cases are formed for β by Reference Dutta et al. (2005) to find the best result of Monte Carlo simulation and the following solution is selected for the related energy range for this study;

$$\beta = \beta_0 + \beta_1 \ln(E_\tau/E_0)$$

$$E_\tau = \exp\left[-\frac{\beta_0}{\beta_1}(1 - e^{\beta_1 \rho x}) + \ln\left(\frac{E_\tau^i}{E_0}\right)e^{-\beta_1 \rho x}\right] E_0 \quad (4.71)$$

where $\beta_0 = 1.2 \times 10^{-6} \text{ cm}^2/g$, $\beta_1 = 1.6 \times 10^{-7} \text{ cm}^2/g$ and $E_0 = 10^{10} \text{ GeV}$. According to the Equation 4.71, the energy of τ decreases when it travels. Also, depends on the energy of τ lepton, it can be escape from the rock before its decay. We need to define a threshold energy to detect the shower more than few tracks in the array and it is $E_{th} = 10 \text{ PeV}$. Thereby the x on the Equation 4.71 transform to X_{th} when $E_{th} = E_\tau(X_{th})$, the threshold distance of travel between the interaction point and the surface of τ has to be enough to generation of shower in the air else the shower detection probability is zero. So, the maximum traveling distance of τ is 50 km in the Earth shell based on its initial energy.

The survival probability of the tau can be represented in terms of the distance it passed Dutta et al. (2005);

$$\frac{dP_{surv}}{dx} = -\frac{P_{surv}}{ct_0 E_\tau/m_\tau} \quad (4.72)$$

where t_0 is the life time of τ lepton.

$$\frac{dP_{surv}}{P_{surv}} = -\frac{dx}{ct_0 E_\tau/m_\tau} = -f(x)dx \quad (4.73)$$

where $f(x) = \frac{dx}{ct_0 E_\tau/m_\tau}$

With Equation 4.73, the survival probability of tau is derived with the knowledge of $E_\tau = E_\tau(x)$

$$P_{surv} = N e^{-\int_0^x f(x)dx} \quad (4.74)$$

where N is the normalization coefficient. Before the tau starts traveling, it is on 0 position so, the survival probability is 1 and N can be calculated as;

$$\begin{aligned}
P_{surv}|_{x=0} &= 1 \\
N &= 1 \\
E_\tau(x) &= \exp\left(-\frac{\beta_0}{\beta_1} + \left(\frac{\beta_0}{\beta_1} + \ln(E_{tau}^i/E_0)\right)e^{-\beta_1\rho x}\right)E_0 \\
P_{surv} &= \exp\left[-\int_0^x \frac{1}{ct_0 E_\tau(x)/m_\tau} dx\right]
\end{aligned} \tag{4.75}$$

where $t_0 = 2.906 \times 10^{-13}$ s is the mean life time of τ lepton and the mass of τ is $m_\tau = 1776.82$ MeV in Equation 4.75. Figure 4.31 shows the survival probabilities of τ leptons with several initial energies versus the distance they passed. As can be seen from the graph, the survival probability is exponentially decreasing while the thickness of the rock was increasing.

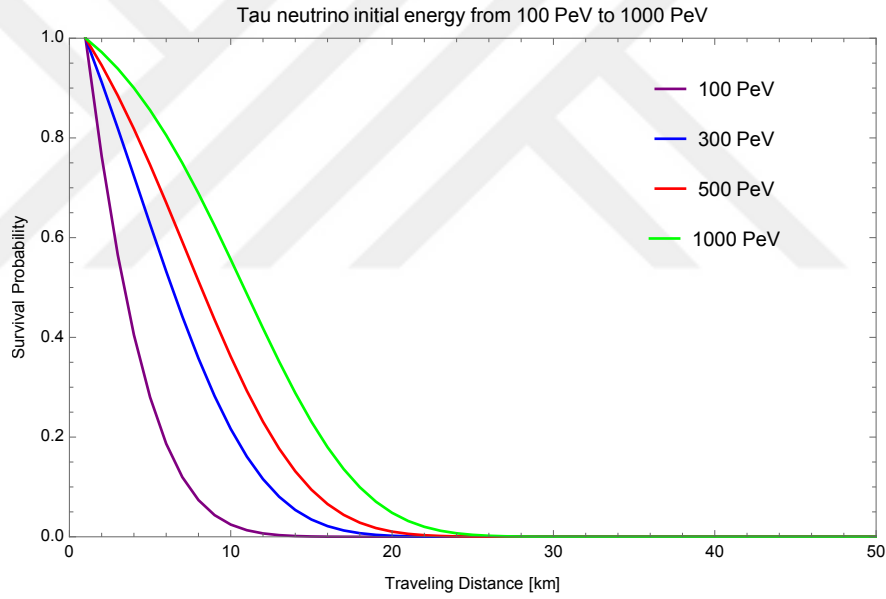


Figure 4.31. The neutrino survival probability with respect to traveling distance in rock for different initial energies.

Finally, the escape probability can be obtained by the integration of the interaction probability for ν_τ and the survival probability for τ to various energies, path length and incline angle as in follows;

$$\begin{aligned}
P_{escape} &= \int P_{int} P_{surv} \\
&= \int_0^L dx e^{-(L-x)/L_{int}} \frac{1}{L_{int}} \exp\left[-\int_0^x \frac{1}{ct_0 E_\tau(x)/m_\tau} dx\right]
\end{aligned} \tag{4.76}$$

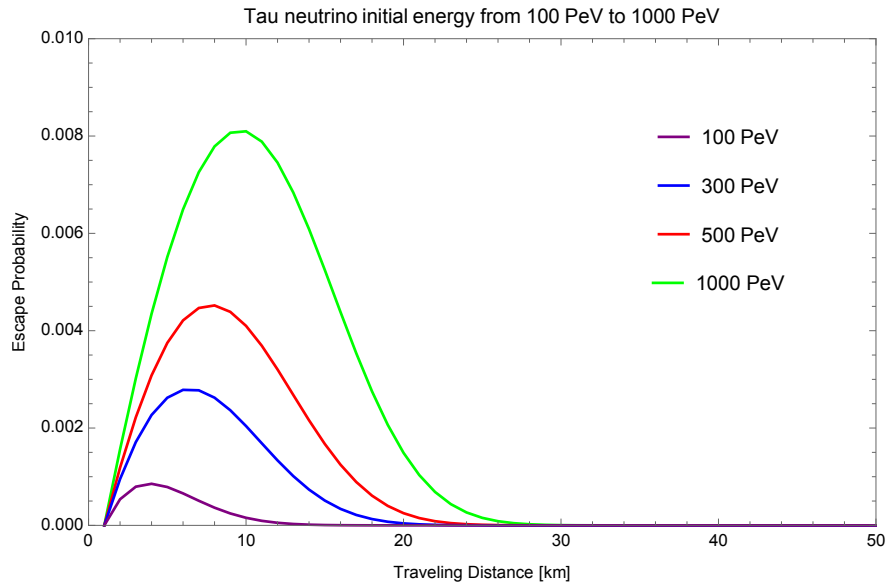


Figure 4.32. The escape probability of τ with respect to traveling distance for different initial energies.

The results for escape probability in terms of traveling distance of τ for different initial energies are in Figure 4.32.

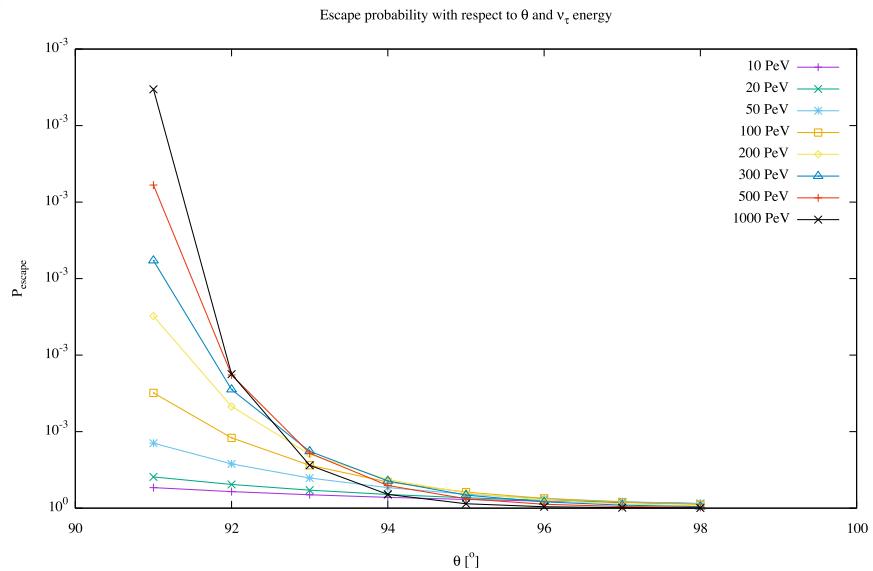


Figure 4.33. The escape probability of τ with respect to traveling distance for different escape directions from shell.

The escape probability values in Figure 4.33 are calculated for incident angle θ from 91 to 98 degree and the integral path is up to 50 km due to τ decay length.

The efficiency is determined by the number of stations having at least 1 hit over total number of stations. The efficiency is used to evaluate the number of the showers in the TAUWER array. The Figure 4.34 shows the efficiency of the TAUWER array in terms of decay channels for the 100 to 1000 PeV energy range.

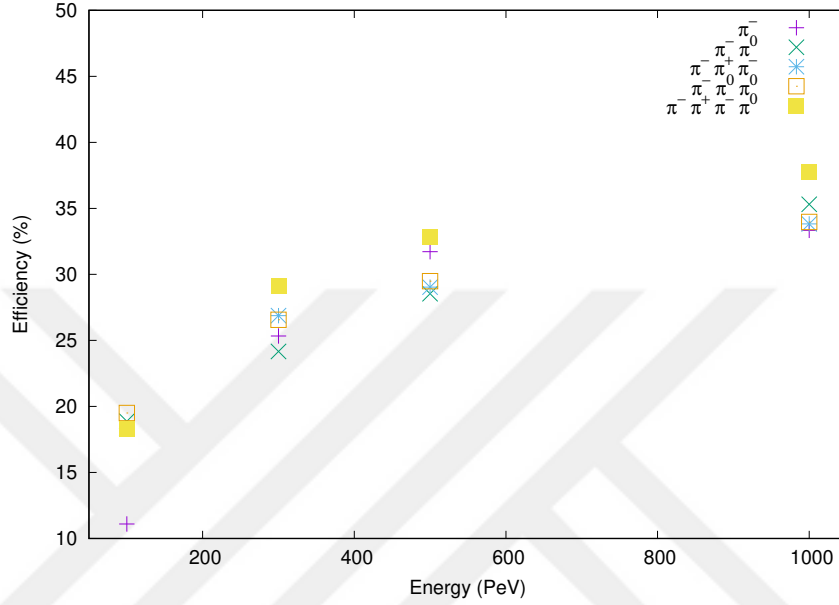


Figure 4.34. The efficiency of TAUWER array for all decay channels and energies.

4.4.2 Discussions

As discussed in Section 4.4.1, the ν_τ interaction length and its charged - current interaction probability are evaluated to calculate the τ survival and escape probabilities during traveling through the Earth and the mountain at PeV energies. Table 4.2 shows the τ escape probabilities calculated for different initial energies and escape directions from the Earth's crust. The escape probability calculations of each energy range are separately added to the calculation of the tau neutrino event N_τ to improve the statistics.

The present neutrino upper limit fluxes are accepted to calculate at the 90% confidence level of the ν_τ event for the TAUWER array. The estimation is calculated with;

Table 4.2. The escape probability with respect to θ and ν_τ energy

$\theta(\text{degree}) / \text{Energy (Pev)}$	10	20	50	100	200	300	500	1000
$\leq 90; L=100 \text{ km}$	3.221×10^{-4}	5.169×10^{-4}	1.180×10^{-3}	2.300×10^{-3}	4.327×10^{-3}	6.082×10^{-3}	9.027×10^{-3}	1.454×10^{-2}
91	2.681×10^{-4}	4.082×10^{-4}	8.490×10^{-4}	1.506×10^{-3}	2.510×10^{-3}	3.236×10^{-3}	4.223×10^{-3}	5.474×10^{-3}
92	2.164×10^{-4}	3.099×10^{-4}	5.782×10^{-4}	9.188×10^{-4}	1.329×10^{-3}	1.550×10^{-3}	1.741×10^{-3}	1.751×10^{-3}
93	1.747×10^{-4}	2.353×10^{-4}	3.938×10^{-4}	5.607×10^{-4}	7.044×10^{-4}	7.425×10^{-4}	7.180×10^{-4}	5.605×10^{-4}
94	1.410×10^{-4}	1.787×10^{-4}	2.683×10^{-4}	3.424×10^{-4}	3.734×10^{-4}	3.560×10^{-4}	2.963×10^{-4}	1.796×10^{-4}
95	1.139×10^{-4}	1.358×10^{-4}	1.829×10^{-4}	2.092×10^{-4}	1.982×10^{-4}	1.708×10^{-4}	1.224×10^{-4}	5.763×10^{-5}
96	9.203×10^{-5}	1.032×10^{-4}	1.248×10^{-4}	1.279×10^{-4}	1.052×10^{-4}	8.207×10^{-5}	5.066×10^{-5}	1.852×10^{-5}
97	7.438×10^{-5}	7.850×10^{-5}	8.517×10^{-5}	7.825×10^{-5}	5.596×10^{-5}	3.948×10^{-5}	2.100×10^{-5}	5.967×10^{-6}
98	6.015×10^{-5}	5.973×10^{-5}	5.819×10^{-5}	4.794×10^{-5}	2.980×10^{-5}	1.902×10^{-5}	8.718×10^{-6}	1.927×10^{-6}

$$N_\tau = \int_{E_{min}}^{E_{max}} \Phi(E) P_\tau(E) (\varepsilon(E) \times \beta_\tau) dE \Delta t \Delta A \Delta \Omega \quad (4.77)$$

where β_τ is tau branching ratios for π^- , $\pi^- \pi^0$, $\pi^- \pi^+ \pi^-$, $\pi^- \pi^0 \pi^0$, $\pi^- \pi^+ \pi^- \pi^0$ modes, ε is efficiency of detector array in terms of the energy range (10 – 1000 PeV), P_τ is the escape probability of τ , 1 year period for Δt , 0.5 km^2 area and 7 km shower development length. To evaluate the events, two scenarios have been taken into account by the Equation 4.77: Earth-Skimming method and the mountain cabin screen strategy.

Table 4.3. The number of events for TAUWER array corresponding to the different upper limit flux in $\text{km}^{-2} \text{sr}^{-1}$ per year.

Flux	Scenario	Energy range (PeV)	N_{event}
$2 \times 10^{-8} (\text{GeV cm}^{-2} \text{s}^{-1} \text{sr}^{-1})$ (all flavor) (Aartsen et al., 2018)	Skimming	[100 – 1000]	0.005
	Skimming	[10 – 1000]	0.08
	Screen	[10 – 1000]	0.09
	Skimming + Screen	[100 – 1000]	0.14
	Skimming + Screen	[10 – 1000]	0.17
$3 \times 10^{-8} (\text{GeV cm}^{-2} \text{s}^{-1} \text{sr}^{-1})$ (all flavor) (Aartsen et al., 2014)	Skimming	[100 – 1000]	0.008
	Skimming	[10 – 1000]	0.12
	Screen	[10 – 1000]	0.13
	Skimming + Screen	[100 – 1000]	0.21
	Skimming + Screen	[10 – 1000]	0.25
$5.1 \times 10^{-8} (\text{GeV cm}^{-2} \text{s}^{-1} \text{sr}^{-1})$ (ν_τ flavor) (Aartsen et al., 2016)	Skimming	[100 – 1000]	0.01
	Skimming	[10 – 1000]	0.21
	Screen	[10 – 1000]	0.22
	Skimming + Screen	[100 – 1000]	0.36
	Skimming + Screen	[10 – 1000]	0.43

The expected number of events by the TAUWER array was estimated using the latest neutrino flux upper limit reported by IceCube experiment (Aartsen et al., 2016, 2018, 2014). The results of different scenarios are summarized in Table 4.3. The TAUWER array has 0.17, 0.25, and 0.43 events in $\text{km}^{-2} \text{sr}^{-1}$ per year, respectively. If the integrated time is selected like in the IceCube's papers: the study done for 9

years Aartsen et al. (2018) and 3 years Aartsen et al. (2016, 2014), the expected event numbers for TAUWER array are 1.50, 0.75 and 3.83 in $km^{-2}sr^{-1}$, respectively.



5. CONCLUSIONS AND RECOMMENDATIONS

In Section 4.1, the unthinning method for restoring information lost in THIN option is described. The proof of this method is made with comparison of the thin and unthinning showers in terms of the particle distributions on the mountain surface. The results shows that there is no deviation for the distribution on the inclined plane.

The Section 4.2 summarizes the particle variation in terms of types, their arrival times, the energy reconstruction procedure, corrected mean arrival time, spherical shower front, thickness for the inclined showers and also the array properties such as, acceptance and effective area. The properties of the TAUWER array are investigated and the results show that the TAUWER array can detect all the simulated showers in this study.

In Section 4.2.6, the main purpose is to determine the arrival directions of the inclined showers detected on TAUWER array. In order to obtain the arrival directions, the core location and the time for the shower core are used. The arrival direction estimation are performed from the coordinates of the detectors on the array, the arrival time of the particles and the number of the particles on the detectors. The core location is achieved with a good precision, and the arrival directions are determined below 0.5 degree for all simulated decay modes, energies and development lengths.

In Section 4.3, the focus is on two goals. The first is to observe more muons in the array with the reducing of the energy cut-off for both hadrons and muons. The second goal is to analogise the performance of the array in terms of particle distributions, shower diameter and arrival direction when reducing the energy cut-off to half value. The total number of particles are comparatively changed with the reducing of ECUT to half. Also the ECUT is more efficient on the high energy scale ($\sim 10^8$ GeV) in comparison with the low energy scale ($\sim 10^7$ GeV). When the ECUT is reduced by half the distribution of the muons on the high energy scale is raised. On the other hand the arrival directions $\theta_{calculated}$ and $\phi_{calculated}$ is not depending to the differences on the ECUT value considerably.

In Section 4.4 the estimation of the expected showers on TAUWER array is studied using the latest neutrino flux upper limits. The results of different scenarios are reported as TAUWER array has 0.17, 0.25, and 0.43 events in $km^{-2} sr^{-1}$ per

year, respectively. To improve the number of showers in TAUWER array the Earth Skimming method and mountain chain screen strategy are used together.

The thesis contains results which can be advisory about the optimization of TAUWER array, the placements of detectors and the determination of the trigger for different characteristic showers.



6. REFERENCES

- Aab A, Abreu P, Aglietta M, et al. (2017) "Observation of a large-scale anisotropy in the arrival directions of cosmic rays above $8 * 10^{18}$ eV", *Science*, 357(6357):1266–1270.
- Aartsen M, Ackermann M, Adams J, et al. (2017) "The IceCube Neutrino Observatory: instrumentation and online systems", *Journal of Instrumentation*, 12(03):P03012.
- Aartsen M et al. (2016) "Search for astrophysical tau neutrinos in three years of IceCube data", *Physical Review D*, 93(2).
- Aartsen M G, Ackermann M, Adams J, et al. (2018) "Differential limit on the extremely-high-energy cosmic neutrino flux in the presence of astrophysical background from nine Years of IceCube data", *Phys. Rev. D*, 98:062003.
- Aartsen M G, Ackermann M, et al. (2014) "Observation of High-Energy Astrophysical Neutrinos in Three Years of IceCube Data", *Phys. Rev. Lett.*, 113:101101.
- Abbasi R, Abdou Y, Ackermann M, et al. (2013) "IceTop: The surface component of IceCube", *Nuclear Instruments and Methods in Physics Research Section A: Accelerators, Spectrometers, Detectors and Associated Equipment*, 700:188–220.
- Abeyssekara A, Alfaro R, Alvarez C, et al. (2013) "Sensitivity of the high altitude water Cherenkov detector to sources of multi-TeV gamma rays", *Astroparticle Physics*, 50-52:26–32.
- Abraham J, Aglietta M, Aguirre C, et al. (2007) "An upper limit to the photon fraction in cosmic rays above 10^{19} eV from the Pierre Auger Observatory", *Astroparticle Physics*, 27(2):155–168.
- Abraham J, Aglietta M, Aguirre I, et al. (2004) "Properties and performance of the prototype instrument for the Pierre Auger Observatory", *Nuclear Instruments and Methods in Physics Research Section A: Accelerators, Spectrometers, Detectors and Associated Equipment*, 523(1):50–95.
- Abreu P, Aglietta M, Ahlers M, et al. (2012a) "Antennas for the detection of radio emission pulses from cosmic-ray induced air showers at the Pierre Auger Observatory", *Journal of Instrumentation*, 7(10):P10011.
- Abreu P, Aglietta M, Ahlers M, et al. (2012b) "Search for Point-like Sources of Ultra-high Energy Neutrinos at the Pierre Auger Observatory and Improved Limit on the Diffuse Flux of Tau Neutrinos", *The Astrophysical Journal Letters*, 755(1):L4.

- Acharya B S, Bhat P N, John A V, Khairatkar S G, Nagesh B K, Rajeev M R, Rao K S, Rao M V S, Reddy A, Sinha S, Sivaprasad K, Stanislaus A J, Venkateshmurthy B L, Vishwanath P R, Viswanathan K, Unnikrishnan P, Upadhya S S, et al. (1993) "Angular resolution of the KGF experiment to detect ultra high energy gamma-ray sources", *Journal of Physics G: Nuclear and Particle Physics*, 19(7):1053.
- Achterberg A, Ackermann M, Adams J, et al. (2006) "First year performance of the IceCube neutrino telescope", *Astroparticle Physics*, 26(3):155–173.
- Aglietta M, Alessandro B, Antonioli P, et al. (1993) "UHE cosmic ray event reconstruction by the electromagnetic detector of EAS-TOP", *Nuclear Instruments and Methods in Physics Research Section A: Accelerators, Spectrometers, Detectors and Associated Equipment*, 336(1):310–321.
- Agnetta G, Ambrosio M, Aramo C, et al. (1997) "Time structure of the extensive air shower front", *Astroparticle Physics*, 6(3):301–312.
- Antoni T, Apel W, Badea F, et al. (2003) "The cosmic-ray experiment KASCADE" *Nuclear Instruments and Methods in Physics Research Section A: Accelerators, Spectrometers, Detectors and Associated Equipment*, 513(3):490–510.
- Aramo C, Insolia A, Leonardi A, Miele G, Perrone L, Pisanti O and Semikoz, D. (2005) "Earth-skimming UHE tau neutrinos at the fluorescence detector of Pierre Auger Observatory", *Astroparticle Physics*, 23(1):65–77.
- Asaoka Y and Sasaki M (2013) "Cherenkov τ shower earth-skimming method for PeV–EeV ν_τ observation with Ashra", *Astroparticle Physics*, 41:7–16.
- Ashton F, Darjazi M. M S, Enderby M J, Nejabat H, Smith A C and Thompson M G (1979) "Determining the arrival directions of extensive air showers from fast timing measurements", In *16th International Cosmic Ray Conference. Vol. 12. Conference Papers. Og, Mg, SP, t. (Late Papers). Proceedings, Kyoto, Japan, August 6-18, 1979*, pages 371–376.
- Atik Yılmaz S, Yılmaz A, Denizli H and Oyulmaz K (2018) "Energy cutoff effect in CORSIKA on the detected particles of $\pi\pi^0$ decay channel", *Canadian Journal of Physics*, 96(7):673–676.
- Bazilevskaya G (2005) "Solar cosmic rays in the near Earth space and the atmosphere", *Advances in Space Research*, 35(3):458–464.
- Bellido J A, Clay R W, Dawson B R and Johnston-Hollitt M (2001) "Southern hemisphere observations of a 10^{18} eV cosmic ray source near the direction of the Galactic Centre", *Astroparticle Physics*, 15(2):167–175.
- Berndlöhr K (1999) "Cosmic-ray air showers", last visit at 18 October 2018.

- Bird D, Corbató S, Dai H, et al. (1994) "The calibration of the absolute sensitivity of photomultiplier tubes in the high resolution Fly's eye detector", *Nuclear Instruments and Methods in Physics Research Section A: Accelerators, Spectrometers, Detectors and Associated Equipment*, 349(2):592–599.
- Bird D J, Corbató S C, Dai H Y, et al. (1993) "Evidence for correlated changes in the spectrum and composition of cosmic rays at extremely high energies", *Phys. Rev. Lett.*, 71:3401–3404.
- Blasi P (2013) "Origin of Galactic Cosmic Rays", *Nuclear Physics B - Proceedings Supplements*, 239-240:140–147.
- Boezio M (2014) "Cosmic Ray Electrons and Protons, and Their Antiparticles", *Brazilian Journal of Physics*, 44(5):441–449.
- Cheng J (2009) *The Principles of Astronomical Telescope Design*, First Edition, Springer, Virginia.
- Cronin J, Gaisser T and Swordy S (1997) "Cosmic Rays at the Energy Frontier", *Scientific American*, 276(1):44–49.
- Dutta S I, Huang Y and Reno M H (2005) "Tau neutrino propagation and tau energy loss", *Phys. Rev. D*, 72:013005.
- Estupiñán A, Asorey H and Núñez L A (2015) "Implementing the De-thinning Method for High Energy Cosmic Rays Extensive Air Showers Simulations", *Nuclear and Particle Physics Proceedings*, 267-269:421–423.
- Fargion D (2002) "Discovering Ultra-High-Energy Neutrinos through Horizontal and Upward τ Air Showers: Evidence in Terrestrial Gamma Flashes?", *The Astrophysical Journal*, 570(2):909.
- Fargion D, Aiello A and Conversano R (1999) "Horizontal tau air showers from mountains in deep valley: Traces of UHECR neutrino tau", In *Proceedings, 26th International Cosmic Ray Conference (ICRC), August 17-25, 1999, Salt Lake City: Invited, Rapporteur, and Highlight Papers*, page 396.
- Forbush S (1946) "Three Unusual Cosmic-Ray Increases Possibly Due to Charged Particles from the Sun", *Phys. Rev.*, 70:771–772.
- Gandhi R, Quigg C, Reno M H and Sarcevic I (1998) "Neutrino interactions at ultrahigh energies", *Phys. Rev. D*, 58:093009.
- Greisen K (1966) "End to the Cosmic-Ray Spectrum?", *Phys. Rev. Lett.*, 16:748–750.
- Haungs A, Blumer J, Fuchs B, et al. (2015) "KCDC - The KASCADE Cosmic-ray Data Centre", *Journal of Physics: Conference Series*, 632(1):012011.

- Hayashida N, Honda K, Honda M, et al. (1994) "Observation of a very energetic cosmic ray well beyond the predicted 2.7 k cutoff in the primary energy spectrum", *Phys. Rev. Lett.*, 73:3491–3494.
- Heck D, Knapp J, Capdevielle J, Schatz G and Thouw T (1998) "CORSIKA: a Monte Carlo code to simulate extensive air showers", Technical report, Institute for Nuclear Physics, Forschungszentrum und Universität Karlsruhe, Karlsruhe.
- Heck D and Pierog T (2013) "Extensive Air Shower Simulation with CORSIKA: A User's Guide", Technical report, Karlsruher Institut Für Technologie (KIT).
- Hess V (1912) "Penetrating radiation in seven free ballon flights", *Physics Zeits*, 13(1084):1–4.
- IceCube Collaboration, Fermi-LAT, MAGIC, AGILE, ASAS-SN, HAWC, H.E.S.S., INTEGRAL, Kanata, Kiso, Kapteyn, Liverpool Telescope, Subaru, Swift/NuSTAR, VERITAS and VLA/17B-403 (2018) "Multimessenger observations of a flaring blazar coincident with high-energy neutrino IceCube-170922A", *Science*, 361:146–154.
- Iori M, Atakisi I, Chiodi G, Denizli H, Ferrarotto F, Kaya M, Yilmaz A, Recchia L and Russ J (2014) "SiPM application for a detector for UHE neutrinos tested at Sphinx station", *Nuclear Instruments and Methods in Physics Research Section A: Accelerators, Spectrometers, Detectors and Associated Equipment*, 742:265–268.
- James F and Roos M (1975) "Minuit - a system for function minimization and analysis of the parameter errors and correlations", *Computer Physics Communications*, 10(6):343–367.
- Jelley J V (1955) "Cerenkov radiation and its applications", *British Journal of Applied Physics*, 6(7):227.
- Kh H H (2016) "A new model-independent approach for finding the arrival direction of an extensive air shower", *Journal of Cosmology and Astroparticle Physics*.
- Krawczynski H, Prahl J, Arqueros F, et al. (1996) "An optimized method for the reconstruction of the direction of air showers for scintillator arrays", *Nuclear Instruments and Methods in Physics Research Section A: Accelerators, Spectrometers, Detectors and Associated Equipment*, 383(2):431–440.
- Lawrence M A, Reid R J O and Watson A A (1991) "The cosmic ray energy spectrum above $4 * 10^{17}$ eV as measured by the Haverah Park array", *Journal of Physics G: Nuclear and Particle Physics*, 17(5):733.
- Linsley J and Scarsi L (1962) "Arrival Times of Air Shower Particles at Large Distances from the Axis", *Phys. Rev.*, 128:2384–2392.
- Linsley J, Scarsi L and Rossi B (1961) "Extremely energetic cosmic-ray event", *Phys. Rev. Lett.*, 6:485–487.

- Mayer H J (1993) "A fast reconstruction method for shower direction at large extended air shower arrays", *Nuclear Instruments and Methods in Physics Research Section A: Accelerators, Spectrometers, Detectors and Associated Equipment*, 330(1):254–258.
- Mishev A and Velinov P I Y (2013) "The influence of low energy hadron interaction models in CORSIKA code on atmospheric ionization due to heavy nuclei", *Journal of Physics: Conference Series*, 409(1):012209.
- Ostapchenko S (2006) "QGSJET-II: towards reliable description of very high energy hadronic interactions", *Nuclear Physics B - Proceedings Supplements*, 151(1):143–146.
- Patrignani C et al. (2017) "2017 Review of Particle Physics", *Chinese Physics C*, 40.
- Sokolsky P (2009) "Observation of the GZK cutoff by the HiRes Experiment", *Nuclear Physics B - Proceedings Supplements*, 196:67–73.
- Sokolsky P (2011) "Final Results from the High resolution Fly's Eye (HiRes) Experiment", *Nuclear Physics B - Proceedings Supplements*, 212-213:74–78.
- Stokes B, Cady R, Ivanov D, Matthews J and Thomson G (2012) "Dethinning extensive air shower simulations", *Astroparticle Physics*, 35(11):759–766.
- The Pierre Auger Collaboration (2015) "Measurement of the cosmic ray spectrum above $4 * 10^{18}$ eV using inclined events detected with the Pierre Auger Observatory", *Journal of Cosmology and Astroparticle Physics*, 2015(08):049.
- The Pierre Auger Collaboration et al. (2015) "The Pierre Auger Cosmic Ray Observatory", *Nuclear Instruments and Methods in Physics Research Section A: Accelerators, Spectrometers, Detectors and Associated Equipment*, 798:172–213.
- Was Z and Jadach S (1992) "TAUOLA Monte Carlo for tau decays", In *Proceedings, 26th International Conference on High-energy Physics (ICHEP 92): Dallas, Texas, USA, August 6-12, 1992*, pages 1777–1780.
- Zas E (2005) "Neutrino detection with inclined air showers", *New Journal of Physics*, 7(1):130.
- Zatsepin G T and Kuzmin V A (1966) "Upper limit of the spectrum of cosmic rays", *JETP Lett.*, 4:78–80.



APPENDICES

7. APPENDICES

Appendix A

The number of particles on mountain slope, detector array and around the center of array are simulated with/without THIN option for 5 different decay modes in 5 different energies with 4 different development lengths.



Appendix B

The arrival direction of 27 showers estimated from the number of the e^\pm in the center of core are selected as at least 1,3,4 and 5 in a station. The energy of the primary particle range between 100 PeV and 1000 PeV with 7 km development length.

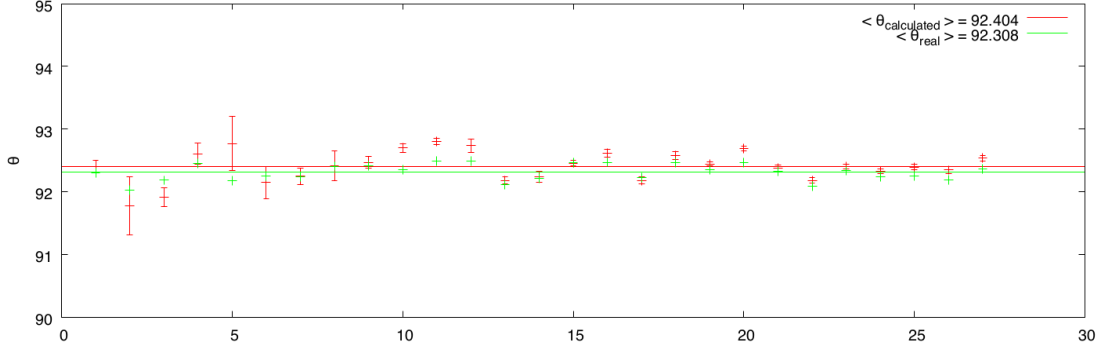


Figure 7.1. The zenith angles θ for 27 different showers are evaluated from at least 1 triggered stations.

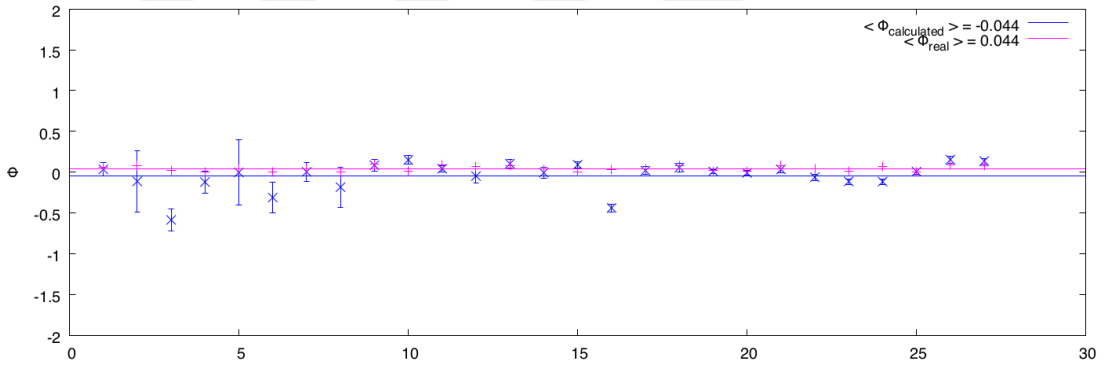


Figure 7.2. The azimuthal angles ϕ for 27 different showers are evaluated from at least 1 triggered stations.

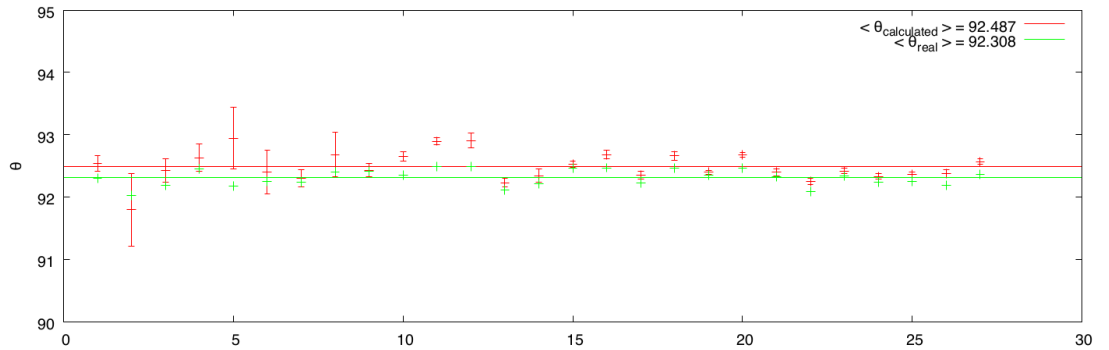


Figure 7.3. The zenith angles θ for 27 different showers are evaluated from at least 3 triggered stations.

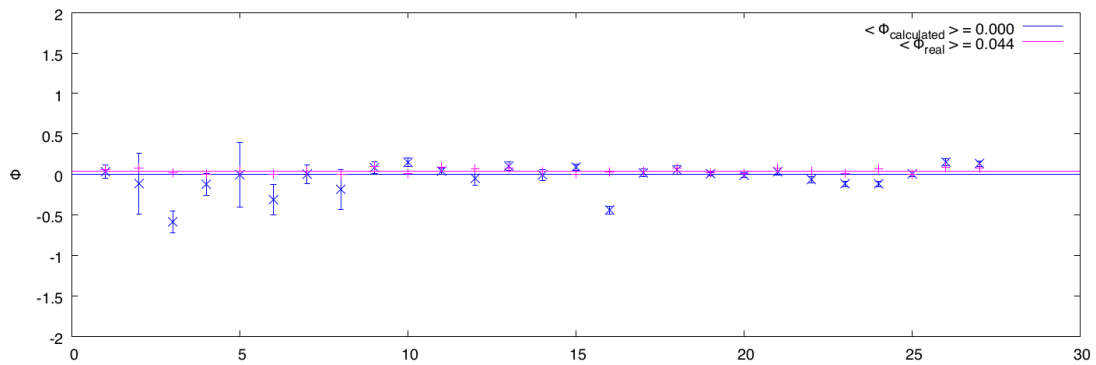


Figure 7.4. The azimuthal angles ϕ for 27 different showers are evaluated from at least 3 triggered stations.

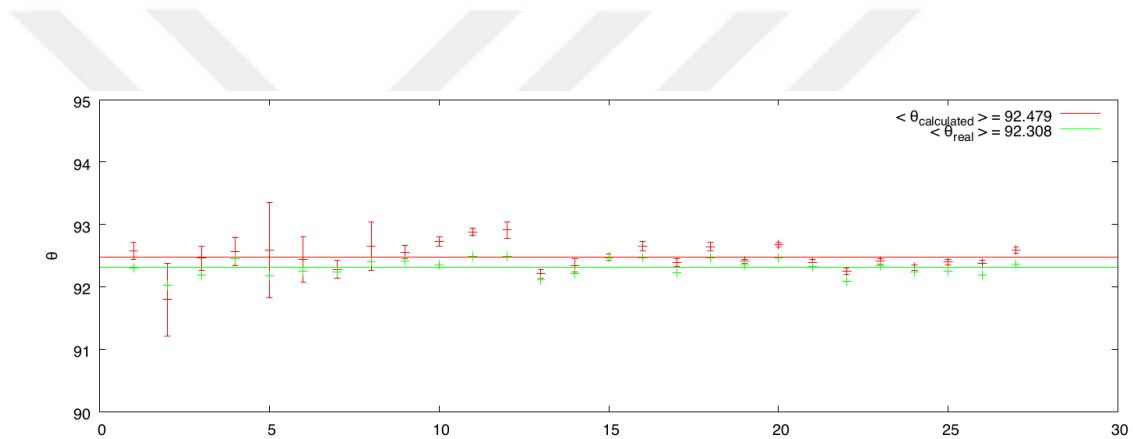


Figure 7.5. The zenith angles θ for 27 different showers are evaluated from at least 4 triggered stations.

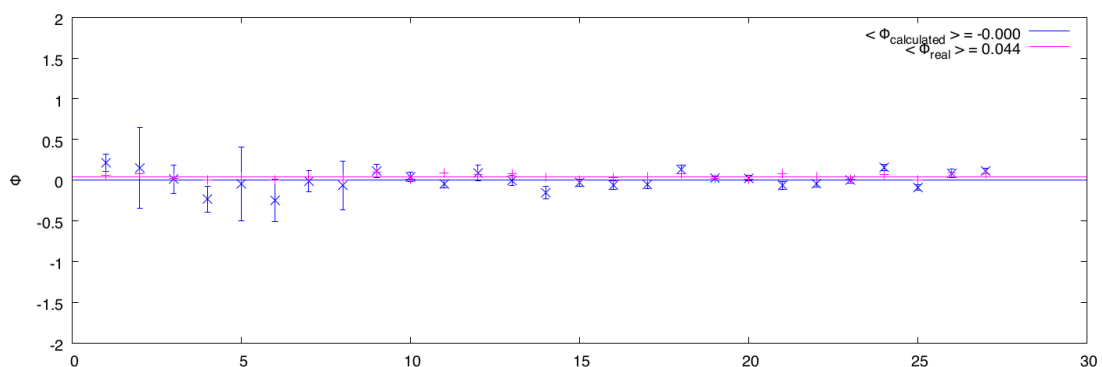


Figure 7.6. The azimuthal angles ϕ for 27 different showers are evaluated from at least 4 triggered stations.

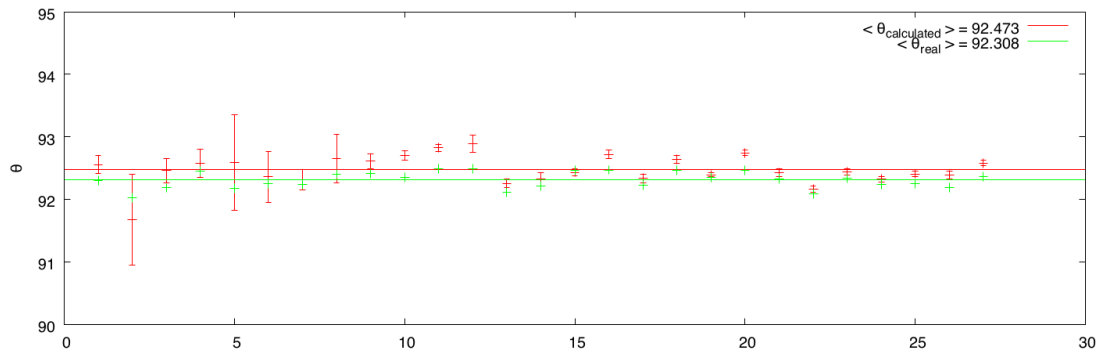


Figure 7.7. The zenith angles θ for 27 different showers are evaluated from at least 5 triggered stations.

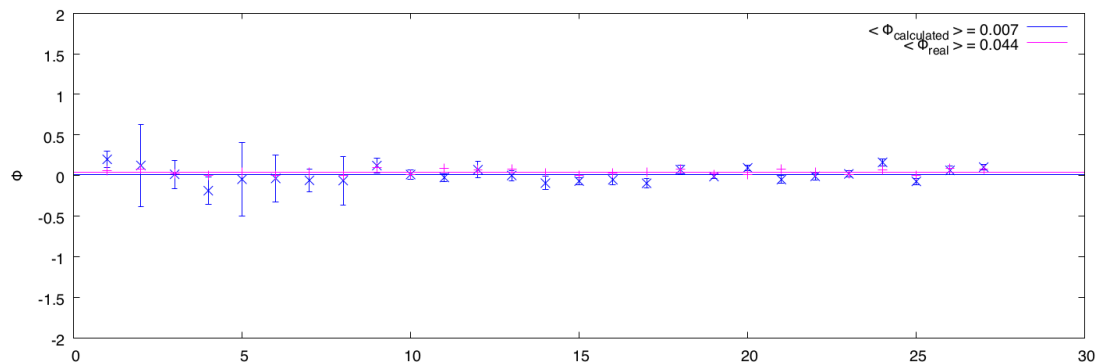


Figure 7.8. The azimuthal angles ϕ for 27 different showers are evaluated from at least 5 triggered stations.

8. CURRICULUM VITAE

Name SURNAME : Şeyma Atik Yılmaz

Place and Date of Birth : Edirne, TURKEY - 29.04.1988

Universities

Bachelor's Degree : Abant İzzet Baysal University, 2011

Master Degree : Abant İzzet Baysal University, 2014

e-mail : seyma.atikyilmaz@ogrenci.ibu.edu.tr

Address : Bolu Abant İzzet Baysal University, Science & Art
Faculty, Gölköy Campus, BOLU, TURKEY.

List of Publications :

S. Atik Yılmaz, M. Iori, A. Yılmaz, K. Y. Oyulmaz, H. Denizli and J. Russ (in review),
“Study of a large array to detect ultra high energy tau-neutrino” Astroparticle Physics,
2018.

Şeyma Atik Yılmaz, Ali Yılmaz, Haluk Denizli, and Kaan Yüksel Oyulmaz, “Energy
cutoff effect in CORSIKA on the detected particles of $\pi\pi^0$ decay channel”, Can. J.
Phys., dx.doi.org/10.1139/cjp-2017-0766, 2018.

A. Yılmaz, M. Iori, H. Denizli, K. Y. Oyulmaz, S. Atik Yılmaz, U. Keskin and J. Russ,
“Simulation of horizontal tau-neutrino induced shower to optimize the site parameters”,
35th International Cosmic Ray Conference - ICRC2017, POS (ICRC2017) 471, 2017.

Seyma Atik, Hakan Yetis, Haluk Denizli and Fatih Evrendilek, “Monitoring spatio
- temporal dynamics of indoor radon concentrations in the built environment of a
university campus”, Fresenius Environmental Bulletin by PSP Volume 25, No 1, 2016.

Seyma Atik, Hakan Yetis, Haluk Denizli and Fatih Evrendilek, “How Do Different Locations, Floors and Aspects Influence Indoor Radon Concentrations? An Empirical Study Using Neural Networks for a University Campus in Northwestern Turkey”, *Indoor and Built Environment*, 22(4):650-658, 2013.

Awards :

Turkish Physical Society 2017 Engin ABAT Best Theoretical Poster Presentation Award, Bodrum TURKEY, 2018.

Turkish Physical Society 2014 Özgen Berkol Doğan Experimental Physics Poster Presentation Award, Bodrum TURKEY, 2015.